

EVENT-TRIGGERED MPC for DC-DC CONVERTERS

by

RANYA BADAWI

A dissertation submitted in partial fulfillment of the
requirements for the degree of

DOCTOR OF PHILOSOPHY IN ELECTRICAL AND COMPUTER ENGINEERING

2025

Oakland University
Rochester, Michigan

Doctoral Advisory Committee:

Jun Chen, Ph.D., Chair

Manohar Das, Ph.D.

Tamas Horvath, Ph.D.

Seyed Ali Arefifar, Ph.D.

© by Ranya Badawi, 2025
All rights reserved

To my family

ACKNOWLEDGMENTS

I would like to express my sincere gratitude to my advisor, Dr. Jun Chen, for his support throughout this journey. I have been faced with many challenges, both academically and personally, but meeting with Dr. Chen always brought me clarity and reassurance that everything will be alright.

Thanks are also due to my advisory committee members: Dr. Manohar Das, Dr. Ali Arefifar and Dr. Tamas Horvath for their constructive feedback related to my thesis formulation and advice on presenting a meaningful contribution.

I would like to thank my husband, Husam, for doing anything possible to make this happen, and my three amazing daughters, Hala, Yara and Lamees for inspiring me to be the best version of myself. I would like to thank my parents, Adel and Fatima, for encouraging me and loving me unconditionally. To my siblings: Marwah, Rawan, Mohammad, Afnan, Raghad and Eman - thank you.

I would also like to thank my coworkers at General Motors: Steven Wybo, Samantha Gunter, Mehrdad Teimorzadeh, Mohammad Anwar, Jeff Yambor, Bill Ivan and Stephen Cichy for mentoring me and instilling in me an interest in Power Electronics. So many people have helped me along the way and to them, I dedicate my work.

Ranya Badawi

ABSTRACT

EVENT-TRIGGERED MPC for DC-DC CONVERTERS

by

Ranya Badawi

Adviser: Jun Chen, Ph.D.

Model Predictive Control (MPC) has been gaining popularity as a time-domain control method for power converters. Event-triggered MPC has been explored as a method to reduce the computational burden of enumeration-based MPC. Existing literature reports MPC's successful use in power converter applications but does not widely explore the use of event-triggered control in similar applications. This investigation proposes a method to utilize event-triggered model predictive control (ET-MPC) in DC-to-DC power converters to achieve significant computational savings by reducing the frequency of control updates to only when needed. The method proposed solves an optimal control problem (OCP) to generate an optimal actuating value only when an event is triggered as opposed to solving the OCP at every time step. The purpose is to reduce the computational load of an enumeration-based time-triggered MPC over a defined time-frame. The novelty of this method lies in the selection of the actuating control signal, where the control actions are selected from the optimal switching sequence as opposed to upholding the last value of the optimal actuating value as reported in prior literature. A Kalman Filter-based estimator is added to the control system to ensure accurate voltage tracking during model mismatch which commonly occurs during load transients. In this work, ET-MPC is successfully implemented on both a DC-to-DC boost and a buck converter showing significant computational savings. The performances of the conventional time-triggered

MPC and the proposed event-triggered MPC are compared through simulation. The effect of the event-trigger threshold is evaluated as a tuning parameter to balance computation and control performance.

TABLE OF CONTENTS

ACKNOWLEDGMENTS	iv
ABSTRACT	v
LIST OF TABLES	xii
LIST OF FIGURES	xiv
CHAPTER ONE INTRODUCTION	1
1.1. Power Converters	1
1.2. Model Predictive Control	3
1.2.1. Mathematical Model	5
1.2.2. Implicit vs Explicit MPC	6
1.2.3. Direct vs Indirect MPC	7
1.3. Optimal Control	7
1.3.1. Optimal Control Problem (OCP) and Feasibility	9
1.3.2. Constraints	10
1.3.3. Prediction Horizon	10
1.3.4. Robustness	11
1.3.5. Performance Objectives	11
1.3.6. Computational Complexity	11
1.4. Optimization Problem Types	12
1.4.1. Least-Squares Problems	12
1.4.2. Convex Optimization	13

TABLE OF CONTENTS—Continued

1.4.3. Non-Convex Optimization	14
1.5. Solution Algorithms	14
1.5.1. Linear Programming (LP)	14
1.5.2. Quadratic Programming (QP)	17
1.5.3. Multiple Integer Linear Programming (MILP)	17
1.5.4. Dynamic Programming (DP)	21
1.6. Summary	21
CHAPTER TWO	
LITERATURE REVIEW	23
2.1. Power Converter System Requirements, Objectives and Constraints	26
2.1.1. Requirements Driven by Regulations	30
2.2. MPC Design Elements	32
2.2.1. Cost Function Selection	34
2.2.2. Weighting Factors	36
2.2.3. Robustness and Effect of Model Mismatch	36
2.3. Event-triggered Control	41
2.4. Contributions of this Thesis	42
CHAPTER THREE	
EVENT-TRIGGERED ENUMERATION-BASED MPC	45
3.1. Time-triggered enumeration-based MPC for boost converter	46

TABLE OF CONTENTS—Continued

3.1.1. Boost Converter Mathematical Model	47
3.1.2. Cost Function and OCP	54
3.1.3. Prediction Horizon	55
3.2. Event-Triggered Enumeration-Based MPC (ET-MPC)	56
3.3. Maximum Computational Savings	62
CHAPTER FOUR	
ET-MPC WITH FULL STATE FEEDBACK	64
4.1. Comparison between TT-MPC and ET-MPC	65
4.1.1. Start-up	65
4.1.2. Step Changes in the Output Reference Voltage	67
4.1.3. Step Change in the Input Voltage	70
4.1.4. Discussion of Computational Savings	71
4.1.5. Summary of results	72
4.2. Evaluation of event-trigger threshold effect	72
4.2.1. Event-Trigger Threshold Impact on Start-up Time	73
4.2.2. Event-Trigger Threshold Impact on Steady-state Operation	74
4.2.3. Event-Trigger Threshold Impact on Step Changes in the Output Reference Voltage	75
4.2.4. Event-Trigger Threshold Impact on Step Change in the Input Voltage	80

TABLE OF CONTENTS—Continued

4.2.5. Summary of results	80
CHAPTER FIVE	
ET-MPC WITH KALMAN FILTER	82
5.1. Introduction and Key Concepts	82
5.1.1. State Estimators, Observers and Filters	83
5.1.2. Observability and Disturbance Observers	84
5.2. Kalman Filter-based Disturbance Observer	84
5.3. Modified Objective Function	88
5.4. Implementation and Simulation Results	89
5.4.1. Converter Startup	91
5.4.2. Steady-state Operation	95
5.4.3. Step Changes in the Output Reference Voltage	99
5.4.4. Step Change in the Input Voltage	102
5.4.5. Response to Load Transients	103
5.4.6. ET-MPC Impact on Efficiency	105
5.5. Remarks	109
CHAPTER SIX	
ET-MPC FOR BUCK CONVERTER	113
6.1. Buck Converter	113
6.2. Discrete Mathematical Model	113
6.2.1. Continuous-time Model	113

TABLE OF CONTENTS—Continued

6.2.2. Discrete-time Model	115
6.3. Implementation and Simulation Results	117
6.3.1. Buck Converter Startup	119
6.3.2. Steady-state Operation	120
6.3.3. Step Changes in the Output Reference Voltage	123
6.3.4. Step Change in the Input Voltage (Line Transient)	123
6.3.5. Response to Load Transients	127
6.4. Remarks	129
CHAPTER SEVEN	
CONCLUSION AND FUTURE WORK	132
7.1. Remarks	132
7.2. Future Work	133
APPENDICES	
A. NOTATION	134
A.1. Mathematical Notation	135
A.2. Symbols	136
A.3. Acronyms	137
REFERENCES	138

LIST OF TABLES

Table 1.1	Knapsack Problem	19
Table 1.2	0/1 Knapsack Problem: Enumeration Method	20
Table 2.1	MPC in Mobility and Energy Management Applications	24
Table 2.2	A Literature Review of the Implementation of MPC in Power Converter Control	37
Table 3.1	Event-triggered Selection of Optimal State trajectory and Switch State Index	58
Table 4.1	Simulation Parameters - Boost Converter	65
Table 4.2	Computational Saving as Measured by Event Frequency	73
Table 4.3	Start-up Time Summary	74
Table 4.4	Event-trigger Threshold Impact on Steady-state Operation - Results Summary	76
Table 4.5	Voltage Reference Converter Response for Different Event Thresholds	78
Table 5.1	Simulation Parameters - Boost Converter with Kalman Filter	93
Table 5.2	Start-up Time Summary	94
Table 5.3	Optimal Switching Sequences in time duration between 4ms and 5ms in Figure 5.6	96
Table 5.4	Event-trigger Impact on Steady-state Operation - Results Summary	98
Table 5.5	Voltage Reference Converter Response for Different Event Thresholds	102
Table 5.6	Load Transient Results	106
Table 5.7	ET-MPC Impact to Efficiency	109

LIST OF TABLES—Continued

Table 6.1	Simulation Parameters - Buck Converter with Kalman Filter	118
Table 6.2	Start-up Attributes Summary-Buck Converter	120
Table 6.3	Event-trigger Impact on Steady-state Operation - Results Summary	124
Table 6.4	Voltage Reference Converter Response for Different Event Thresholds	127

LIST OF FIGURES

Figure 1.1	Power Converter Closed Loop Feedback and Feedforward Control	2
Figure 1.2	Model Predictive Control Overview	4
Figure 1.3	Implicit MPC for Power Converter Control	6
Figure 1.4	Explicit MPC for Power Converter	7
Figure 1.5	Direct MPC for a Power Converter	8
Figure 1.6	Indirect MPC for Power Converter	8
Figure 1.7	Common Optimal Control Techniques	9
Figure 1.8	Farmer's Problem - Graphical Solution	16
Figure 1.9	Solving 0/1 Knapsack Problem in Dynamic Programming	22
Figure 2.1	Prediction Horizon in MPC	25
Figure 2.2	Boost Converter with Synchronous Rectifiers to Improve Efficiency	28
Figure 2.3	Shoot-through condition in synchronous rectifier buck converter	31
Figure 2.4	Direct MPC with Hysteresis Bounds	33
Figure 2.5	Non-minimum phase behavior of Boost Converter - PWM controlled example	35
Figure 3.1	Boost converter circuit diagram	45
Figure 3.2	Enumeration-based Model Predictive Control for Boost Converter	47
Figure 3.3	Current conduction modes: CCM, CRM, DCM	48

LIST OF FIGURES—Continued

Figure 3.4 Continuous-time model state machine representation Figure 3.5 The three operating modes in DCM Figure 3.6 Discrete-time model state machine representation Figure 3.7 Discrete Math Model Operating Modes Figure 3.8 Prediction horizon move blocking scheme Figure 3.9 Event-trigger decision and increment process Figure 3.10 Event-trigger Flowchart for Boost Converter control Figure 3.11 Minimum Achievable Event Frequency ($n_s = 4$)	49 50 52 53 57 59 61 63
Figure 4.1 DC-DC boost converter with ET-MPC control Figure 4.2 Boost Converter Start-up (TT-MPC) Figure 4.3 Boost Converter Start-up (ET-MPC, $\delta = 0.05$) Figure 4.4 Reference voltage step-up from 15V to 30V (TT-MPC) Figure 4.5 Reference voltage step-up from 15V to 30V (ET-MPC) Figure 4.6 Reference voltage step-down from 20V to 15V (TT-MPC) Figure 4.7 Reference voltage step-down from 20V to 15V (ET-MPC)	64 66 67 68 69 69
Figure 4.8 Input voltage step-up from 10V to 15V (TT-MPC) Figure 4.9 Input voltage step-up from 10V to 15V (ET-MCP) Figure 4.10 Start-up ($v_s = 10V$ and $v_{o,ref} = 20V$) Figure 4.11 Start-up and steady-state operation ($v_s = 10V$ and $v_{o,ref} = 30V$)	71 72 75 77

LIST OF FIGURES—Continued

Figure 4.12	Reference voltage step-up from 15V to 30V (ET-MPC)	78
Figure 4.13	Reference voltage step-down from 20V to 15V (ET-MPC)	79
Figure 4.14	Input voltage step-up from 10V to 15V (ET-MPC)	81
Figure 5.1	The use of a state estimator in MPC	82
Figure 5.2	The use of a disturbance observer in MPC to eliminate the effect of disturbances	85
Figure 5.3	DC-DC boost converter with ET-MPC control and Kalman Filter-based DOB	91
Figure 5.4	Start-up (TT-MPC)	94
Figure 5.5	Start-up (ET-MPC)	95
Figure 5.6	Steady-State (ET-MPC) $v_s = 10V$, $v_{o,ref} = 15V$	97
Figure 5.7	Reference voltage step-up from 15V to 30V (TT-MPC)	99
Figure 5.8	Reference voltage step-up from 15V to 30V (ET-MPC)	100
Figure 5.9	Reference voltage step-down from 25V to 15V (TT-MPC)	101
Figure 5.10	Reference voltage step-down from 25V to 15V (ET-MPC)	101
Figure 5.11	Inductor Saturation (No current information in OCP)	103
Figure 5.12	Inductor Saturation Addressed: Shifted Voltage Reference from 10ms to 9.92ms	104
Figure 5.13	Inductor Saturation Addressed: Add Inductor Current to OCP	105

LIST OF FIGURES—Continued

Figure 5.14 Input voltage step-up from 10V to 15V (TT-MPC)	106
Figure 5.15 Input voltage step-up from 10V to 15V (ET-MCP)	107
Figure 5.16 Load Transient for TT-MPC	107
Figure 5.17 Load Transient for ET-MPC, $\delta = 0.01$	111
Figure 5.18 Load Transient for ET-MPC, $\delta = 0.025$	112
Figure 6.1 Buck converter circuit diagram	114
Figure 6.2 Buck Converter ET-MPC Implementation Block Diagram	117
Figure 6.3 Buck Converter Start-up without (a) and with Soft-Start (b) (TT-MPC)	121
Figure 6.4 Buck Converter Start-up without and with Soft-Start (ET-MPC - $\delta = 0.025$)	122
Figure 6.5 Reference voltage step-up from 3.3V to 5V (TT-MPC and ET-MPC)	125
Figure 6.6 Reference voltage step-down from 5V to 3.3V (TT-MPC and ET-MPC)	126
Figure 6.7 Input voltage step-down from 12V to 16V (TT-MPC and ET-MPC ($\delta = 0.025$))	128
Figure 6.8 Load Transient for TT-MPC and ET-MPC ($\delta = 0.15$) - Buck Converter	130
Figure 6.9 Average event frequency during load transient - ($\delta = 0.01$, $\delta = 0.015$, $\delta = 0.035$, $\delta = 0.045$)	131

CHAPTER ONE

INTRODUCTION

1.1 Power Converters

Power converters utilize the fundamentals of power electronics to efficiently convert electric power from one form to another. Converters generally consist of semiconductor devices (e.g., MOSFETs and diodes), magnetic devices (e.g., inductors and transformers) and capacitors. Ideally, these components switch, store and release energy and are considered lossless. Realistically, however, these components are non-ideal and contain many forms of power losses. Regardless, a power converter outperforms its linear regulator counterpart as an efficient method to convert power. The clear advantage especially presents itself in high-power applications.

In the case of a DC to DC power converter, the system converts the voltage and, in turn, current level from one to another. The goal of the converter is to maintain a voltage level provided by a reference voltage, also known as the command voltage, despite disturbances seen throughout operation. These disturbances appear in the form of variations at the voltage source, voltage reference, and load. Variations can also appear due to circuit component tolerances.

Under varying conditions, the converter must perform corrective actions to maintain regulation. This can be achieved through open-loop or closed-loop control. In open-loop control, the controller does not comprehend information about the system's present status. In closed-loop feedback control, measurements of the system are fed back to the controller. These measurements can include input voltage, output voltage and for converters that contain magnetic devices; the inductor current. The role of the control system is to assess how far the measurements deviate from the desired behavior and

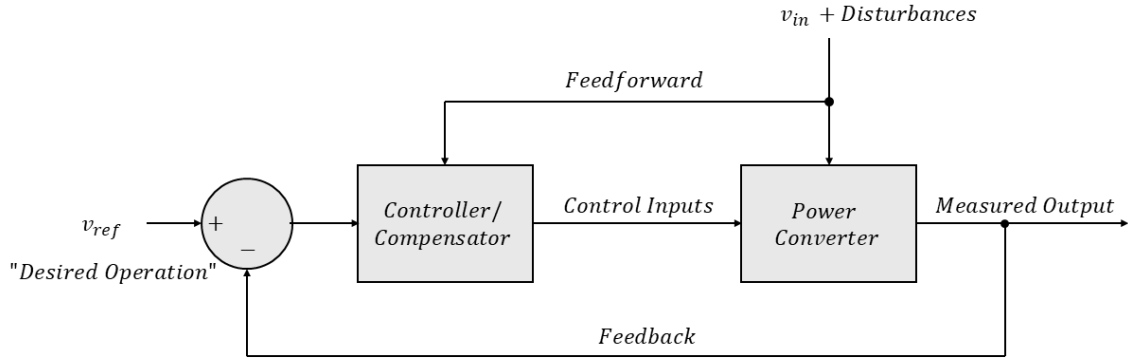


Figure 1.1: Power Converter Closed Loop Feedback and Feedforward Control

actuate the system so that it can be restored to nominal operation [1]. A general block diagram of a closed-loop feedback system with feed-forward is shown in Figure 1.1.

Power converter control has been a widely investigated topic. Control techniques can be classified into classical control and modern control. In a general sense, classical control refers to methods in which a system is represented with a transfer function in the frequency domain using Laplace transforms. Then, a form of Proportional Integral Derivative (PID) control is implemented to improve the smoothness and responsiveness of a Linear Time-Invariant (LTI) system's closed loop feedback response.

In practice, power converters have vastly implemented classical control methods. Due to the switching nature of power converter systems, classical control methods cannot be applied directly without implementing averaging techniques to obtain a system model. These techniques include state-space averaging and circuit averaging [2]. Once a model is obtained, and a transfer function is developed, a compensator can be designed to improve the closed-loop performance of the system to meet system objectives.

Modern control has generally referred to the use of state-space methods which allow for developing a system model in time domain and for easier implementation to

control Multiple-Input Multiple-Output (MIMO) systems. The advancement of computers allowed for the furtherance of modern control systems. More recently, modern control theory is a term which describes the use of advanced techniques that can handle nonlinear, time-varying and nondeterministic systems. These techniques include optimal control, robust control, adaptive control and nonlinear control.

1.2 Model Predictive Control

This chapter will give an overview of Model Predictive Control (MPC) and its advantages. It will also cover the main elements of MPC within the context of power converters. These elements include the system math model, prediction horizon and the Optimal Control Problem (OCP). A brief introduction to optimization theory with a focus on optimization solution techniques and algorithms will be covered.

MPC has been gaining popularity as a control method for power converters [3–7]. MPC is an intuitive control method which utilizes a system model and a control objective to select an optimal actuating control signal. This is achieved by solving a cost function which generates an optimal control sequence across a prediction horizon [8]. Figure 1.2 gives an overview of MPC control for a general system.

Traditional MPC utilizes a receding horizon approach in which the first control signal in the optimal control sequence is selected at each time step the OCP is triggered. The rest of the sequence is dismissed, and a new one is generated at the following time step. This is to ensure robustness and adaptability of the system to adjust when uncertainties and disturbances are introduced [9].

The predictive nature of the controller enables a fast system response. Another advantage of the MPC controller is that it can handle multiple inputs and outputs since it captures their interactions through the system model. Additionally, the inclusion of control objectives and constraints within the cost function can reduce the need for some of

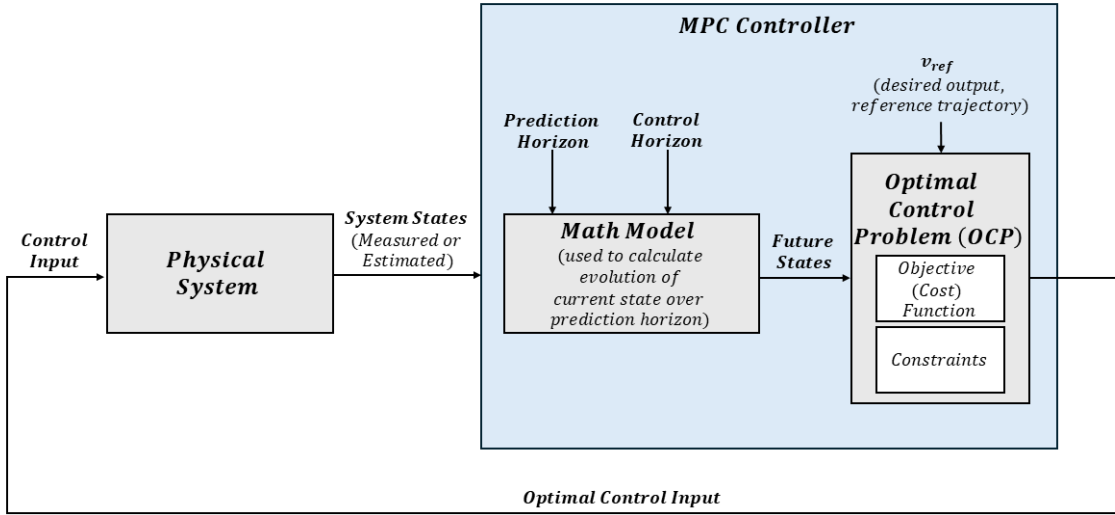


Figure 1.2: Model Predictive Control Overview

the protection circuitry. The ability to add state estimators gives the system designer the option to reduce the number of sensors and improve the accuracy of the model which improves the quality of control [10–15].

Recent advancements in the processing speed of modern microcontrollers has allowed for a wider use of MPC in power converter control. MPC also shares the the advantages of digital control such as reduced hardware implementation cost and physical size, incorporation of more operating features and higher accuracy.

The control objective of a DC-DC boost or buck converter is to have the output voltage track a reference voltage. Regulation must be achieved despite input voltage disturbances and load variations. Additional control objectives can include current limiting to protect components from overheating and magnetic devices from saturation. Another control objective is limiting the switching frequency to reduce switching losses. Without imposing a restriction to the switching frequency or the amount of switching

within the cost function, the frequency of the converter can reach up to $1/(2T_s)$, since the actuation occurs at every time step [16].

1.2.1 Mathematical Model

MPC requires an accurate model of the system to predict the optimal actuation signal every time step, T_s . Switched-mode power converters are time-variant and non-linear systems, and the modeling of such systems can be done in multiple ways. The time-variant property is due to the switching nature of the converter. Non-linear behavior can be introduced when the state of the system changes based on circuit variables or system states. An example is during transitions between Continuous Conduction Mode (CCM) and Discontinuous Conduction Mode (DCM).

Averaged models ignore the switching dynamics of the converter and linearize around the operating point only to capture disturbance dynamics. One common approach in Pulse-Width Modulation (PWM) converter control is to create an AC equivalent circuit model by averaging the inductor voltage and capacitor current waveforms over a single switch cycle. Small AC variations around a quiescent operating point are then introduced into the model and the system is then linearized by removing second order AC (nonlinear) terms [2].

A power converter is considered a time-variant system when its behavior is observed at the switching frequency. This is why average models lose their accuracy at half the switching frequency [17]. Another modeling approach could consider power converters as linear time-invariant systems (LTI) connected by switches. Such a consideration is a hybrid system. This thesis will address the implementation of direct MPC control, and so, the consideration of a switched-model which captures the dynamics of the converter at the switching frequency is suitable. In this scenario, one may utilize

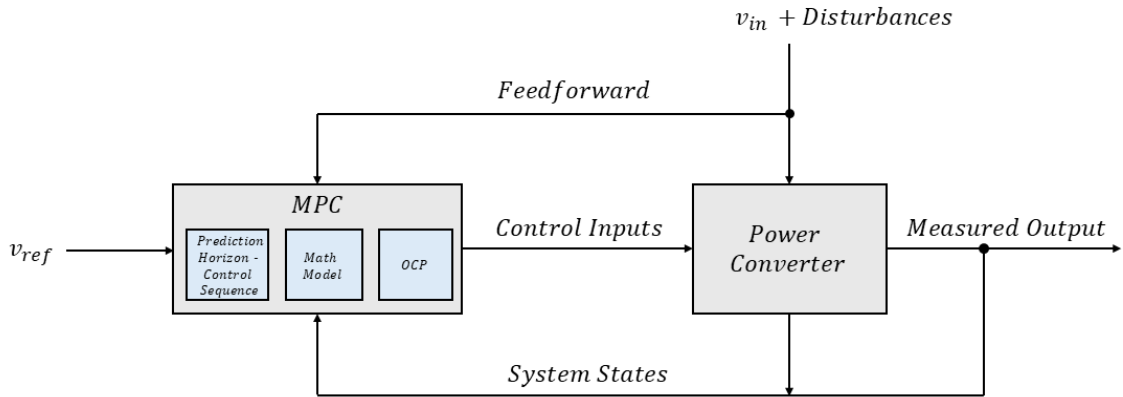


Figure 1.3: Implicit MPC for Power Converter Control

switched state-space modeling. The derivation of the math model for the boost and buck converter applications will be included in Chapters 3 and 6 respectively.

1.2.2 Implicit vs Explicit MPC

When comparing methods into how an optimal solution is obtained through physical hardware implementation, we may consider both online and offline solving methods. Implicit MPC generally refers to the method an optimal solution is found online by an iterative numerical procedure. Explicit MPC is a method in which the optimization problem is solved offline to generate a lookup table that is used during the online control effort [18]. Once the state-feedback control law is developed for all possible states of the system, the controller's effort shifts to finding the solution in the lookup table using methods such as a Binary Search Tree. Explicit MPC reduces the computation burden of the controller in real time and has been explored in previous work such as [19]. Figure 1.3 and Figure 1.4 both give a brief overview highlighting the differences between the two methods. The drawback of Explicit MPC is its high utilization of data memory resources.

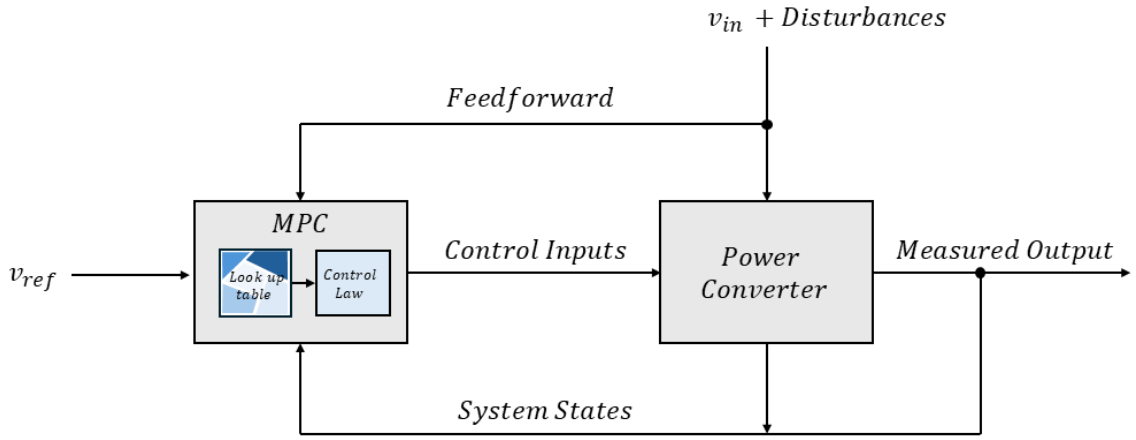


Figure 1.4: Explicit MPC for Power Converter

1.2.3 Direct vs Indirect MPC

Direct MPC describes a control system that applies the control output directly to actuate the controllable parameter, i.e. the switch in the case of a DC-DC converter. Indirect MPC generates a value that is then applied to a modulator. The modulator, in turn, generates a PWM signal that is applied to the switch [9]. Figure 1.5 and Figure 1.6 illustrate the differences between direct and indirect MPC respectively.

1.3 Optimal Control

In the following sections, an overview of optimal control and the main concepts related to it are introduced. In general, optimal control is the process of solving a problem and using the solution to control a system. The solution to the problem typically minimizes or maximizes an objective or cost function. Commonly used optimal control techniques and a general summary of each are summarized in Figure 1.7 [8, 20–23].

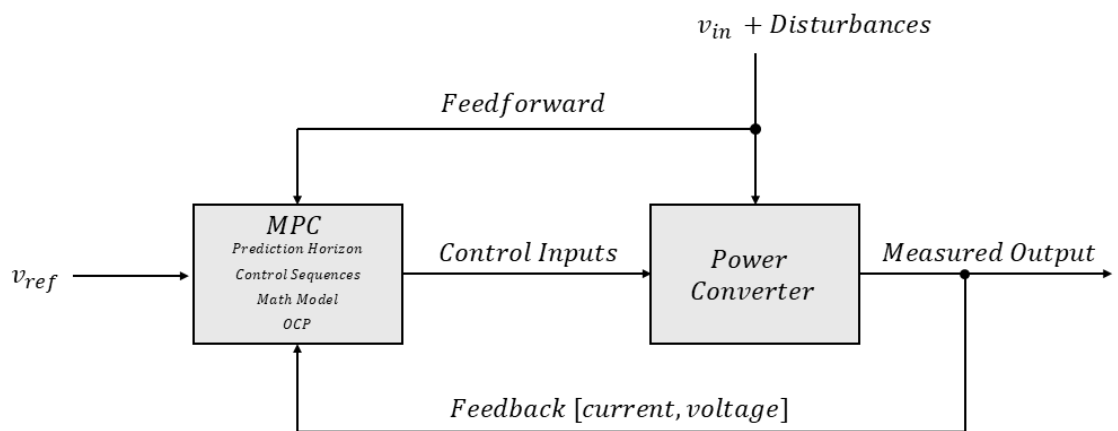


Figure 1.5: Direct MPC for a Power Converter

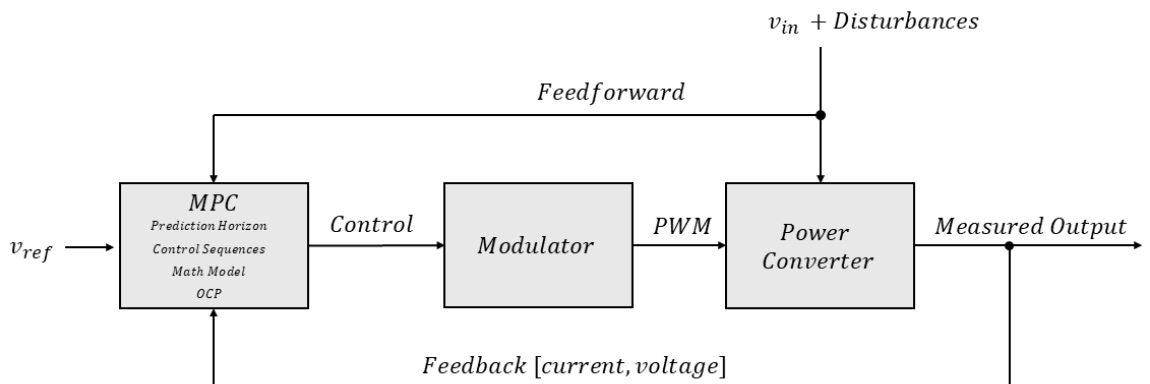


Figure 1.6: Indirect MPC for Power Converter

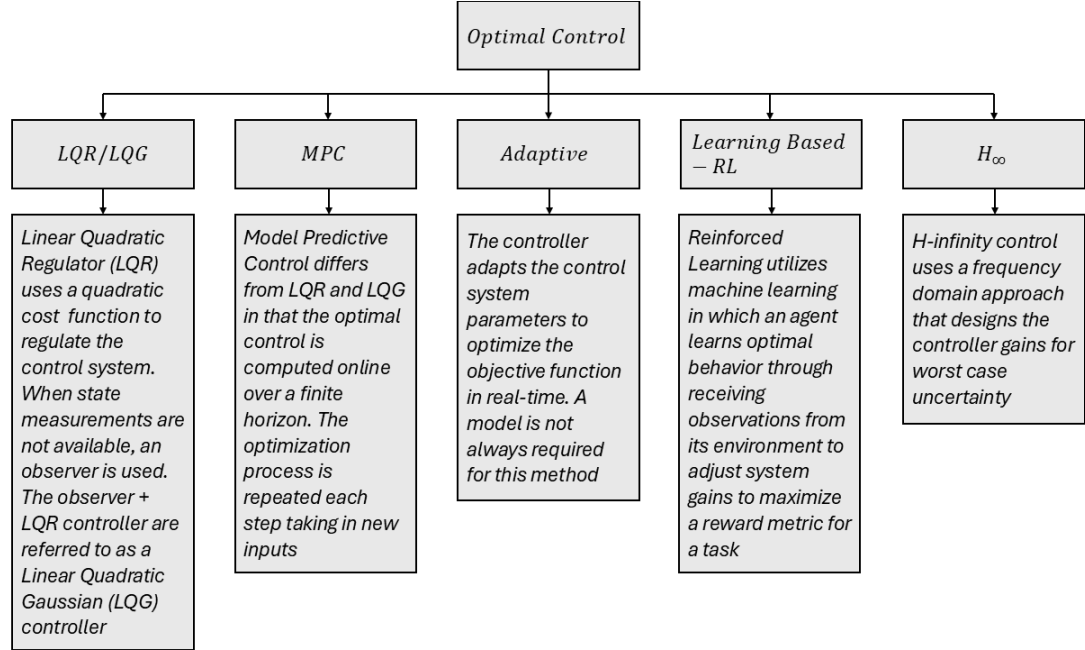


Figure 1.7: Common Optimal Control Techniques

1.3.1 Optimal Control Problem (OCP) and Feasibility

The OCP is an optimization problem written in the following form [24]:

$$\min_{x \in \mathbb{R}^n} f_0(x) \quad (1.1a)$$

$$\text{subject to } f_i(x) \leq 0, \quad i = 1, \dots, m \quad (1.1b)$$

$$h_i(x) = 0, \quad i = 1, \dots, p \quad (1.1c)$$

where x is the optimization variable, $f_0(x) : \mathbb{R}^n \mapsto \mathbb{R}$ is the objective function and is a function of the control input, x . The objective function comprehends and quantifies the control objective which in most power converter control cases aims at reducing tracking error. Tracking error is the difference between the predicted output and the reference. In many cases, the optimization process is subjected to constraints on the inputs

and outputs of the system. In (1.1), f_i are the inequality constraint functions and $h_i(x) = 0$ are equality constraints.

Feasibility refers to the ability of the OCP to find a solution that ensures a control action, thus leading to system stability. Any x that satisfies the constraints in (1.1) is called a feasible solution. A feasible solution is called the optimal solution (x^*) if it achieves the smallest objective value. State and control constraints could lead to infeasibility specifically if the current state is too far from the desired state or if the constraints are too tight.

1.3.2 Constraints

Constraints in (1.1) may be applied to the states and control input. Typically, physical systems and their control inputs have physical limits which cannot be violated. These limitations need to be incorporated in the MPC controller through hard constraints. Soft constraints are applied to system states so that the system can operate within safe limits and are usually added to maintain components within their safe and/or desirable operating zones [8, 9]. One example of a soft constraint is limiting current to prevent overheating of electrical components. When control objectives are included as constraints, the feasibility of a solution is not always guaranteed. An alternative to this is to include the control objectives in the cost function. The impact of the control objectives can be adjusted depending on how much influence is desired using weights [8].

1.3.3 Prediction Horizon

The prediction horizon is the time period the current state of the system is predicted to evolve when given a number of control steps. The prediction horizon shall be selected so that it is long enough to capture the immediate dynamics of the system, but not

too long in which it causes more computational burden and an increase in memory requirements [9].

1.3.4 Robustness

MPC is generally more robust to disturbances when compared to classical control methods such as PI-control due to its predictive nature. According to [25], robustness of the control loop refers to its ability to maintain stability and meet performance specifications despite model variations and exposure to noise. These variations and noise signals shall be defined within an uncertainty range, as it is not practical for a system to tolerate undefined operating conditions or ones that exceed the practical limitations of the system.

1.3.5 Performance Objectives

The main objective of a power converter is to maintain regulation throughout operation. Additional objectives can include reducing switching frequency and current limiting. These objectives can be included in the OCP through weighting factors and are not imposed as constraints.

1.3.6 Computational Complexity

Computational complexity theory classifies computation problems according to their resource usage. These resources are mainly storage and time. Optimization problems are one type of computational problems and can be classified as *P*, *NP*, *NP – Complete*, or *NP – Hard* problems. The following is a general description to provide the reader with sufficient background for the purpose of this dissertation. The reader is referred to [26] to gain more insights and an understanding of computational complexity.

Algorithms are step-by-step procedures which solve computational problems. Intractable problems are ones with that have constraints imposed on the solutions which

can make the solution impractical. Another instance in which a problem can be intractable is when there is no algorithm that could solve the problem quickly. "Quickly", in theoretical computer science, generally implies that an algorithm can solve the problem in polynomial time (P -time), e.g., $\mathcal{O}(n^2)$, as opposed to exponential time, e.g., $\mathcal{O}(2^n)$, where n is the length of input to the algorithm. There are exceptions to this general statement depending on the length of n .

A nondeterministic polynomial time (NP -time) problem is a type of computational problem in which when provided an answer, the answer can be verified in polynomial time, however, there is no way to find an answer quickly.

1.4 Optimization Problem Types

There are several methods to classify optimization problems with the form in ((1.1)). The major categories covered in [24] include least-squares, convex and non-convex optimization problems. A brief overview is given in this section.

1.4.1 Least-Squares Problems

Least-squares problems are optimal control problems, but do not have constraints. They are commonly found in regression analysis and in data fitting methods. The objective problem is a sum of the squares of the terms $a_i^T x - b_i$:

$$\text{minimize } f_0(x) = \|Ax - b\|_2^2 = \sum_{i=1}^k (a_i^T x - b_i)^2 \quad (1.2)$$

Where $A \in \mathbb{R}^{k \times n}$ (with $k \geq n$), a_i^T are the rows of A , and $x \in \mathbb{R}^n$ is the optimization variable.

Least-square problems are reduced to linear equations to facilitate a quick solution. The solution to (1.2) can be reduced to:

$$(A^T A)x = A^T b \quad (1.3a)$$

$$\text{hence } x = (A^T A)^{-1} A^T b \quad (1.3b)$$

which can be solved analytically in polynomial time [24].

1.4.2 Convex Optimization

Convex optimization problems are ones in which both the objective function and inequality constraint are convex. Additionally, the equality constraint $h_i(x)$ in (1.1) must be affine [24]. The importance of convexity is in the fact that every local minimum is also a global minimum which is a key factor in solving optimization problems and finding feasible solutions. Another key property is that convex problems can be solved in polynomial time, hence, they can be solved quickly.

A convex optimization written in standard form [24]:

$$\min_{x \in \mathbb{R}^n} f_0(x) \quad (1.4a)$$

$$\text{subject to } f_i(x) \leq 0, \quad i = 1, \dots, m \quad (1.4b)$$

$$a_i^T x = b_i, \quad i = 1, \dots, p \quad (1.4c)$$

A function $f_0(x)$ is convex if it satisfies the relationship in (1.5) for all $x, y \in \mathbb{R}$ and all values of $\alpha \in [0, 1]$:

$$f_0(\alpha x + (1 - \alpha)y) \leq \alpha f_0(x) + (1 - \alpha)f_0(y) \quad (1.5)$$

Note that least squares and Linear Programming (LP) problems are special cases of convex optimization problems. LP is described in a later section.

1.4.3 Non-Convex Optimization

The objective and constraint functions in non-convex optimization problems are not linear. Additionally, these problems exhibit multiple local minima and can be intractable. Examples of non-convex problems are Multiple Integer Linear and Quadratic (MILP and MIQP) problems. The straightforward method to solve these types of problems is to use enumeration for the binary variables. The disadvantage to this technique is the number of computations is on the exponential order. Other techniques have been explored to reduce the number of computations; one example is the Branch and Bound technique.

1.5 Solution Algorithms

There are multiple optimization techniques to solve OCP which include linear programming, dynamic programming, nonlinear programming and convex optimization. The following include common methods to solve optimization problems.

1.5.1 Linear Programming (LP)

LP includes different methods to solve optimization problems that contain constraints. Particularly, LP is used to find an optimal solution of a linear cost function (1.1) while satisfying constraints written as linear inequalities. Linear program problems are written in the general format in (1.6) and are considered convex optimization problems [24]:

$$\text{minimize} \quad \mathbf{c}^T \mathbf{x} \tag{1.6a}$$

$$\text{subject to} \quad \mathbf{Gx} \preceq \mathbf{h} \tag{1.6b}$$

$$\mathbf{Ax} = \mathbf{b}, \tag{1.6c}$$

Where $\mathbf{c} \in \mathbb{R}^n$, $\mathbf{G} \in \mathbb{R}^{m \times n}$, $h \in \mathbb{R}^m$ and $\mathbf{A} \in \mathbb{R}^{pxn}$ and $\mathbf{b} \in \mathbb{R}^p$. The geometric interpretation of the constraints is a polyhedron, while the objective function $c^T x$ can be visualized as hyper planes orthogonal to c . We illustrate this visualization with the Farmer's problem example below.

1.5.1.1 Farmer's Problem At the beginning of the planting season, a farmer has 3 tons (3000kg) of potato seeds, 4 tons (4000kg) of carrot seeds and 5tons (5000kg) of fertilizer that is used at a 1:1 ratio with the product (i.e., 1kg of potatoes or carrots need 1kg of fertilizer). Once they become produce, potatoes are sold for \$1.20/kg and carrots are sold for \$1.70/kg. The goal is to maximize the farmer's profit. How much potatoes and carrot seeds should the farmer plant?

This can either be solved through a graphical method by defining the feasibility region which contains all feasible solutions. The optimal solution is then obtained by intersecting the line of constant revenue up as much as possible while maintaining an intersecting point with the feasible region. This point is the optimal solution. To illustrate this method, we start by formulating an OCP in (1.7) with variables x_p and x_c representing the weight of the potatoes and carrots seeds respectively.

$$\text{maximize} \quad 1.2x_p + 1.7x_c \quad (1.7a)$$

$$\text{subject to} \quad x_p \leq 3000 \quad (1.7b)$$

$$x_c \leq 4000 \quad (1.7c)$$

$$x_p + x_c \leq 5000 \quad (1.7d)$$

$$x_p, x_c \geq 0 \quad (1.7e)$$

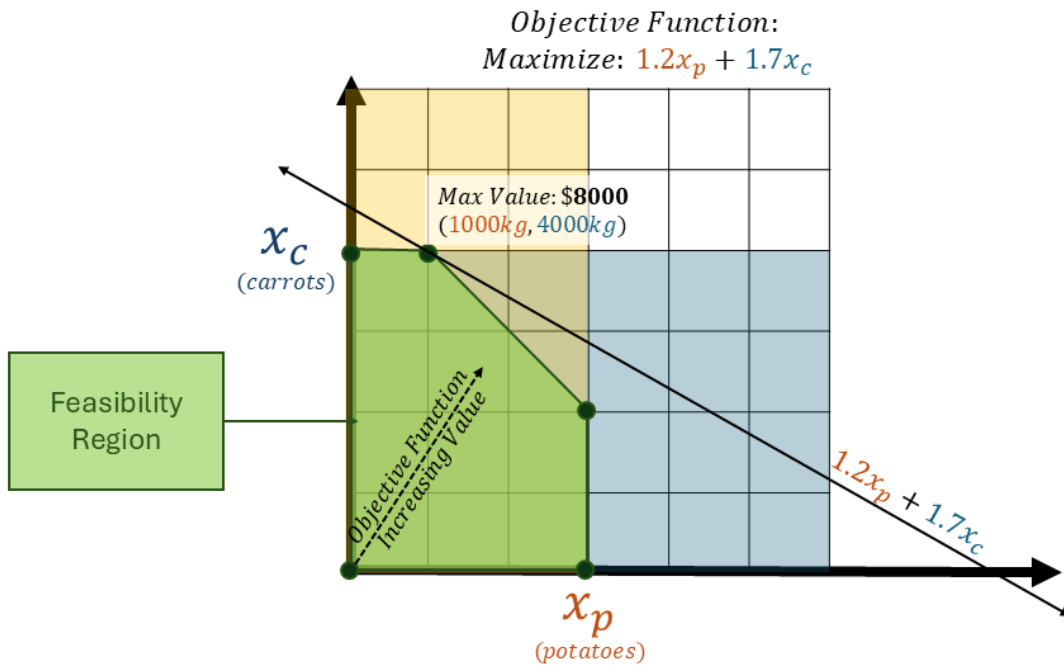


Figure 1.8: Farmer's Problem - Graphical Solution

The graphical method is utilized in Figure 1.8 and shows that the maximum value, or revenue, the farmer can gain is when 1000kg of potato seed and 4000kg of carrot seed is used. The revenue total is \$8000.

A more iterative method for solving LP problems is the Simplex Method. The cost function and constraints are written in normal form and utilize slack variables. A more detailed explanation can be found in [27] if the reader wishes to learn more. Additional methods include Interior Point and Newton-Barrier Methods.

Solving large linear programming problems in real-time can be very challenging. While we highlighted some methods that can be used to solve linear programs, [24] states that solving them is a mature technology and generally can be solved in polynomial-time.

1.5.2 Quadratic Programming (QP)

QP is a type of programming used to optimize quadratic problems. Quadratic problems are convex problems if the objective function is (convex) quadratic and the constraint functions are affine. It is formulated as follows [24]:

$$\text{minimize } f(x) = \frac{1}{2}\mathbf{x}^T \mathbf{P}\mathbf{x} + \mathbf{q}^T \mathbf{x} + \mathbf{r} \quad (1.8a)$$

$$\text{subject to } \mathbf{G}\mathbf{x} \preceq \mathbf{h} \quad (1.8b)$$

$$\mathbf{A}\mathbf{x} = \mathbf{b}, \quad (1.8c)$$

where $\mathbf{P} \in \mathbf{S}_+^n$, $\mathbf{G} \in \mathbb{R}^{m \times n}$, and $\mathbf{A} \in \mathbb{R}^{p \times n}$.

Similar to linear programming, the geometric interpretation of this type of problem is a polyhedron which defines the feasible set, but in the case of convex quadratic programs, the objective function forms ellipsoids which intersect the feasible set as contour lines. Note that linear programming is a special case of quadratic programming, where $\mathbf{P} = 0$.

A QP can be either P -hard (solved in polynomial-time) if P is positive definite, or NP -hard if P is indefinite or has any negative eigenvalues which would render the computational time one that grows exponentially. QPs can be solved using an extension to the Simplex method, interior-point method, and many others that can be found in literature [24].

1.5.3 Multiple Integer Linear Programming (MILP)

MILP optimization problems are non-convex and are NP -hard. They are identified by having a binary component which makes solving them as convex problems difficult as multiple global minima points may exist. MILP optimization problems are

written in the following format [28]:

$$\text{minimize} \quad \mathbf{c}^T \mathbf{x} \quad (1.9a)$$

$$\text{subject to} \quad \mathbf{Gx} \preceq \mathbf{h} \quad (1.9b)$$

$$\mathbf{Ax} = \mathbf{b} \quad (1.9c)$$

$$\mathbf{x}_b \in \{0, 1\}^{n_b}, \quad (1.9d)$$

where $\mathbf{x} = [\mathbf{x}_r^T, \mathbf{x}_b^T]^T$, with $\mathbf{x}_r \in \mathbb{R}^{nr}$, $\mathbf{x}_b \in \{0, 1\}^{n_b}$, and $n = n_r + n_b$.

Using enumeration to solve MILP can guarantee the optimal solution but suffers from high computational burden. In the enumeration technique, all solutions are listed and then evaluated in the objective function which is considered a brute-force method. Many famous optimization problems can be formulated in a way so that they are solved using enumeration. One example is the 1/0 Knapsack Problem [29].

The Knapsack problem states that we are given a set of items, each with a weight and a value. The solver must determine which items to include in the collection so that the total mass is less than or equal to a given mass and the total value of the objects is as large as possible. In this scenario, we assume a bounded Knapsack problem which means that the solver can only use one of each item.

The straight-forward method to solve this problem is to formulate the OCP into an MILP. This is done by assigning each object a variable x_i , in which $x_i \in \{0, 1\}$ and indicates whether an object is placed in the knapsack ($x_i = 1$) or not ($x_i = 0$).

1.5.3.1 Example: 0/1 Knapsack Using Enumeration Find the most profitable items to take from the list of items in Table 1.1 while not exceeding a total weight equal to 7.

Table 1.1: Knapsack Problem

Object Label (x_i)	Weight (wt)	Value (val)
x_1	1	1
x_2	3	4
x_3	4	5
x_4	5	7

This optimization problem can be formulated into the following structure:

$$\text{maximize } f(x) = 1x_1 + 4x_2 + 5x_3 + 7x_4 \quad (1.10a)$$

$$\text{subject to } 1x_1 + 3x_2 + 4x_3 + 5x_4 \leq 7 \quad (1.10b)$$

$$x_1, x_2, x_3, x_4 = 0 \text{ or } 1, \quad (1.10c)$$

where the objective function is a sum of the profit values for each respective object weighted by x_i . Setting $x_i = 1$ represents adding an object to the knapsack, while setting $x_i = 0$ means that the object was not added. The constraint clause limits the total weight of the added objects to less than or equal 7.

In explicit enumeration, we list out all possible solutions, determine whether it is feasible according to the constraint listed, then calculate the cost function. The solution with the maximum cost is selected as optimal. This process is shown in Table 1.2.

Table 1.2 identifies the one combination of objects that will both fit into the knapsack and create the highest value for the owner are x_2 and x_3 . Notice that the number of computations is of exponential time $\mathcal{O}(2^n)$. In this case, for each additional object introduced to the knapsack problem, the run time and storage needs double. Implicit

Table 1.2: 0/1 Knapsack Problem: Enumeration Method

x_1	x_2	x_3	x_4	Total Weight	Total Value
0	0	0	0	0	0
0	0	0	1	5	7
0	0	1	0	4	5
0	0	1	1	9	Infeasible
0	1	0	0	3	4
0	1	0	1	8	Infeasible
0	1	1	0	7	9*
0	1	1	1	12	Infeasible
1	0	0	0	1	1
1	0	0	1	6	8
1	0	1	0	5	6
1	0	1	1	10	Infeasible
1	1	0	0	4	5
1	1	0	1	9	Infeasible
1	1	1	0	8	Infeasible
1	1	1	1	13	Infeasible

enumeration may be used to reduce the number of enumerated sequences or eliminate infeasible ones from entering the algorithm using several techniques, however, these are out of the scope of this thesis.

Mixed-Integer Quadratic Problems (MIQP) face the same challenges as MILP. The main difference is that the objective function is quadratic.

1.5.4 Dynamic Programming (DP)

DP is a method to break down the optimization problem into smaller sub-problems. The solutions to these sub-problems are then reconstructed to solve the original optimization problem. DP is more flexible when compared to LP as it can tackle problems with non-linear relationships.

Back to the Knapsack example, one may utilize a DP method to solve the problem more quickly. A common DP method is tabulation which is shown in Figure 1.9.

1.6 Summary

In this chapter, we introduced power converters, MPC and optimization taxonomy. The intention was to provide the reader with sufficient background to understand our work. While this thesis mainly focuses on the use of the enumeration technique for MILP, we also wanted to foster a deeper understanding of the scope of optimization and its potential use in MPC and power converter control.

0/1 Knapsack Problem – Dynamic Programming – Tabulation/Recursive Method

Profit function: $P[i, m] = \max\{P[i - 1, m_i], P[i - 1, m - m_i] + V_i\}$ where i : rows, m : columns

		Capacity of Bag									
			0	1	2	3	4	5	6	7	
x_i	m_i	V_i	0	$P[0,0]$	$P[0,1]$	$P[0,2]$	$P[0,3]$	$P[0,4]$	$P[0,5]$	$P[0,6]$	$P[0,7]$
x_1	1	1	1	$P[1,0]$	$P[1,1]$	$P[1,2]$	$P[1,3]$	$P[1,4]$	$P[1,5]$	$P[1,6]$	$P[1,7]$
x_2	3	4	2	$P[2,0]$	$P[2,1]$	$P[2,2]$	$P[2,3]$	$P[2,4]$	$P[2,5]$	$P[2,6]$	$P[2,7]$
x_3	4	5	3	$P[3,0]$	$P[3,1]$	$P[3,2]$	$P[3,3]$	$P[3,4]$	$P[3,5]$	$P[3,6]$	$P[3,7]$
x_4	5	7	4	$P[4,0]$	$P[4,1]$	$P[4,2]$	$P[4,3]$	$P[4,4]$	$P[4,5]$	$P[4,6]$	$P[4,7]$

Completed Profit Table (Winning Combination Highlighted in Blue)										
			0	1	2	3	4	5	6	7
x_i	m_i	V_i	0	0	0	0	0	0	0	0
x_1	1	1	1	0	1	1	1	1	1	1
x_2	3	4	2	0	1	1	4	5	5	5
x_3	4	5	3	0	1	1	4	5	6	9
x_4	5	7	4	0	1	1	4	5	7	9

Figure 1.9: Solving 0/1 Knapsack Problem in Dynamic Programming

CHAPTER TWO

LITERATURE REVIEW

Power electronic converters are used to control and supply voltages and currents that are suitable for an end-user's needs. They are found in many applications that touch our lives and have existed for more than four decades [30–32]. Power electronic converters can be categorized into four main categories depending on the form of the electrical power being processed: AC-DC (rectifiers), DC-AC (inverters) DC-DC, and AC-AC (frequency converters) [31]. These converters find applications in all areas including residential, commercial, industrial, transportation, utility systems, aerospace and telecommunications [33].

MPC incorporates the fundamentals of optimal control in its design. It uses a dynamic model of the system to predict future behavior while making the best control decision to optimize system response over a prediction horizon [8]. Figure 2.1 illustrates this concept by showing future trajectories of a system output for a given sequence of future control signals. MPC first appeared in the 1970s and gained popularity as an advanced process control technology in the 1980s where it was prevalently used in chemical plants. It has found a wide range of applications in industry such as mining, material processing and fuel management [34–37].

Modern MPC applications include applications in energy management [6, 7, 11–13], advanced autonomous vehicle driving [38, 39] and power grid stabilization. Table 2.1 provides a summary of previous work highlighting these applications.

The prior examples display the applicability of MPC in large system control in which process dynamics and control take place on the order of milliseconds, seconds, and

Table 2.1: MPC in Mobility and Energy Management Applications

Field	Application	References
Renewable Energy Management	MPC was used to provide maximum power point tracking (MPPT) for a Photovoltaic (PV) System	[6, 7]
Power grid stabilization	MPC used to ensure electric grid stability through controlling machine power following a fault condition	[40]
Building Energy Management	MPC was explored in the control of building HVAC	[41]
Electric Vehicle (EV) energy management	Vehicle speed is controlled using MPC while minimizing battery energy consumption	[13]
EV battery cell balancing	MPC used to actively balance battery cells within EV battery pack	[12]
Autonomous Vehicle (AV) path tracking	MPC and Event-triggered MPC were utilized to control the path of an AV respectively	[42], [38, 39]
Adaptive Cruise Control	An MPC-based adaptive cruise control system is developed to control vehicle distance and speed based on sensor inputs	[43]

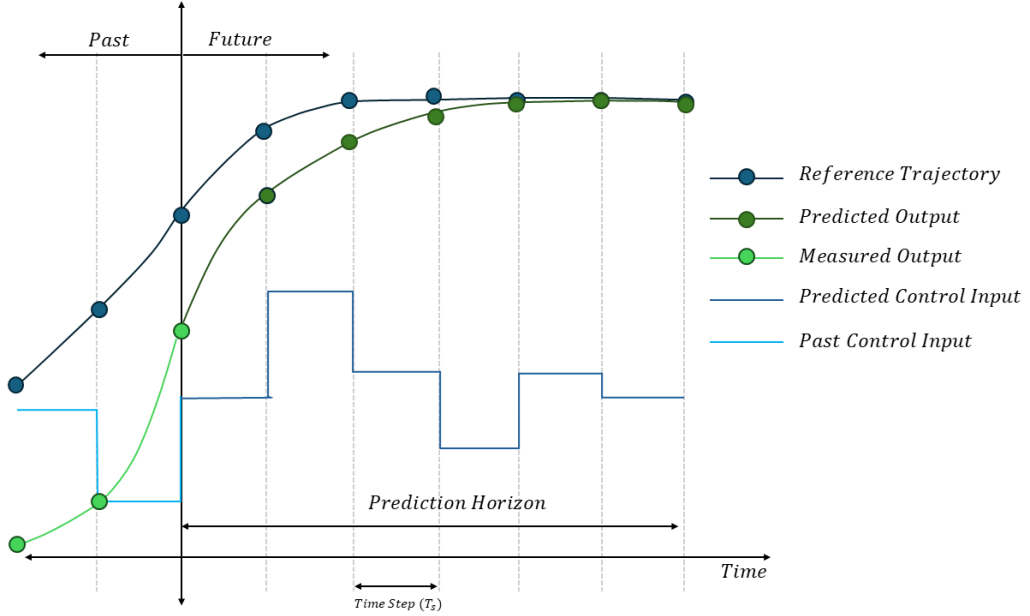


Figure 2.1: Prediction Horizon in MPC

in some cases, minutes. When MPC is applied in the control of power converters, the system must take action at the switch level which is typically within a number of microseconds. For example, high voltage (HV) to low voltage (LV) DC-DC converters found in EV applications typically operate at frequencies in the hundred kilohertz range. Electric vehicle traction inverters typically have single-digit kilohertz switching frequencies and may go up to the 10 – 20 kilohertz range.

MPC is a method that has been gaining popularity in the control of power converters due to the ease of its design and the increased capabilities of microprocessors to deal with system and control dynamics in real-time. The simplicity of implementation arises from the fact that control objectives and protections can be seamlessly integrated into the cost function. Additional advantages include fast dynamics and inherent robustness due to its predictive nature [9, 10, 14–16, 19, 32, 44, 45]. Additionally, with the increased capability of modern microprocessors, it is feasible to implement a switched

model that represents the converter's operation in all modes. This leads to a more accurate model which in turn enables more precise control [32].

2.1 Power Converter System Requirements, Objectives and Constraints

When designing an MPC strategy for power converters, several factors must be considered to develop system objectives and constraints. Included below are common converter requirements, challenges and control objectives for power converters along with some examples of prior work conducted to address them [1, 3, 46].

- Voltage regulation — this is the ability of the converter to maintain a consistent output voltage within a specific range. A vast majority of converter applications state their main objective as the ability to closely track an output voltage reference within an $\pm x\%$ of the command or reference voltage. In MPC, the deviation of the output voltage to the output reference voltage is included in the objective function and is weighted to increase its influence against other requirements within the objective function.
- Load regulation — is the ability of the converter to follow a reference voltage across different steady-state load currents and impedance. It is common for power converters to experience a drop in output voltage as loads increase due to internal voltage drops on parasitic resistances of wires and switches in addition to forward voltage drops of diodes. Collectively, the drop in voltage across load current is referred to as the closed-loop output impedance of the converter.
- Voltage regulation during transient loads — describes the ability of the converter to follow the reference voltage while providing fast dynamics with quick changes to the load impedance or current. The converter control loop must be able to respond

quick enough to maintain the output voltage within a specified range without losing stability.

- Line regulation — is the ability of the system to maintain a regulated output voltage despite changes on the input source.
- Current limiting — another state constraint that is applied to protect semiconductor switches from overheating and inductors from saturating is current limiting. Current limiting can be implemented through constant current limiting which sets the current limit to a single value. This value is selected based on the specifications of the parts that require protection. Other methods include current fold-back and hiccup mode.
- Current regulation and control — in many applications, such as low harmonic rectifiers (also known as power factor correction (PFC) converters) the task of the converter is to track a reference current waveform [2]. PFC is explained in a later section.
- Soft-Start — during converter startup, it is necessary to limit the inrush of current. One common scenario in which inrush occurs in many converters is due to the output filter capacitance. For example, a boost converter has an unimpeded connection between the input to the output capacitance so there is no way to stop the inrush of current into the output capacitor without including additional circuitry or implementing special measures within the control circuitry. Soft startup using an MPC-based controller was implemented in [47] to reduce the inrush of current in a Dual Active Bridge (DAB) converter.
- High efficiency — while power converters may outperform their linear voltage regulator counterparts, there is still a need to improve efficiency as demands for more energy consumption along with an increase in government regulations are

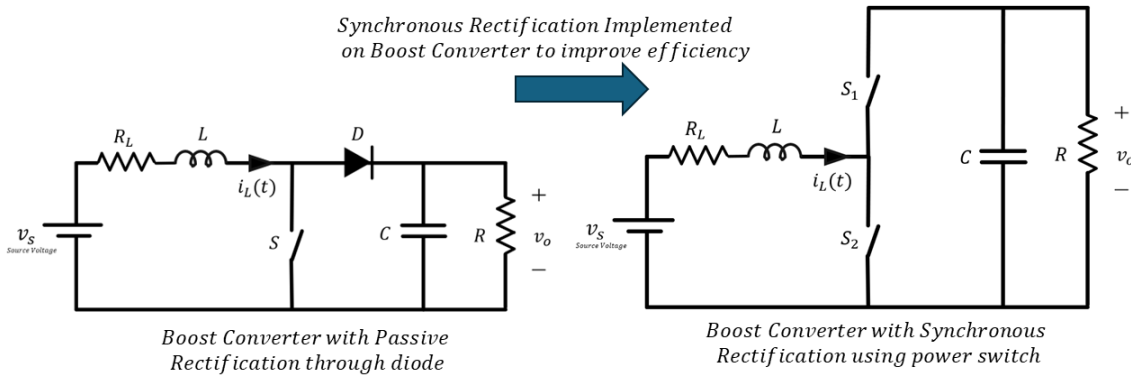


Figure 2.2: Boost Converter with Synchronous Rectifiers to Improve Efficiency

emphasizing the need to do so. There are many sources of power loss in power converters which include [46]:

1. Conductive losses — in DC-to-DC converters, these are $I_{rms}^2 R$ losses that are generated due to wires and PCB traces, windings in magnetics, and the drain-to-source resistance of the power MOSFETs. In diodes, the power loss is due to the forward voltage drop multiplied by the conducting current, I_{fwd} ($P_{diode-loss} = V_d \times I_{fwd}$). These types of losses are typically reduced through design optimization such as selecting design parameters which lower the rms currents within components, and selecting devices with low parasitic resistances or forward voltage drop. One example is by replacing diodes with synchronous rectifiers as shown in Figure 2.2.
2. Switching losses — these occur as the power switches are turned *ON* and *OFF*. In a power MOSFET, there are three main mechanisms which contribute to these losses.

- Switching loss due to the charging of the gate capacitance during switching

$$P_{gate} = V_{DRV} \times Q_G \times f_{sw} \quad (2.1)$$

where V_{DRV} is the voltage applied to the gate circuit, Q_G is the total gate charge required for switching and f_{sw} is the switching frequency.

- Switching loss due to the capacitance between the drain and source which charges and discharges as the switch blocks voltage or turns *ON*.

$$P_{DS} = \frac{1}{2} C_{DS} \times V_{DS}^2 \times f_{sw} \quad (2.2)$$

where C_{DS} is the total capacitance at the drain of the MOSFET, V_{DS} is the blocking voltage across the drain to source.

- Switching loss due to the overlap between the voltage and current waveforms as the main power switched is switched *ON* and *OFF*.

$$P_{overlap} = \frac{1}{2} V_{DS} \times I_{ON} \times t_T \times f_{sw} \quad (2.3)$$

where I_{ON} is change in current during the transition t_T is the transition time.

All three terms above are frequency dependent and can be reduced through penalizing switching in the objective function of the MPC controller. The last term specifically, can be reduced through additional means such as selecting a topology which enables soft-switching, i.e., zero-voltage-switching (ZVS) and/or zero-current-switching (ZCS). These methods can reduce the overlap of the voltage and current. Implementation of soft-switching using Explicit MPC was investigated in [48] showing that soft-switching can be maintained during transient conditions due to the favorable response time of the MPC controller.

- Reduction of common-mode voltage [3] — in some applications, such as voltage source PWM inverters applied to variable-speed drive applications, high frequency common-mode voltages may induce leakage currents through parasitic capacitive coupling between the motor's neutral and ground. This can impact electromagnetic compatibility performance. Common-mode voltages may also generate shaft voltages across motor bearings which can cause electric discharges that are destructive to the bearings [49]. In [50], Finite Control Set MPC (FCS) was introduced as an alternative to common-mode voltage PWM mitigating techniques. The method proposed indicated promising results.

- Fault management — a power converter must implement protections against system faults and ideally return to its original function once the fault is removed. One example is protection against faults such as shoot-through events which is a scenario in which failure event when two adjacent switches such as the ones in Figure 2.3 are on simultaneously thus short-circuiting the supply voltage. Additional fault conditions include over-voltage conditions, reversed polarity conditions, over current and under-voltage conditions.

2.1.1 Requirements Driven by Regulations

- Power Factor (PF): This is of particular interest in AC line powered supplies. PF is the ratio of the average power measured to the apparent power at the terminals of device. The factor comprehends both the phase shift between voltage and current due to capacitive and/or inductive loading. It also comprehends the distortion in the current drawn by the load [1]. Active Power Factor Correction (PFC) is typically implemented with a boost converter pre-regulator. Through special controls, the boost pre-regulator improves the current wave shape so that it follows the line voltage. This allows the converter to appear as a resistive load to the AC grid (i.e.,

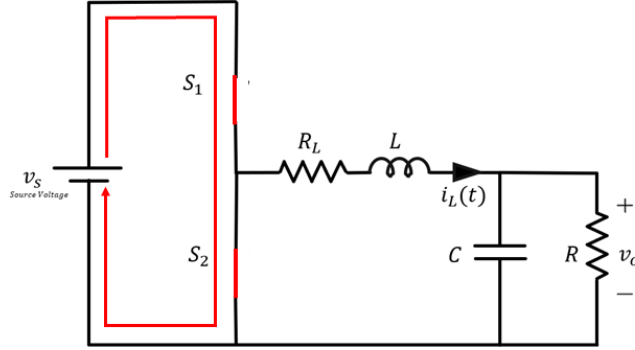


Figure 2.3: Shoot-through condition in synchronous rectifier buck converter

input resistor emulation [2]), reduce peak currents which strain grid-related and converter components and reduce noise interference as it works to reduce distortion harmonics.

- Total Harmonic Distortion (THD) — is the measure of the distortion in a current signal caused by the undesirable frequency components [1] and is defined in 2.4. THD and PFC are closely related as defined in 2.5.

$$THD = \sqrt{\frac{\sum_{n>1} I_n^2}{I_1}} \quad (2.4)$$

$$PF = \sqrt{\frac{1}{1 + THD^2}} \quad (2.5)$$

Regulations were enacted to require high power factor for grid connected converters such as the IEC 61000-3-2 international standard, which places limits for current harmonics rms values at each harmonic above the 230V(AC) fundamental up to the

39^{th} harmonic. In the United States, Energy Star EPS 2.0 required a power factor of at least 0.9 at rated load when tested at $115V(AC), 60Hz$ for power supplies up to $250W$ [46] MPC was investigated as a method for Active PFC and reduction of THD in [51] and [52].

- Electromagnetic Compatibility (EMC) — high-frequency harmonics causing electromagnetic interference (EMI) are inevitable due to the switching nature of power converters [53]. These harmonics are generated due to the fast changing voltage and current waveforms. While most EMI is combated through good design practices such as sufficient filtering, shielding and proper PCB layout - there are methods to reduce EMI through control. These methods include [46]:
 1. Limiting the switching frequency — in an MPC implementation, this can be achieved by penalizing the switching, i.e., actuation of the switch devices.
 2. Limiting rise time of the gate signals applied to the switches — i.e. reducing rate of voltage change (dv/dt). High (dv/dt) can also cause insulation and semiconductor device issues.
 3. Spread-Spectrum Frequency Dithering (SSFD) — which is modulating the switching frequency of the power supply to spread out the energy of each harmonic across the frequency spectrum

In [54], MPC was implemented to reduce dv/dt for a multi-level converter to improve efficiency and the reliability. Additional advantages were realized such as improvement in EMC performance.

2.2 MPC Design Elements

MPC used in the control of power converters can be generally categorized as direct MPC or indirect MPC [16]. Direct MPC is when the output of the controller directly

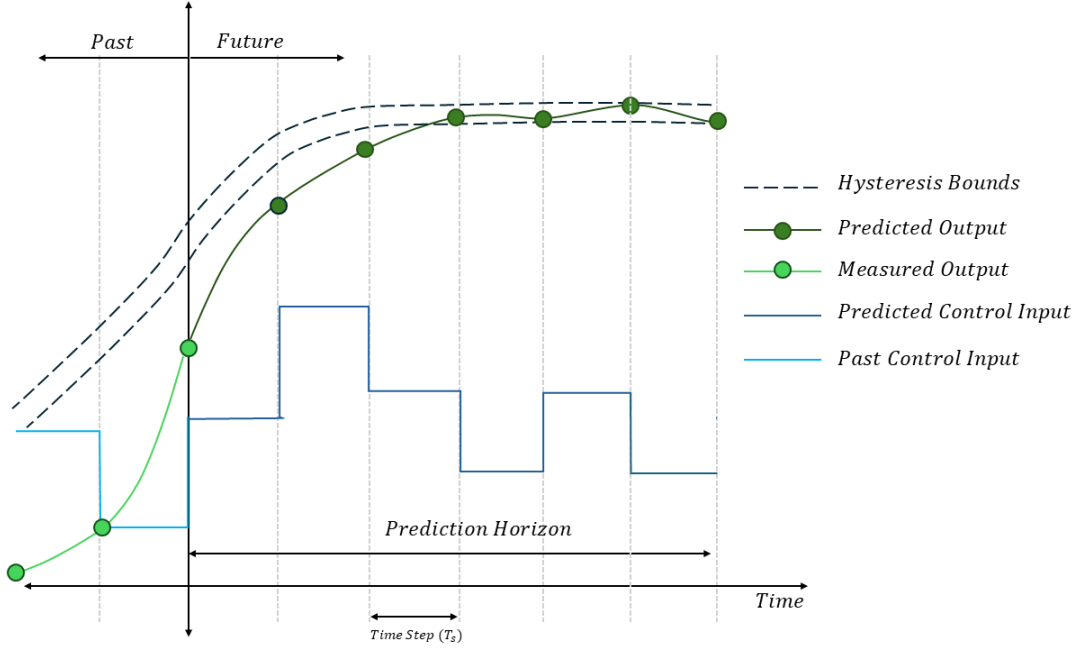


Figure 2.4: Direct MPC with Hysteresis Bounds

actuates the switch and it has been implemented in [55–57]. Indirect control MPC implements a modulator which receives an optimal duty cycle from the controller and has been implemented in [14, 19, 58–60].

There are multiple categories under Direct MPC that have been reported in literature which include controllers with reference tracking, hysteresis bounds and an implicit modulator [9]. Direct MPC with hysteresis bounds aims to maintain the state variable within desired bounds and not to a set trajectory or reference voltage as shown in Figure 2.1. Control actions are optimized over a defined prediction horizon while considering constraints and control objectives. Figure 2.4 illustrates this concept. Direct MPC with hysteresis bounds has been implemented in [61] for direct power control of a three-phase-grid-connected NPC converter while minimizing switching frequency.

Direct MPC with implicit modulator manipulates both switching signals and the time at which they are applied (i.e., emulating PWM behavior) to gain more controllability of the switching and improve its performance to minimize harmonic distortion. A more detailed explanation of the sub-groups for this method can be found in [9]. Direct MPC with reference tracking is also known as Finite Control Set (FCS) since it utilizes a finite number of possible switch positions to define the switching sequences [44, 62–64]. FCS-MPC is widely found in literature and favored due to its intuitive design method. One major drawback of FCS-MPC is its extensive need for computational resources. This stems from the fact that FCS-MPC problems are formulated as MILP or MIQP which are NP-hard. This is especially an issue for converters with non-minimum phase behavior such as boost and buck-boost converters [56]. Non-minimum phase behavior in a boost converter translates to an initial delay in the response of the converter when the main switch is set to the *ON* position. This results in a slight dip in the output voltage, which then adjusts after several switching cycles. Figure 2.5 illustrates this behavior in a PWM controlled Boost converter. In an enumeration based MPC control scheme, this response requires an extension of the switching sequence prediction horizon NT_s .

2.2.1 Cost Function Selection

The cost function, or the objective function, in 1.1 is a weighted sum of deviations in the system output and control signal increments. There may also be linear terms for minimization or maximization of certain variables. There are two main parameters that are to be considered in the design of the cost function: the choice of ℓ -norm and control effort penalization. The definition of ℓ_p -norm:

$$\|\mathbf{x}\|_p = (|x_1|^p + |x_2|^p + \dots + |x_n|^p)^{1/p} \quad (2.6)$$

A fundamental difficulty associated with boost converters happens when the output voltage is being controlled without an intermediate current loop. To increase the output voltage, the switch needs to be closed, but initially the output voltage drops

The impact of actuating the main switch is delayed at the output so a longer prediction horizon length is required to predict future converter response

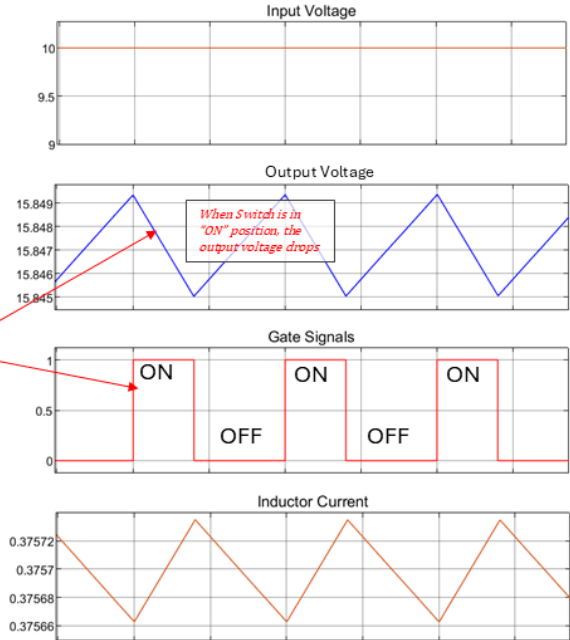


Figure 2.5: Non-minimum phase behavior of Boost Converter - PWM controlled example

where $p \geq 1$ and \mathbf{x} is a vector, $x \in \mathbb{R}^n$. It was reported in [9] that the use of ℓ_1 -norm is a reasonable choice for FCS Direct MPC due to the excessive computational power needed as the prediction horizon grows. ℓ_2 -norm has been found more prevalent in Indirect MPC.

The selection of output variables that are included in the objective function is application dependent. In the case of the DC-DC converters covered in this thesis, the output variable of interest is the output voltage v_o . Additional controlled parameters, such as the inductor current i_L may be included in the objective function.

In the case of Direct-MPC, penalizing the control effort directly impacts the switching frequency, in which increasing the penalty of the control input increment leads to a lower switching frequency. Additionally, according to the findings in [9], the full

potential of MPC is not realized without penalizing the control effort as it leads to poorer system performance.

2.2.2 Weighting Factors

Weighting factors is one of the tuning parameters that impacts the performance of the MPC controller; along with the prediction horizon length and sampling time. The selection of these factors is primarily dependent on heuristics. The authors of [44] develop a more methodical method to design the weighting factors in cost functions of FCS-MPC.

2.2.3 Robustness and Effect of Model Mismatch

It is inevitable for a system to be subjected to disturbances, variations in component values due to tolerances, temperature and other conditions. Operating conditions also vary where the converter and controller need to behave robustly. As mentioned in Chapter 1, MPC relies heavily on an accurate model of the system and many of these disturbances will cause model mismatch. State estimators are implemented to measure the state variables in addition to disturbance observers to measure the disturbances caused by the mismatch. These measurements are fed back to the MPC controller and compensated for in the control. Kalman filters have been widely used in the applications that were studied [4, 19, 60, 65] and has been cited as an effective state estimator for high model uncertainty.

Table 2.2 summarizes previous papers that were reviewed for this work. The intent is to identify the broad application of MPC in power converter control, to understand how MPC was implemented for each application, and to provide a general description of the design parameters for each paper.

Table 2.2: A Literature Review of the Implementation of MPC in Power Converter Control

Converter Topology	MPC Classification	Output Variables	Objective Function (J)	Robustness	Reference
DC-DC Synchronous Buck	Indirect (Modulator) Explicit (Lookup table)	$[i_L, v_o]$	$J = \ Q\epsilon(k+\ell k)\ _1$ $\epsilon = [v_{o,err}, \Delta d]^T$, constraints on i_L	Kalman Filter disturbance observer	[59, 66]
DC-DC Synchronous Boost	Indirect Explicit MPC	$[\hat{i}_L, v_o]$	$J = \ \hat{[v_{o,err}]}\ _1$, constraints on i_L	Extended Kalman Filter	[19]
DC-DC Boost Converter	Direct FCS-MPC	$[\hat{i}_L, v_o]$	$J_p = v_{o,err} + \lambda \Delta u $ J_c penalizes prediction horizon	Kalman Filter	[62]
Full Bridge Buck-Boost DC-DC Converter	Implicit MPC	$[v_o]$	$J = x^T Qx + u^T u, x = [i_L, v_o]^T$ i_L, β, u constraints	Sequential Quadratic Programming good for dynamics	[15]
DC-DC Boost Converter	Direct FCS-MPC	$[\hat{i}_L, v_o]$	$J = v_{o,err} + \lambda \Delta u $	Kalman Filter	[32]
SiC Three-Phase Grid-tied Inverter	SVM MPC (Indirect)	$[i_{inv}, v_{grid}]$	$J = i_{inv,err}, n = a, b, c$ constraints on i_{inv}	Variiable frequency led to harmonics	[67]
Three-Phase Five-Level Nested Neutral Point Piloted Converter	Direct FCS-MPC	$[i_o, v_{cl}, v_{c2}]$	$J = \ i_{o,err} + K_1 v_{cl,err} + K_2 v_{c2,err}\ _1$	Not implemented	[63]
Three-Phase Two-Level Inverter	Indirect SVM	$[v_c, i_t, i_o]$	$J = \lambda_{i_c}^2 v_{c,err}^2 + \lambda_{i_t}^2 i_{t,err}^2 + \lambda_{i_o}^2 i_{o,err}^2$	Grid voltage estimation for robustness	[64]
Modular Multilevel DC Transformer	Direct MPC	$[i_{cm}, v_c]$	$J = \lambda_1 g_1 + \lambda_2 g_2$ g_1 suppresses circulating current g_2 : capacitor voltage balance	PI Controller	[68]
Naturally Clamped Current-fed Half-Bridge Isolated Boost DC-DC	Indirect MPC	$[i_{L_1}, i_{L_2}, v_o]$	$J = q_i(i_{L,err})^2 + q_d(d_{err})^2$	Extended Kalman Observer	[69]
Interleaved DC-DC Boost Converters with Coupled Inductors	Direct MPC	$[[i_{L1}, i_{L2}], v_o]$	$J = v_{a,err}^2 + \lambda_{i,branch,err}^2$ $+ \lambda_{b,branch,err}^2$	Extending Prediction Horizon for improved response	[70]
Multi-level Cascaded H-Bridge Inverter	GAVV online & offline MPC	$[i, v_o]$	$J = i_{err} $	Not robust under certain operating conditions	[71]

Continuation of Table 2.2 — A Literature Review of the Implementation of MPC in Power Converter Control

Converter Topology	MPC Classification	Output Variables	Objective Function (J)	Robustness	Reference
Five-level Active Neutral Point Clamped Voltage Source Inverter	Direct MPC	$[i_n, v_n, v_{ph}]$	$J = \lambda_m v_{n,err} + \lambda_{ph} v_{ph,err} + \Delta u $ voltage constraints		[72]
Multi-Modular Grid-tied Inverter	Indirect Implicit MPC with Laguerre's Function	$[i_d, i_q, v_d, v_q]$	$J = x^T Q x + \eta^T R \eta$, with constraints	Proven through sensitivity analysis	[73]
Buck-Boost DC-DC Converter	Indirect Explicit MPC	$[i_L, v_o]$	Quadratic Program	Adaptive Model Linear Parameter Varying	[74]
Step-down DC-DC Converter	Indirect MPC	$[i_L, v_o]$	$J = v_{o,err} + q \Delta d $	Integrator added for robustness	[75]
Single-Inductor Multiple-Output Buck Converter	Direct MPC with enumeration	$[i_L, v_o]$	$J = v_{o,err}^2 + \lambda \Delta S$	Robust to load and reference variations	[76]
Step-down DC-DC Converter	Enumeration-based MPC with combinatorial approach	$[i_L, v_o]$	$J = v_{o,err} + q \Delta d $	Resistive load predicted and compensated	[77]
Buck Converter	Direct MPC with enumeration	$[i_L, v_o]$	$J = v_{o,err} + \lambda \Delta u $	Kalman Filter	[78]
Three-Phase Inverter with LC output filter	Direct MPC	$[i_o, v_c]$	$J = v_{c,err} $, control input not penalized due to ET-MPC	Event-trigger performance similar to conventional formulation	[79]
Modular Multilevel Converter	Event-triggered ESO-Based Robust Direct MPC	$[P, Q]$	$J = v_{g,err} + \lambda_{a_i} \theta_P + \lambda_{b_i} \theta_Q $	Extended State Observer	[80]
Interleaved Boost Converter	Indirect MPC	$[i_L, i_{L2}]$	$J = (i_{L1,err})^2 + (i_{L2,err})^2$	Extended State Observer	[81]
Voltage Source Inverter (VSI)	Direct MPC FCS	$[i_p, v_o]$	$J = i_{\alpha,err} + i_{\beta,err} $ additional cost functions were evaluated	Not fully explored in this work	[55]
Boost Converter	Direct MPC	$[i_L, v_o]$	$J = (v_{o,err})^2$ for VMC $J = (i_{L,err})^2$ for CMC	Integral parameter to address load variations	[56]
Grid-side Converter	Direct MPC	$[i_{dq}, v_c]$	$J_1 = \dot{i}_{dq,k} - i_{dq,k} _2 + \lambda_1 i_{dq} _2$ $J_2 = J_1 + \lambda_{VP} \Delta U_{c,k}^2$	Kalman Filter	[82]

Continuation of Table 2.2 — A Literature Review of the Implementation of MPC in Power Converter Control

Converter Topology	MPC Classification	Output Variables	Objective Function (J)	Robustness	Reference
Interleaved DC-DC Boost Converter	Indirect Current Control	$[\dot{i}_{L1}, \dot{i}_{L2}, v_o]$	$J = (\dot{i}_{L1,err})^2 + \lambda (\dot{i}_{L2,err})^2$	Kalman Compensation	[83]
Full-bridge Neutral-point Clamped Inverter	Indirect SVM MPC	$[\dot{i}_{filter}, v_o]$	$J = v_{o,err} $	Luenberger Disturbance Observer	[84]
Multi-level Flying Capacitors Inverter	Adaptive Observer Indirect SVM MPC	$[v_{c1}, v_{c2}, i_o]$	$J = \ v_{c1,err}\ _2 + \ v_{c2,err}\ _2$ $\ k_{o,err}\ _2$, normalized	Kalman Filter Disturbance Observer	[85]
Three-phase AC-DC Converter	Indirect MPC DPC (SVM)	$[P, Q]$	$J = p_{pw}(P_{err})^2 + q_{wf}(q_{err})^2$	Improved cost function to address interference and improve dynamic performance	[86]
Active Front End Rectifier	Finite-Set MPC (SVM)	$[v_{DC}, P, Q]$	$J = P_{err} + Q_{err} $	Achieved through controlling input currents	[52]
Three-Phase Voltage Source Inverters	Indirect SVM	$[\dot{i}_{phase}]$	$J = i_{\alpha,err}^2 + i_{\beta,err}^2$ no non-zero vectors	Use of two non-zero vectors within single sampling period to optimize CM voltage	[87]
Dual Active Bridge DC-DC Converter	Explicit (Lookup Table) Indirect	$[i_{Ln}, v_{Cn}]$	$J = v_{o,err}^2$	Robustness achieved through additional optimization algorithm	[88]
Bidirectional DC-DC Buck and Boost-Ultra-capacitor ESS	TS-Fuzzy Model Indirect MPC	$[\dot{i}_L, v_o]$	$J = \ \mathcal{Q}\epsilon(k+i k)\ _2, \epsilon = [v_{c,err}, \Delta d]^T,$ constraints on d and \dot{i}_L	Kalman Filter	[89]
Step-up Phase-shifted Full-Bridge DC-DC Converter	Indirect MPC (Modulator)	$[i_o, v_o]$	$J = \dot{i}_{o,err} $	Robust Current Control	[90]
Step-up Phase-shifted Full-Bridge DC-DC Converter	Indirect MPC	$[\dot{i}_L, v_o]$	$J = x^T \mathcal{Q}x + \eta^T R\eta$, Laguerre functions constraints on control bounds	Offset-free tracking through system augmentation	[91]
Non-Isolated AC-AC Zeta Converter	FCS MPC Current Control (Direct)	$[\dot{i}_{L1}, \dot{i}_{L2}, v_o]$	$J = (\dot{i}_{L1,err})^2$ or $J = (\dot{i}_{L2,err})^2$	Prediction two samples ahead	[92]
AC-AC Converter with Input and Output LC Filter	FCS Model (Direct)	$[v_i, \hat{i}_{Lo}, v_o]$	$J = W_1 i_{in,err}^2 + W_2 v_{Lo,err}^2 + W_3 v_{o,err}^2$	Full-State Observer and added i_{in}, v_i to improve control	[93]

Continuation of Table 2.2 — A Literature Review of the Implementation of MPC in Power Converter Control

Converter Topology	MPC Classification	Output Variables	Objective Function (J)	Robustness	Reference
Inverter with Output LC Filter for UPS	Indirect SVM MPC	$[i_f, v_c, i_o]$ with observer	$J = v_{\alpha,err}^2 + c\beta_{err}^2$	Use of observer enhances control against noise	[94]
Active Front-End Rectifier	Indirect SVM for Direct Power Control	$[P, Q]$	$J = Q_{in,err} + P_{in,err} $	Robust to errors in inductance values through control delay	[95]
Flying Capacitor Converter	Indirect SVM MPC	$[i_L, v_1, v_2]$	$J = e'[l] _p^2 + \lambda_2 \Delta u ^2$ where: $e' = [v_{1,err}, v_{2,err}, W_f i_L]^T$	Balancing of capacitors provides good transient response	[96]

2.3 Event-triggered Control

Previous work has been done to reduce the computational burden of an enumeration based FCS-MPC, including adaptive prediction horizon [62], limiting switching sequences to eliminate unlikely switching scenarios or reduce switching frequency [9, 16], and move blocking schemes [72]. Another approach is dynamic quantized resolution for PWM DC-DC converters as proposed in [77].

Implementing an event-triggered MPC (ET-MPC) method saves on computational resources [97–99] and has been implemented in different applications and referenced in [38, 39, 100–103] and on a boost converter in [104, 105]. The results show significant computational savings with comparable performance to the time-triggered formulation. In [79], event-trigger control applied to a FCS MPC is used to regulate the voltage of a three-phase inverter. When the voltage is within the set criteria, the control action is held, but if the criteria is not met, the FS-MPC algorithm is run and a new action is calculated and applied. Since the use of event-trigger reduced the control signal (switching) variation, it allowed the removal of the switching penalty from the cost function.

ET-MPC is utilized to control a buck converter in [106, 107]. The work in [106] developed a method to design the event trigger condition and removed the switching criteria from the cost function. The results show a reduction in overall computational burden and switching losses. A similar technique was also implemented in [108] to control a current-source-mode single-inductor multiple-output (CSM-SIMO) buck converter to minimize cross-regulation across the different outputs and reduce the overall computational burden of FCS-MPC. In [109], ET-MPC is applied to the power control loop of a three-phase two-level grid-connected power converter to control active and reactive power. The work in [80] furthers the ET-MPC mechanism by applying an extended state observer to address math model uncertainties for a modular multilevel converter.

Compared to these literature, the contribution of our work is the introduction of the event-triggered mechanism to a time-triggered enumeration based MPC in which the actuation signals are selected from the optimal switching sequence. An event is triggered when the measured (or estimated) output voltage deviates beyond the value in the optimal state trajectory based on the set trigger-threshold. Once an event is triggered, the MPC controller will run and generate a new optimal switch sequence and state trajectory. The actuation signals are initially predicted across the prediction horizon using a move blocking scheme. The optimal control sequence and state signals are cycled through the controller and reused. What distinguishes our work from previous work is the use of the actuation signals and assessing how much the measured output deviates from the projected state variable, while previous work [80, 106–109] only upholds the last actuation value until the output voltage deviates from the reference voltage beyond a trigger-threshold. A more detailed explanation of our method is presented in a later section along with an evaluation of the impact of the trigger-threshold on the converter’s performance. This work furthers our results which were originally reported in [104, 105] by adding a Kalman Filter-based state and disturbance estimator. We also provide further enhancements to the controller by utilizing the inductor current measurement for current limiting.

2.4 Contributions of this Thesis

The goals of this thesis are:

- Define an event-triggered MPC framework for a DC-DC boost converter to reduce the control effort of a time-triggered enumerated MPC. Additionally, the purpose is to achieve an overall reduction of the number of times the computational effort is conducted over a specific period of time while maintaining comparable performance to a time-triggered MPC formulation. This objective was covered in the following papers:

- R. Badawi and J. Chen, "Enhancing Enumeration-Based Model Predictive Control for DC-DC Boost Converter with Event-Triggered Control," 2022 European Control Conference (ECC), London, United Kingdom, 2022, pp. 723-728, doi: 10.23919/ECC55457.2022.9838010.
- R. Badawi and J. Chen, "Performance Evaluation of Event-Triggered Model Predictive Control for Boost Converter," 2022 IEEE Vehicle Power and Propulsion Conference (VPPC), Merced, CA, USA, 2022, pp. 1-6, doi: 10.1109/VPPC55846.2022.10003282.
- Prove the robustness of our ET-MPC framework with a Kalman-filter based disturbance observer implementation, which was covered in the following journal paper:
 - Badawi, R., & Chen, J. (2024). Event-triggered boost converter model predictive control with Kalman filter. *Systems Science & Control Engineering*, 12(1). <https://doi.org/10.1080/21642583.2024.2438866>
- Develop a similar framework for a DC-DC buck converter and evaluate its performance to common power converter metrics which is covered in Chapter 6.

In the next chapters, the contribution of this thesis will be highlighted and expanded upon. Chapter 3 starts out with the implementation of time-triggered MPC on a boost converter and from there, a framework for an enumeration-based event-triggered MPC is developed. Chapter 4 applies ET-MPC with full state feedback and evaluates the impact of the event-trigger threshold on the performance of the converter. Chapter 5 improves the robustness of the converter by implementing a Kalman-based disturbance observer to address model mismatch during load transients. In Chapter 6, ET-MPC is applied to a buck converter. It was found that additional modifications to the event-trigger threshold

had to be made in order to apply our method. Chapter 7 concludes this thesis with main takeaways from the work and proposes future development.

CHAPTER THREE
EVENT-TRIGGERED ENUMERATION-BASED MPC

A boost converter is capable of generating a DC output voltage that is higher than its input voltage. Boost converters are found in many applications including LED drivers, fuel cell applications, photovoltaic systems, and many more in consumer electronics and communication applications. They are also commonly found in pre-regulator stages such as the PFC stage of an onboard EV charger.

The topology of a dc-dc boost converter is shown in Figure 3.1. A key feature of a boost converter is that it transmits power in a two-step process where the inductor acts as a temporary storage element [46] as detailed in the following.

The operation starts with closing switch S , the input current, $i_L(t)$ flows into the inductor L from the input voltage source v_s and energy is stored in the inductor's increasing magnetic field. Note that only L is modeled with a parasitic resistance R_L which mostly represents its winding resistance. All other components are considered ideal. Diode D in this state is reverse biased, so energy from the input is not transferred to the output. In this scenario, the output capacitor C holds up the output voltage v_o and

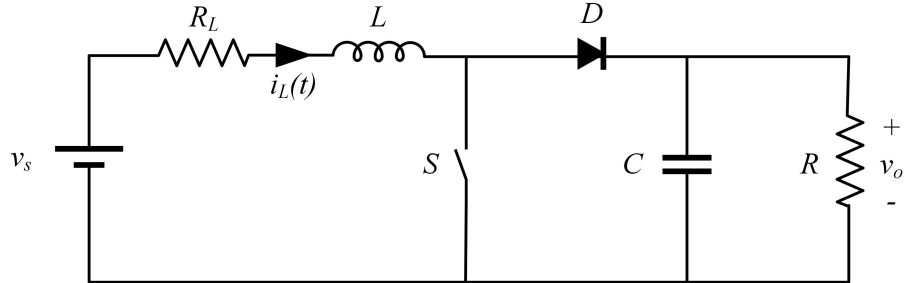


Figure 3.1: Boost converter circuit diagram

supports the load. Keeping S closed, i.e., in the *ON* position, will allow the current to increase indefinitely according to the inductor characteristics that are derived from Faraday's law of induction. This is why every *ON* cycle in which current increases through the inductor winding needs to be countered with an *OFF* cycle in which the inductor magnetic field falls.

During the *OFF* cycle, the polarity of the voltage across the inductor reverses which causes the diode to forward bias and allows current to flow from the input source to the output load.

3.1 Time-triggered enumeration-based MPC for boost converter

We start with an explanation of a time-triggered enumeration-based MPC implementation for a boost converter. Figure 3.2 gives an overview of the MPC control process. MPC starts with a math model of the converter. The model receives a set of switching sequences that span across the selected prediction horizon. The prediction horizon duration is equal to the number of switching states N multiplied by the time step T_s . The model solves the OCP using the switching sequences along with the inductor current and output voltage measurements it receives to decide which sequence achieves voltage regulation while meeting other system objectives. Voltage regulation is defined as the deviation of the output voltage from the *Reference Voltage*, $v_{o,ref}$. From the aforementioned, the main components of the MPC control are identified:

1. Discrete-time Mathematical Model
2. Cost function and OCP
3. Prediction Horizon

The following sections describe these components in better detail.

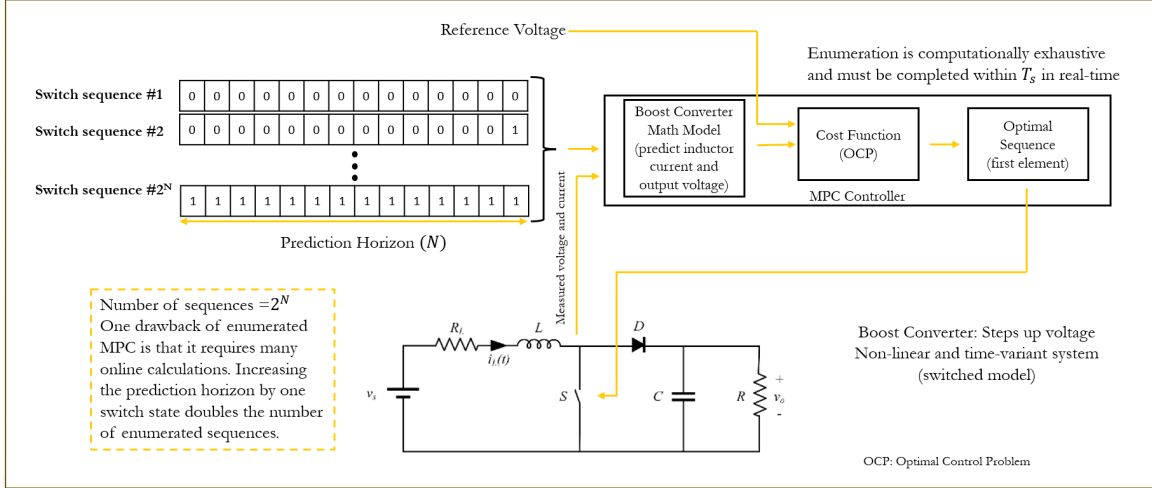


Figure 3.2: Enumeration-based Model Predictive Control for Boost Converter

3.1.1 Boost Converter Mathematical Model

This section introduces the development of the dynamical model that will be utilized in the MPC controller. The derivation is based on a switched state-space model adopted from the work in [32]. We begin our derivation in continuous time domain and then convert the model into discrete-time domain for implementation in the controller.

3.1.1.1 Continuous-time Model Three different operating modes can be defined for the boost converter in Figure 3.1 depending on the position of switch S and the inductor current i_L during a single time step, T_s . Prior to developing the model, there are three current conduction operating modes that shall be comprehended in our model which are displayed in Figure 3.3 and described below:

- The Continuous Conduction Mode (CCM) describes the operation of the converter in which the inductor current is continuous and does not reach zero. This is the case when the average inductor current is relatively high in comparison to the inductor current ripple.

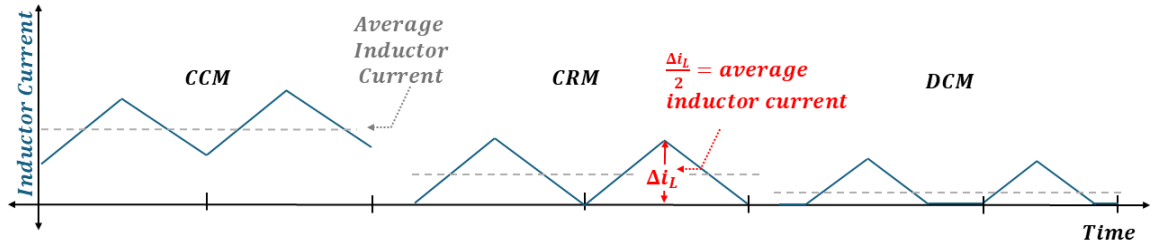


Figure 3.3: Current conduction modes: CCM, CRM, DCM

- The Discontinuous Conduction Mode (DCM) presents itself at light loads when the inductor current ripple is larger than the average inductor current and the converter contains unidirectional-current devices such as diodes that do not permit negative current to flow. The inductor current reaches zero prior to the end of the switch cycle. A switch cycle is defined by the start of two consecutive *ON* – state of switch S .
- The Critical Conduction Mode (CRM) is a special scenario when the inductor current reaches zero at the end of the switch cycle.

We can now begin to develop the state-space representation of the system by developing a state-space model for each switch configuration and inductor current. The state machine in Figure 3.4 shows the conditions for the transitions between the three operating modes. Variable u represents the switch position where $u = 1$ indicates that the switch S is *ON*, while $u = 0$ indicates that the switch S is *OFF*.

The first mode (Mode 1) happens when $u = 1$ and inductor current is positive and increasing. In this mode, the diode is not conducting current, so the output is supported by the capacitor. The transition to Mode 2 happens when $u = 0$. In this case, the inductor will induce a voltage that will force the current to continue flowing in the same direction through the diode to the load. The system remains in Mode 2 as long as $u = 0$ and the

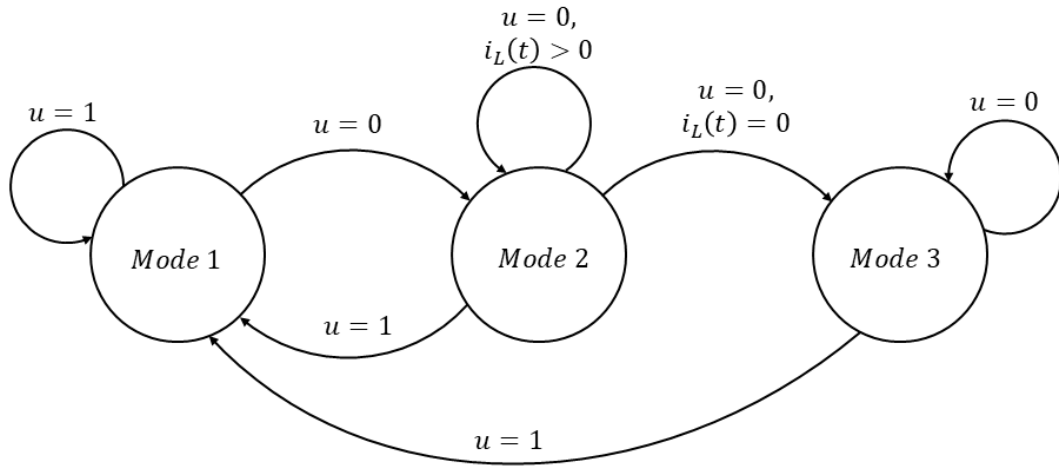


Figure 3.4: Continuous-time model state machine representation

inductor current i_L is greater than zero. If the inductor current reaches 0 before $u = 1$ then the system transitions to Mode 3. In this case, the diode is also *OFF* and the converter is said to be operating in DCM. The system remains in Mode 3 until the next switch cycle occurs, i.e., $u = 1$. The system states and corresponding circuit arrangements for each mode are displayed in Figure 3.5.

The next step is to develop state-space equations for each mode using the state variable defined in (3.1), where i_L is the inductor current and v_o is the output voltage (capacitor voltage).

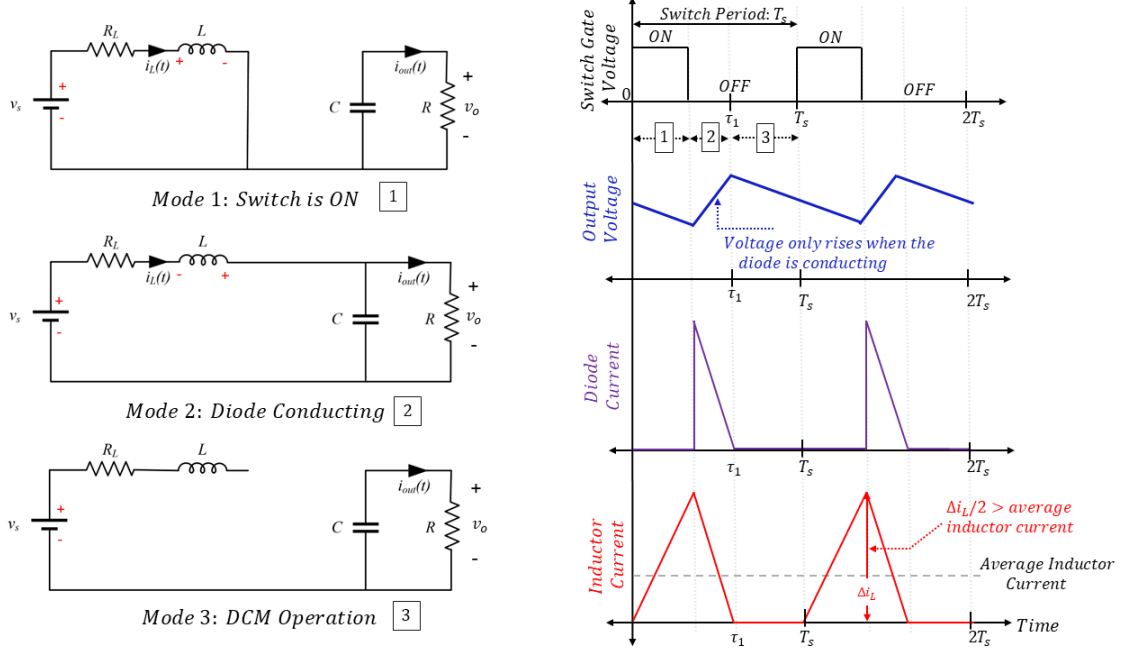


Figure 3.5: The three operating modes in DCM

$$\mathbf{x}(t) = \begin{bmatrix} i_L(t) & v_o(t) \end{bmatrix}^T \quad (3.1)$$

The state-space equations for each mode are defined in (3.2). Additional details can be found in [104].

Mode 1:

$$\dot{\mathbf{x}}(t) = \begin{bmatrix} -\frac{R_L}{L} & 0 \\ 0 & -\frac{1}{RC} \end{bmatrix} \mathbf{x}(t) + \begin{bmatrix} \frac{1}{L} \\ 0 \end{bmatrix} v_s(t) \quad (3.2a)$$

Mode 2:

$$\dot{\mathbf{x}}(t) = \begin{bmatrix} \frac{-R_L}{L} & -\frac{1}{L} \\ \frac{1}{C} & -\frac{1}{RC} \end{bmatrix} \mathbf{x}(t) + \begin{bmatrix} \frac{1}{L} \\ 0 \end{bmatrix} v_s(t) \quad (3.2b)$$

Mode 3:

$$\dot{\mathbf{x}}(t) = \begin{bmatrix} 0 & 0 \\ 0 & -\frac{1}{RC} \end{bmatrix} \mathbf{x}(t) + \begin{bmatrix} 0 \\ 0 \end{bmatrix} v_s(t) \quad (3.2c)$$

$$\mathbf{y}(t) = \begin{bmatrix} 0 & 1 \end{bmatrix} \mathbf{x}(t) \quad (3.2d)$$

3.1.1.2 Discrete-time Model It was reported in [9] that the most commonly used techniques to discretize continuous-time data are forward Euler, backward Euler or exact discretization. Forward and backward Euler are computationally cheaper, however, forward Euler is easier to implement due to its explicit nature. The main drawback of the forward and backward Euler methods is that system model loses accuracy as the time-step, T_s increases, and it has been reported that forward Euler method may cause stability issues. [16] provides a recommendation for the selection of T_s to be two orders of magnitude greater than the targeted switching frequency.

The forward Euler approximation (3.3) is used to derive a discrete-time model from the continuous-time model in (3.2) where the time increment is defined by T_s and $k \in \mathbb{N}$ indicates the discrete time-step.

$$\frac{\mathbf{x}[k+1] - \mathbf{x}[k]}{T_s} = f(\mathbf{x}[k]) \quad (3.3)$$

where $f(\mathbf{x}[k])$ is substituted with the equations in (3.2) for each mode.

The discrete-time model shares the same three modes as the continuous-time model, however, Mode 3 in continuous-time becomes Mode 4 in the discrete model, and a fourth mode (Mode 3) is added to represent the moment the inductor current decreases from a positive value and reaches 0. This time instant is defined as τ_1 . Hence, the converter operates in four different modes, depending on the shape of the inductor current

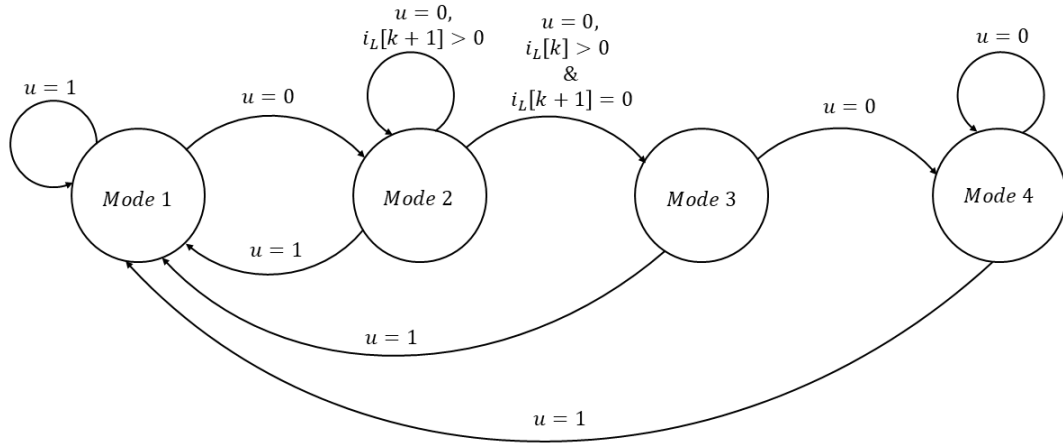


Figure 3.6: Discrete-time model state machine representation

and switch position. The state-machine diagram is updated to represent the discrete time operation with all four modes in Figure 3.6 with the four modes identified in Figure 3.7 and state-space representations defined in (3.4).

1. Mode 1 represents the converter when switch S is ON and the inductor current is increasing.
2. Mode 2 is when switch S is OFF and the inductor current is decreasing and is positive.
3. Mode 3 is the average of Modes 2 and 4 and includes the moment the inductor current decreases from a positive value to 0, which is defined as τ_1 .
4. Mode 4 is when both switch S and diode D are OFF and the inductor current is 0.

The discrete-time state space matrices for all four modes are included below:

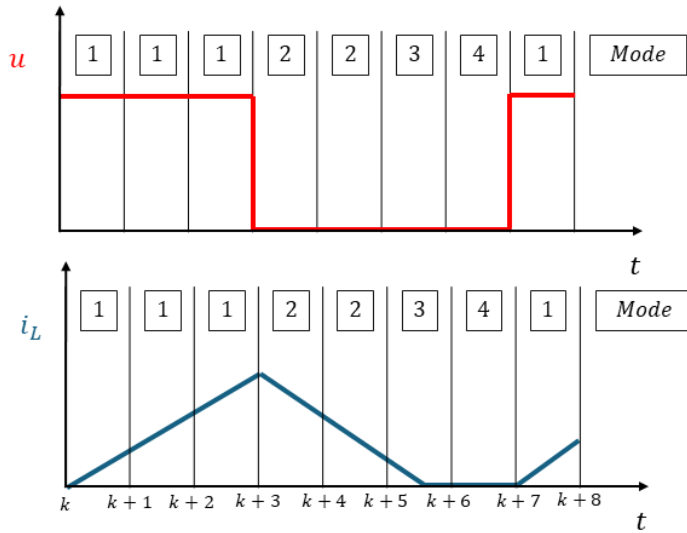


Figure 3.7: Discrete Math Model Operating Modes

Mode 1:

$$\mathbf{x}[k+1] = \begin{bmatrix} 1 - \frac{R_L T_s}{L} & 0 \\ 0 & 1 - \frac{T_s}{RC} \end{bmatrix} \mathbf{x}[k] + \begin{bmatrix} \frac{T_s}{L} \\ 0 \end{bmatrix} v_s[k] \quad (3.4a)$$

Mode 2:

$$\mathbf{x}[k+1] = \begin{bmatrix} 1 - \frac{R_L T_s}{L} & -\frac{T_s}{L} \\ \frac{T_s}{C} & 1 - \frac{T_s}{RC} \end{bmatrix} \mathbf{x}[k] + \begin{bmatrix} \frac{T_s}{L} \\ 0 \end{bmatrix} v_s[k] \quad (3.4b)$$

Mode 3:

$$\mathbf{x}[k+1] = \begin{bmatrix} 1 - \frac{R_L \tau_1}{L} & -\frac{\tau_1}{L} \\ \frac{\tau_1}{C} & 1 - \frac{T_s}{RC} \end{bmatrix} \mathbf{x}[k] + \begin{bmatrix} \frac{\tau_1}{L} \\ 0 \end{bmatrix} v_s[k] \quad (3.4c)$$

Mode 4:

$$\mathbf{x}[k+1] = \begin{bmatrix} 1 & 0 \\ 0 & 1 - \frac{T_s}{RC} \end{bmatrix} \mathbf{x}[k] \quad (3.4d)$$

Output:

$$\mathbf{y}[k] = \begin{bmatrix} 0 & 1 \end{bmatrix} \mathbf{x}[k] \quad (3.4e)$$

3.1.2 Cost Function and OCP

The MPC solves an optimal control problem (OCP) for each switching sequence, formulated as follows:

$$\min_{U_o} \sum_{\ell=k}^{k+N-1} (|v_{o,err}[\ell+1|k]| + \lambda_u |\Delta u[\ell|k]|) \quad (3.5a)$$

$$\text{s.t. System dynamics(3.4)} \quad (3.5b)$$

The objective (cost) function is defined in (3.5a). The first term in the objective function penalizes the error between the calculated output voltage and the reference voltage and is found using the following:

$$v_{o,err}[k] = v_{o,ref} - v_o[k] \quad (3.6)$$

The second term in the objective function penalizes the difference between two successive switch states and is calculated using:

$$\Delta u[k] = u[k] - u[k-1] \quad (3.7)$$

Penalizing the change in the switch state effectively reduces the switching frequency, f_{sw} . The effect of this term is manipulated by multiplying it with a weighting factor λ_u , where

increasing this factor generally reduces the switching frequency and keeping this factor set to 0 allows the switching frequency to reach $1/(2T_s)$ if $R_L = 0$ and $v_o = 2v_s$ [16]. We note here that the objective function (3.5) does not place limits on the control input or state variables so feasibility is guaranteed since the MPC is solving an unconstrained optimization problem.

3.1.3 Prediction Horizon

At each time step, the MPC controller evaluates the cost function (3.5a) for a set of predefined switching sequences $U[k]$. The prediction horizon is defined over a finite horizon $N \in \mathbb{N}^+$ in which the switching sequences are defined:

$$\mathbf{U}[k] = \begin{bmatrix} \mathbf{u}[k] & \mathbf{u}[k+1] & \dots & \mathbf{u}[k+N-1] \end{bmatrix}^T \quad (3.8)$$

in which the total number of switching sequences is 2^N . The optimization variable, $\mathbf{U}[k]$, the input (source) voltage, v_s and the current state variable $\mathbf{x}[k]$ are then entered into the OCP (3.5) for which the output voltage trajectory is predicted, and the objective function is evaluated. For real-time implementation, the computational time required to process these sequences is small compared to the sample time, T_s .

The switching sequence with the minimum cost function value is then selected as the optimal switching sequence $\mathbf{U}_o[k]$. The first element of the sequence is applied to the switch, S . For time-triggered MPC, this procedure is repeated at the next time-step, based on new measurements acquired at the following sampling instance, T_s .

3.1.3.1 Receding Horizon Policy In time-triggered enumeration-based MPC (TT-MPC), after the first control input \mathbf{u}_o within the optimal switch sequence $\mathbf{U}_o[k]$ is applied to switch, S , the rest of the sequence is disregarded and the optimization process is repeated

after T_s . This provides a form of closed-loop feedback to the MPC controller which adds robustness to the controller [9].

3.1.3.2 Move Blocking Scheme Since boost converters experience a non-minimum phase behavior, a long prediction horizon is required to anticipate for the initial drop in output voltage when the switch is actuated *ON* ($u = 1$). In an enumeration-based MPC, all switching sequences are evaluated by the controller, so every added switch state doubles the number of sequences to be evaluated which in turn increases the computational burden of the controller. To address this, a move blocking scheme is implemented [32].

Move blocking assigns the first number of switch steps N_1 with sample time T_s . The remaining steps N_2 are assigned a longer time sample by multiplying N_2 with a factor n_s . With a move blocking scheme, the total prediction horizon time is covered with fewer prediction steps. The example shown in Figure 3.8 displays two prediction horizon implementations in which the same time duration is covered in a different number of steps. Without move blocking, the prediction horizon is $N = 17$, which makes the total length = $17T_s$. With move blocking, the new prediction horizon is $N = 13$, where: $N_1 = 9$, $N_2 = 4$, $n_s = 2$, making the total length = $(9 + (4 \times 2))T_s = 17T_s$. i.e., the same prediction length is covered with fewer steps, but the number of computations is reduced significantly (i.e., $\mathcal{O}(2^{17})$ reduces to $\rightarrow \mathcal{O}(2^{13})$.

3.2 Event-Triggered Enumeration-Based MPC (ET-MPC)

ET-MPC is introduced to reduce the computational burden of the enumeration time-triggered MPC (TT-MPC) by triggering the OCP only when the control objective is being compromised. In this case, the control objective is voltage reference tracking. In TT-MPC, all 2^N switching sequences are evaluated at each time step T_s which requires significant computational effort by the controller especially as the prediction steps N

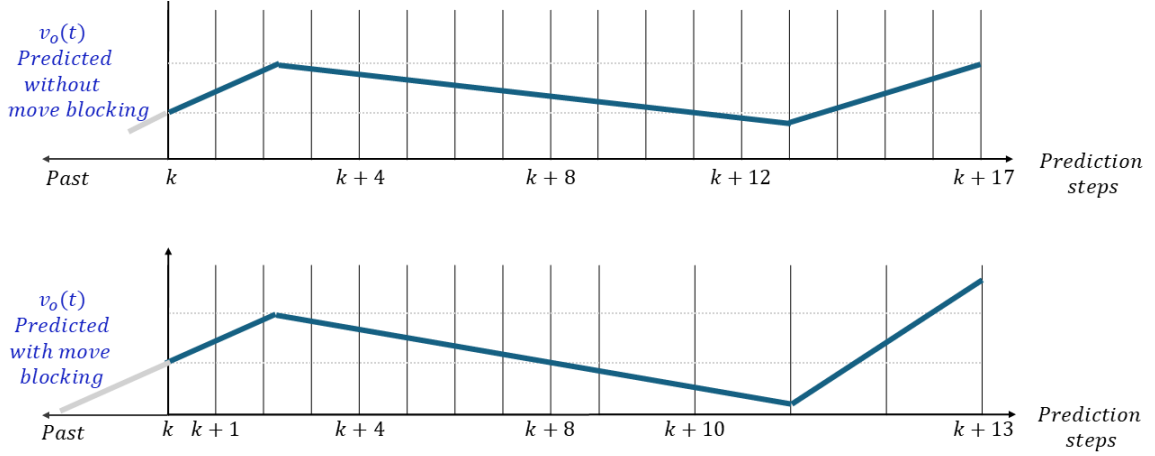


Figure 3.8: Prediction horizon move blocking scheme

increase. ET-MPC is proposed to solve the optimization problem only when an event is triggered, as opposed to solving at every time step. The algorithm starts with an event trigger which generates an optimal switching sequence \mathbf{U}_t and optimal state trajectory \mathbf{X}_t . The first element in $\mathbf{U}_t[k]$ is used to actuate the main switch S and is fed back to the controller with a time delay. The controller also outputs the optimal switch sequence, \mathbf{U}_t , and state trajectory, \mathbf{X}_t with a time delay along with counter t . \mathbf{U}_{t1} and \mathbf{X}_{t1} indicate the optimal switch and state trajectory that have been passed to the MPC controller after the time delay.

Upon the next time step, the counter, t is incremented by T_s . The counter is used to increment index k to select the next optimal switch state, but due to the move blocking scheme, index k may need to be held for up to n_s time samples. Index selection matrix T is developed to address this. T allocates counter t to an equivalent index k with consideration of the move blocking scheme. An example of T is defined in Table 3.1. The example in Table 3.1 assumes $N = 6$, $N_1 = 4$, $n_s = 4$ and $Ts = 5\mu s$.

Table 3.1: Event-triggered Selection of Optimal State trajectory and Switch State Index

Counter t	$5\mu s$	$10\mu s$	$15\mu s$	$20\mu s$	$25\mu s$	$30\mu s$	$35\mu s$	$40\mu s$	$45\mu s$	$50\mu s$	$55\mu s$	$60\mu s$
Index k	1	2	3	4		5				6		
$T[k]$	$5\mu s$	$10\mu s$	$15\mu s$	$20\mu s$		$40\mu s$				$60\mu s$		
$\mathbf{U}_t[k]$	$U_t[1]$	$U_t[2]$	$U_t[3]$	$U_t[4]$		$U_t[5]$				$U_t[6]$		
$\mathbf{X}[k]$	$X[1]$	$X[2]$	$X[3]$	$X[4]$		$X[5]$				$X[6]$		

At the next time sample, T_s , given the optimal state sequence X_{t1} computed at the last event (at time t_1), and the current output voltage measurement, v_o , an event-trigger e is evaluated using the following criteria:

$$e = \begin{cases} 1 & \text{if } ||X_{t1}[2,k] - v_o|| > \delta \text{ or } k > k_{max} \\ 0 & \text{Otherwise} \end{cases}, \quad (3.9)$$

where δ is defined as the trigger threshold and represents how much the output voltage, v_o , deviates from the corresponding optimal state trajectory, $X_{t1}(2,k)$.

An event is triggered when $e = 1$, which triggers the controller to evaluate the OCP. An event can also be triggered if k_{max} is reached which is the maximum allowable number of elements that can be used in the switching sequence. This generates a new optimal state trajectory and switching sequence which are fed back to the controller. Otherwise, when $e = 0$, the control action is determined using the next switch state in the optimal sequence U_{t1} computed at the last event, which eliminates the need to run the optimization problem for the 2^N switching sequences [38]. A visualization of the process is shown in Figure 3.9

The event-triggered control algorithm is described in Algorithm 3.1 and in the flow chart in Figure 3.10. J represents the cost function in (3.5a).

Move Blocking Factor $n_s = 4$

$N_1 = 4, N = 6$

$T_s = 5\mu s$

$5\mu s$	$10\mu s$	$15\mu s$	$20\mu s$	$40\mu s$				$60\mu s$			
$5\mu s$	$10\mu s$	$15\mu s$	$20\mu s$	$25\mu s$	$30\mu s$	$35\mu s$	$40\mu s$	$45\mu s$	$50\mu s$	$55\mu s$	$60\mu s$
1	2	3	4	5				<u>6</u>			

Vector $T(k)$

Counter t

Index k (k_{max})

$k = 1$ (index)

0	1	1	1	0	0
i_{L1}	i_{L2}	i_{L3}	i_{L4}	i_{L5}	i_{L6}
v_{o1}	v_{o2}	v_{o3}	v_{o4}	v_{o5}	v_{o6}

Optimal Switching Sequence (U_t)

Optimal State Trajectory (X_t)

where: $i_{Lk} = X_t[1, k]$
 $v_{ok} = X_t[2, k]$

1 – Increment t (counter) by T_s at beginning of MPC control sequence

2 – Find k such that $t \geq T[k]$ and $t < T[k + 1]$

3 – Compare absolute measured v_o against $X_t[k, 2]$

→ If they diverge beyond δ , set $t = 0$ and run

the optimization process to get a new u , U , and X

Set $e = 1$

→ Else, set u to $U_t[k + 1]$, and pass U_t and X_t through

Set $e = 0$

Figure 3.9: Event-trigger decision and increment process

Algorithm 3.1: Event-Triggered MPC Algorithm

```
procedure ETMPC( $u, \mathbf{U}_{t1}, \mathbf{X}_{t1}, t, i_l, v_o, v_s$ )
     $J^*(k) = \infty;$ 
     $t \leftarrow t + T_s$ 
     $k \leftarrow$  select  $k$  from  $T$  using  $t$  see Table (3.1)
     $e \leftarrow$  compute (3.9);
    if  $e = 1$  then
         $t \leftarrow 0$ 
        for all  $U$  over  $N$  do
             $J = 0$ 
            for  $\ell = k$  to  $k+N-1$  do
                 $x(\ell+1) \leftarrow$  compute from (3.4)
                 $J \leftarrow$  compute from (3.5)
            end
            if  $J < J^*(k)$  then
                 $J^*(k) = J, u = U(1)$ 
            end
        end
         $\mathbf{U}_t \leftarrow \mathbf{U}$ 
         $X_t \leftarrow x$ 
    end

    if  $e = 0$  then
         $u \leftarrow \mathbf{U}_{t1}(k)$ 
         $\mathbf{U}_t \leftarrow \mathbf{U}_{t1}$ 
         $\mathbf{X}_t \leftarrow \mathbf{X}_{t1}$ 
    end

return  $u, t, \mathbf{U}_t, \mathbf{X}_t$ 
end procedure
```

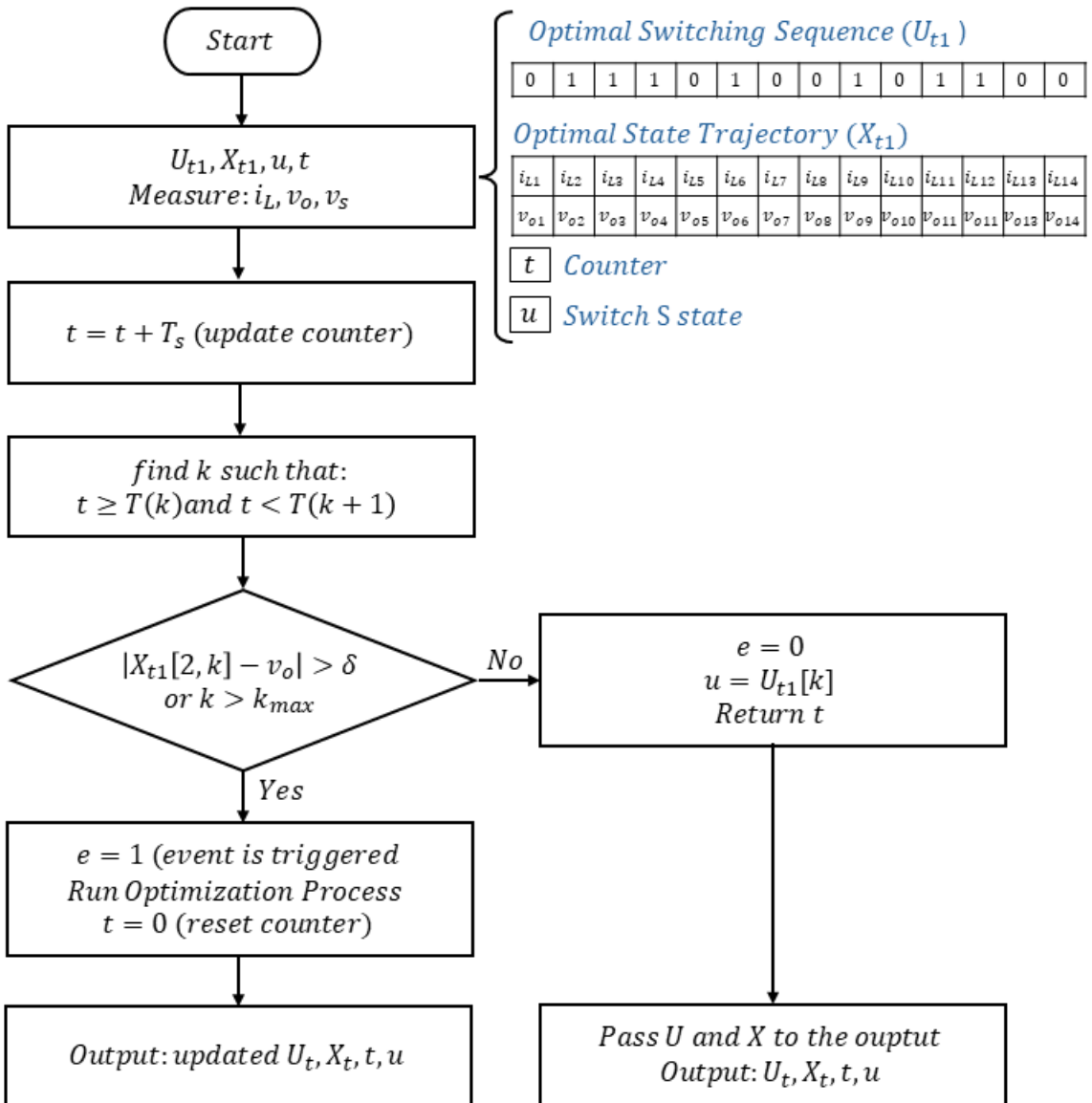


Figure 3.10: Event-triggered Flowchart for Boost Converter control

3.3 Maximum Computational Savings

The maximum computational savings can be achieved when events are not triggered. Equation 3.10 shows that given an event is not triggered, we are able to skip the optimization problem at each time step for up to:

$$\text{Number of time steps OCP is skipped} = \begin{cases} N_1 + (k_{max} - N_1)n_s & \text{if } k_{max} \geq N_1 \\ k_{max} & \text{if } k_{max} < N_1 \end{cases} \quad (3.10)$$

time steps. When an event is not triggered, the MPC will only shift the index within the optimal control sequence and apply the actuating signal to switch S without calculating the OCP. In a TT-MPC formulation, the number of operations per second (OPS) is calculated with Eq. (3.11):

$$OPS_{TT} = \frac{2^{N_1+N_2}}{T_s} \quad (3.11)$$

While the number of OPS in an ET-MPC can reach a minimum number given in (3.13). The assumption here is the optimal sequence is cycled through in its entirety and an event is only triggered when the counter reaches (3.12):

$$t_{max} = \begin{cases} N_1 T_s + (k_{max} - N_1)n_s T_s & \text{if } k_{max} \geq N_1 \\ k_{max} T_s & \text{if } k_{max} < N_1 \end{cases} \quad (3.12)$$

$$OPS_{ET} = \begin{cases} \frac{2^{N_1+N_2}}{(N_1 + (k_{max} - N_1)n_s)T_s} & \text{if } k_{max} \geq N_1 \\ \frac{2^{N_1+N_2}}{k_{max}T_s} & \text{if } k_{max} < N_1 \end{cases} \quad (3.13)$$

The minimum event frequency is found using (3.14) and a plot showing the general trend relating the prediction horizon unweighted steps (N_1) and k_{max} to the minimum achievable

event-frequency given a move blocking factor equal to 4 ($n_s = 4$).

$$\text{Minimum event frequency: } f_{min-ET} = \begin{cases} \frac{1}{(N_1 + (k_{max} - N_1)n_s)} & \text{if } k_{max} \geq N_1 \\ \frac{1}{k_{max}} & \text{if } k_{max} < N_1 \end{cases} \quad (3.14)$$

The maximum computational savings given an event is not triggered can be found using (3.15).

$$CS_{max} = (1 - f_{min-ET}) \times OPS_{TT} \quad (3.15)$$

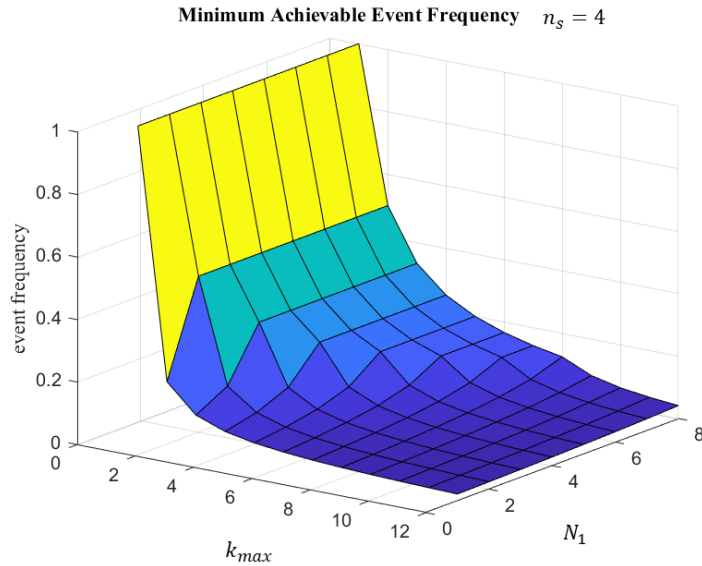


Figure 3.11: Minimum Achievable Event Frequency ($n_s = 4$)

CHAPTER FOUR

ET-MPC WITH FULL STATE FEEDBACK

In this chapter, simulation results for both time-triggered and event-triggered control are presented. Both TT-MPC and ET-MPC formulations for the boost converter are implemented using MATLAB/SIMULINK. The block diagram for the proposed ET-MPC system is shown in 4.1. TT-MPC is implemented using the same system, with the event-trigger threshold δ is set to 0.

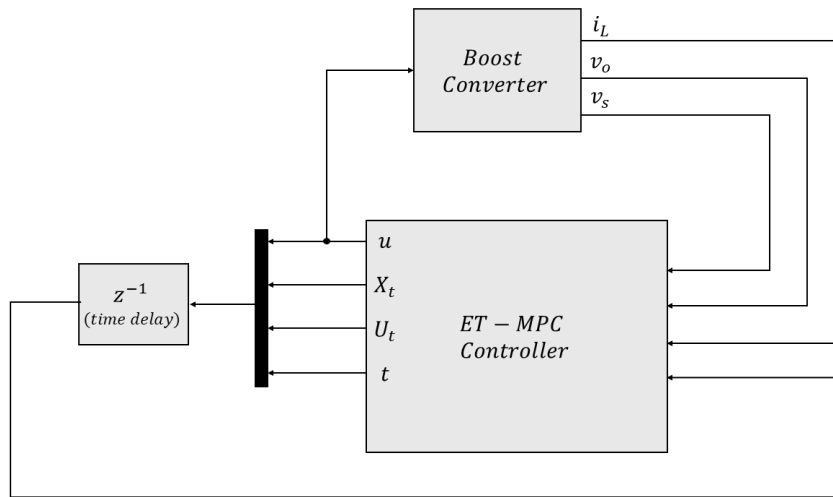


Figure 4.1: DC-DC boost converter with ET-MPC control

The performance of the boost converter is evaluated during startup, steady-state operation, step changes in voltage reference, and step change in the input voltage . The parameters used in all simulations are listed in Table 4.1. The input voltage v_s is set to 10V and the output voltage reference $v_{o,ref}$ is 15V unless stated otherwise. In all

Table 4.1: Simulation Parameters - Boost Converter

Converter and Controller Parameter	Value
Inductor (L)	$550\mu H$
Inductor DC Resistance (R_L)	1.3Ω
Output Capacitance (C)	$220\mu F$
Load Resistance (R)	73Ω
Sampling Period (T_s)	$5\mu s$
Prediction Horizon (N)	14
N_1	1
Move Blocking Coefficient (n_s)	4
Weight in Objective Function Lambda (λ)	0.5
δ	0.05
k_{max}	14
Minimum event frequency (f_{min-ET})	1.9%

simulations, $k_{max} = N$, where N is the prediction horizon. We start the evaluation with the trigger-threshold δ set to 0.05.

4.1 Comparison between TT-MPC and ET-MPC

4.1.1 Start-up

A start-up under normal condition is simulated, with results shown in Figure 4.2 and Figure 4.3. For ET-MPC, Figure 4.3, we additionally plot the event frequency to denote computational savings. Note that for the ease of presentation, the event frequency is averaged using a moving window to show the average triggering frequency.

The start-up time is defined as the time it takes for the converter to reach voltage regulation when it is first powered on and begins converting power. As can be seen from the simulated waveforms, the converter reaches the desired reference at about 2ms without overshoot using both TT-MPC and ET-MPC. Initially, the controller keeps switch S open to charge the output capacitor as quickly as possible to the reference voltage. Once the output voltage is within the range of the input voltage, the controller begins to operate, and the converter begins to boost the voltage to the reference voltage. Note that during the converter's initial operation, the event frequency is at its highest value due to the difference between output voltage and reference voltage.

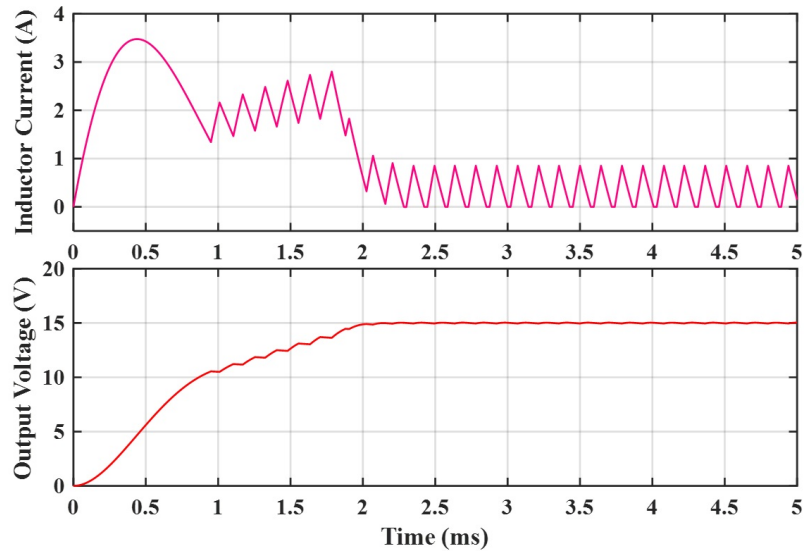


Figure 4.2: Boost Converter Start-up (TT-MPC)

Once the output voltage reaches the reference voltage, the inductor current decreases. With ET-MPC, once the converter reaches DCM, the number of event triggers

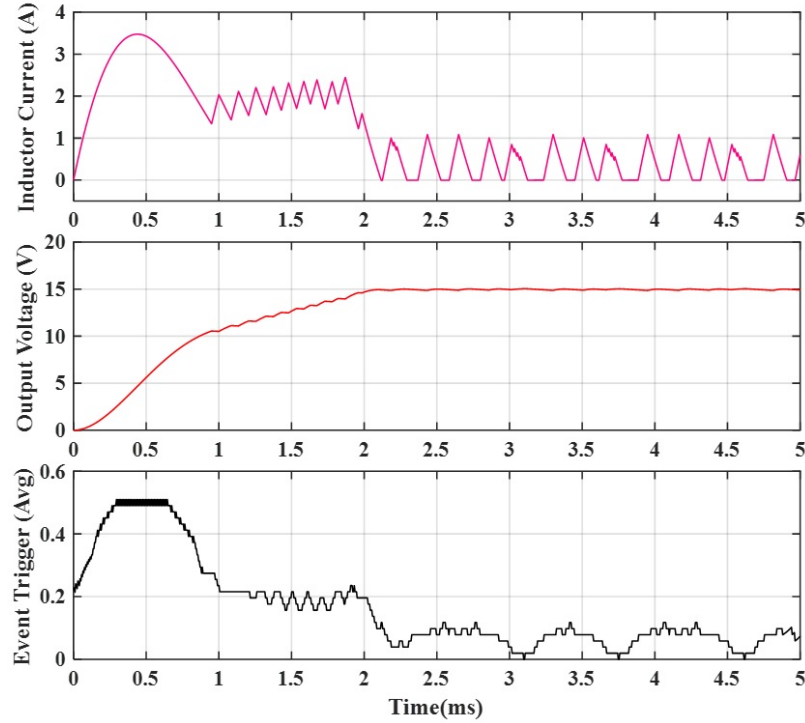


Figure 4.3: Boost Converter Start-up (ET-MPC, $\delta = 0.05$)

is significantly decreased as shown in Figure 4.3. Using event-triggered MPC, we were able to achieve similar results while using significantly less computation.

4.1.2 Step Changes in the Output Reference Voltage

The performance of the converter with both TT-MPC and ET-MPC were evaluated when the output reference voltage was stepped up from 15V to 30V at 7.5ms. As can be seen from Figure 4.4 and Figure 4.5, the output achieves a regulated 30V output at approximately 19ms for time-triggered MPC. The inductor current slightly increases during the step up in reference voltage to increase the output voltage. Once the converter reaches regulation, the inductor current is reduced. For ET-MPC, the converter reaches a regulated 30V output at approximately 21.5ms, a 2.5ms delay compared to time-triggered

formulation. The converter's performance is almost equivalent for the two techniques, with the average number of computations significantly reduced with the latter method.

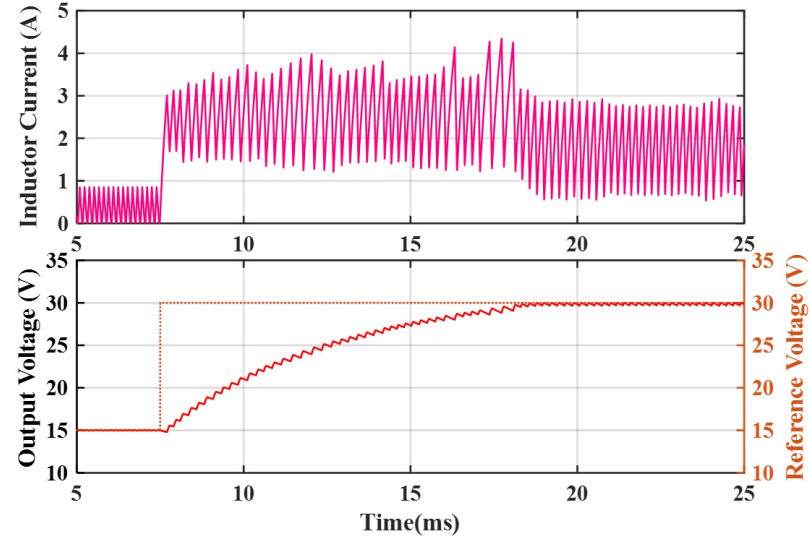


Figure 4.4: Reference voltage step-up from 15V to 30V (TT-MPC)

Next, the output voltage reference is changed from 20V to 15V at 10ms. The response of the converter using both TT-MPC and ET-MPC methods are illustrated in Figure 4.6 and Figure 4.7. Both control methods allow the converter to reach regulation within 5ms with the latter achieving similar performance with significantly reduced calculations. During the step down in reference voltage, the inductor current goes to zero allowing the capacitor to discharge into the load to reduce the output voltage to the new reference voltage.

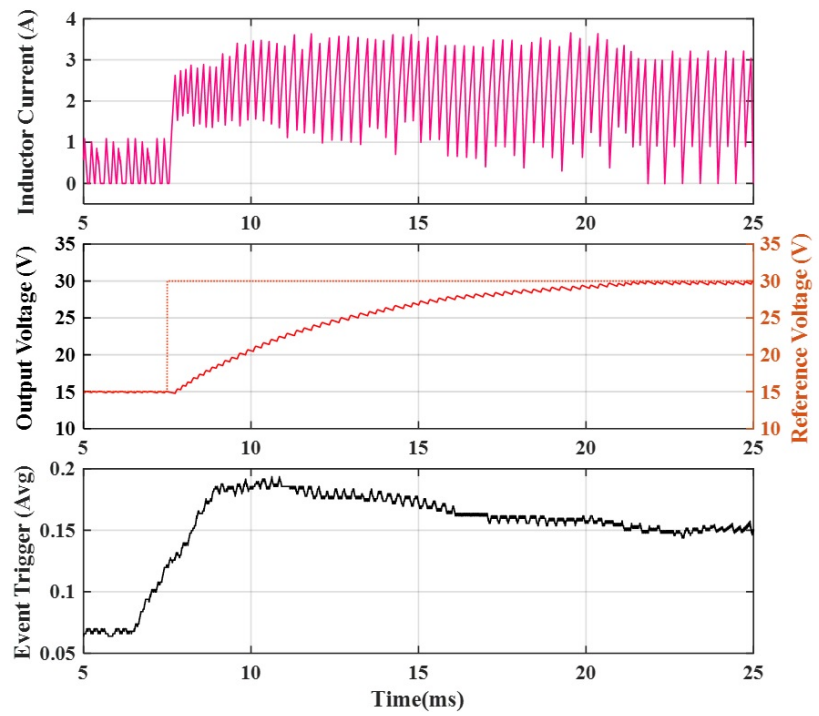


Figure 4.5: Reference voltage step-up from 15V to 30V (ET-MPC)

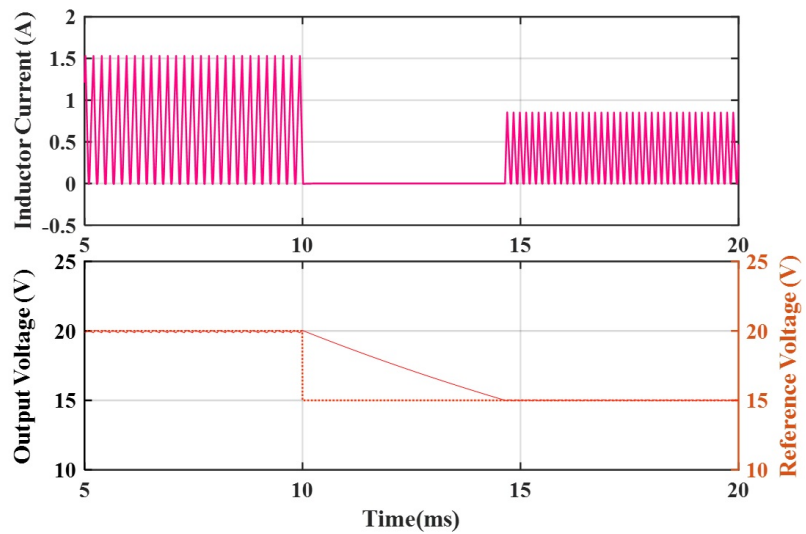


Figure 4.6: Reference voltage step-down from 20V to 15V (TT-MPC)

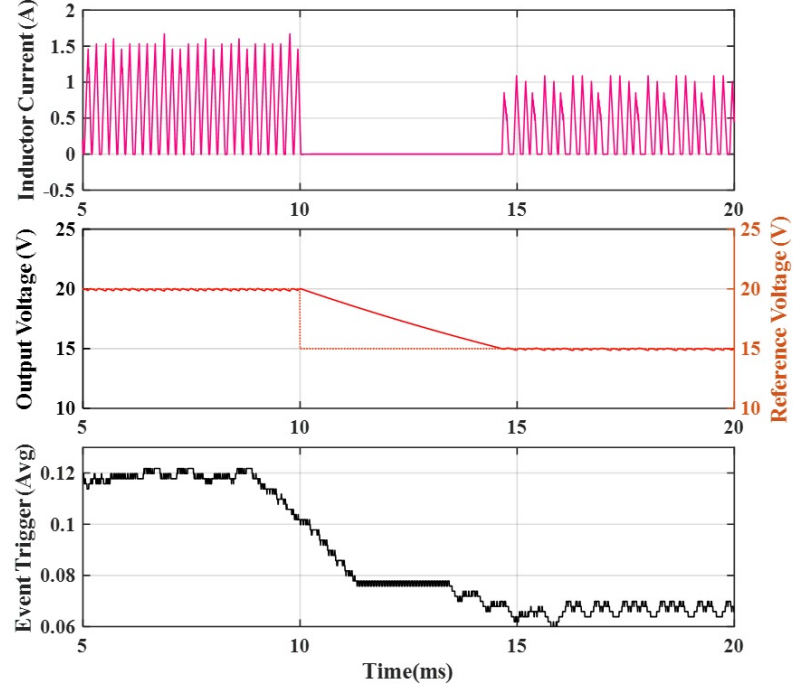


Figure 4.7: Reference voltage step-down from 20V to 15V (ET-MPC)

4.1.3 Step Change in the Input Voltage

In this case, a step change in the input voltage is simulated. More specifically, the input, v_s , is stepped up from 10V to 15V at 20ms after steady state operation with the reference voltage, $v_{o,ref}$, set to 30V. The line transient response of the converter for both methods is displayed in Figure 4.8 and Figure 4.9. The output voltage remains almost undisturbed during the input transient.

The number of event triggers decreases once the input increases to 15V. The plot did not include the start-up profile of the converter, but it was noted that the number of events continuously decreases as the converter approaches steady state. It does take the converter more time to reach 30V steady state using event-triggered control. The

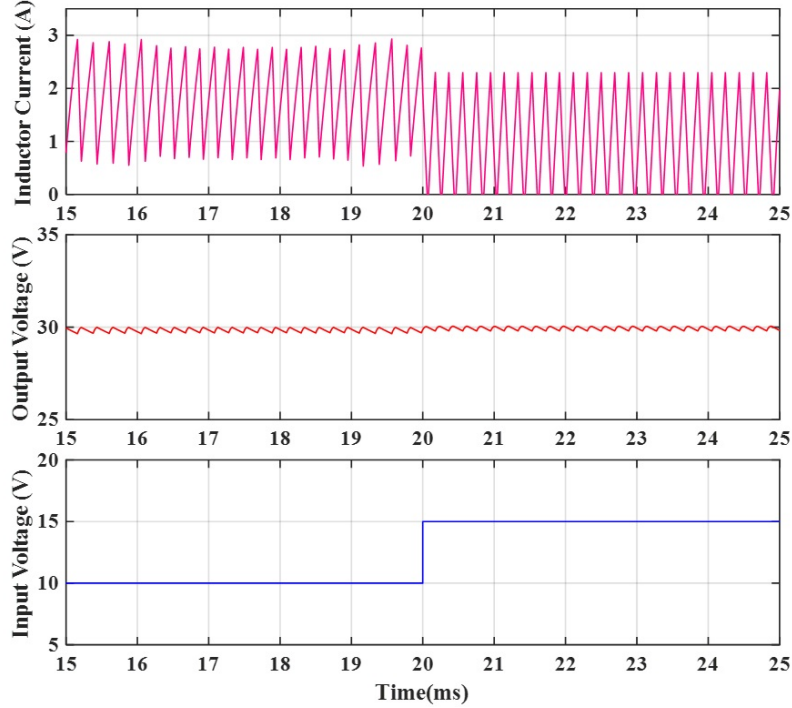


Figure 4.8: Input voltage step-up from 10V to 15V (TT-MPC)

event-triggered controlled converter reached steady state at 16ms while the time-triggered controlled converter reached steady state at 13ms.

4.1.4 Discussion of Computational Savings

Finally, the computational savings for all simulated cases are summarized in Table 4.2, measured by the average event frequency. As can be seen, the proposed ET-MPC requires only 7% – 20% control effort as compared to TT-MPC, while maintaining comparable performance. Note that the balancing between computation reduction and control performance can be achieved by calibrating the threshold parameter δ , and a thorough analysis of its impact is discussed in the following section.

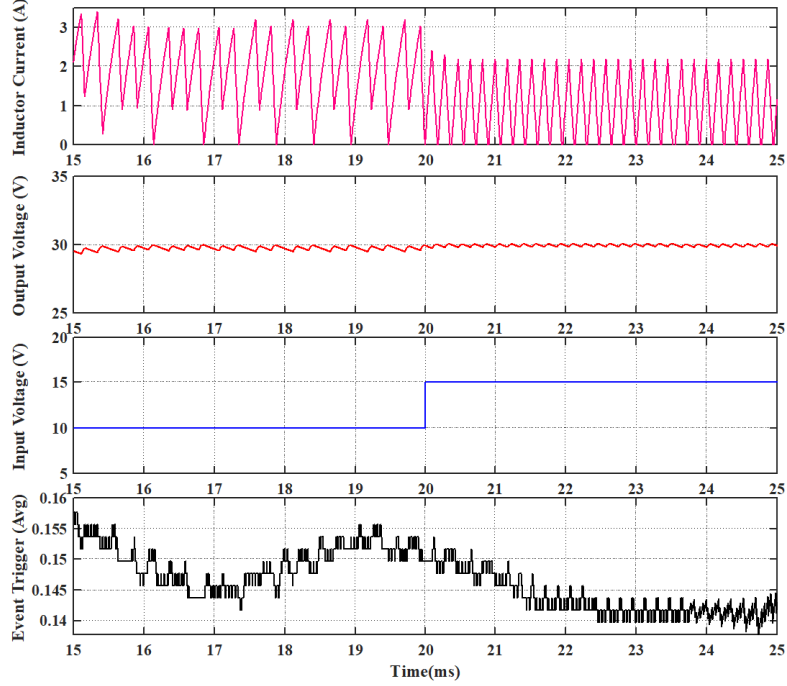


Figure 4.9: Input voltage step-up from 10V to 15V (ET-MCP)

4.1.5 Summary of results

This section investigated the use of event-triggered enumeration-based model predictive control (MPC) for a DC-DC boost converter control. Specifically, ET-MPC is used to reduce the computational burden of conventional TT-MPC. Simulation results demonstrate the effectiveness of the proposed methodology by reducing the average online computations by up to 93%, while maintaining a comparable control performance.

4.2 Evaluation of event-trigger threshold effect

The selection of the event-trigger threshold, δ , significantly impacts the performance of the converter. To assess this impact, we evaluate the boost converter and

Table 4.2: Computational Saving as Measured by Event Frequency

Operation Modes (Conditions as listed in IV)	Average Computation
Start-up	20%
Steady state $v_s = 10V, v_o = 15V$	7%
Steady state $v_s = 10V, v_o = 20V$	12%
Steady state $v_s = 10V, v_o = 30V$	16%
Steady state $v_s = 15V, v_o = 30V$	14%
Step-up in reference voltage	19%
Step-down in reference voltage	8%
Step-up in input voltage	15%

ET-MPC control performance using different values of δ . The simulation results are discussed and reported in the following section.

The performance of ET-MPC control for the boost converter is again evaluated during startup, step change in input voltage and step changes in voltage reference with different values of trigger threshold δ . The parameters used in all simulations are listed in Table 4.1, while δ listed in the Table is varied. Throughout our investigation, we plot the averaged event frequency using a moving window to indicate average computational savings.

4.2.1 Event-Trigger Threshold Impact on Start-up Time

Different start-up conditions were simulated in which the event-trigger threshold of the MPC controller was varied. In all cases, the controller kept switch S open initially during start-up to charge the output capacitor to the input voltage which caused an initial

Table 4.3: Start-up Time Summary

Operating Conditions	TT-MPC	ET-MPC
$v_s = 10V, v_o = 15V$	2.2ms	2.2ms
$v_s = 10V, v_o = 20V$	3.9ms	4.3ms
$v_s = 10V, v_o = 30V$	13.2ms	16ms
$v_s = 15V, v_o = 20V$	1.6ms	1.6ms
$v_s = 15V, v_o = 30V$	3.9ms	3.9ms

inrush of current. Once the output capacitor was charged to the input voltage, the controller began to actuate the switch, and the converter boost the voltage to the voltage setpoint ($v_{o,ref}$). It was observed that the desired reference is reached at about the same time for both TT-MPC and ET-MPC implementations for most operating conditions. Start-up time was mostly independent of our selection of the event-trigger threshold δ value. However, start-up time was dependent on operating conditions with the results tabulated in Table 4.3. Simulated waveforms for different trigger thresholds for the operating case: $v_s = 10V$ and $v_{o,ref} = 20V$ are shown in Figure 4.10.

4.2.2 Event-Trigger Threshold Impact on Steady-state Operation

With ET-MPC, once the converter reaches steady-state, the number of event triggers is significantly decreased. Event frequency for different steady state operating conditions, in addition to the tracking error were tabulated in Table 4.4, where tracking error was calculated by

$$T.E. = \sqrt{\frac{\sum_{i=1}^n (v_o[i] - v_{o,ref}[i])^2}{n}}. \quad (4.1)$$

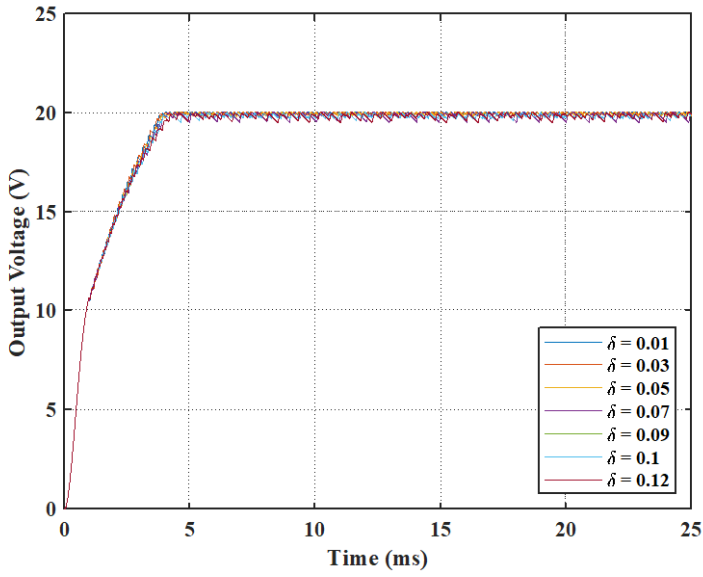


Figure 4.10: Start-up ($v_s = 10V$ and $v_{o,ref} = 20V$)

The results reported in Table 4.4 show that increasing the trigger threshold δ significantly reduces the computation burden of the controller during steady state operation but increases the tracking error. Increasing δ also increases the output voltage ripple and peak inductor current. It was noted in Figure 4.11 that the converter was not able to reach the reference voltage when $v_s = 10V$ and $v_{o,ref} = 30V$ for $\delta \geq 0.09$. Additionally, during steady-state operation the converter experienced irregularities in the output waveform when $v_s = 10V$ and $v_{o,ref} = 15V$ for $\delta \geq 0.1$.

4.2.3 Event-Trigger Threshold Impact on Step Changes in the Output Reference Voltage

The performance of the converter with different trigger thresholds was evaluated when the output reference voltage was stepped up from 15V to 30V. As can be seen from Figure 4.4, the output achieves a regulated 30V output at approximately 19ms for TT-MPC. The performance of the converter with different trigger thresholds was

Table 4.4: Event-trigger Threshold Impact on Steady-state Operation - Results Summary

Event Frequency:		
Steady-State Conditions	$\delta = 0.01$	$\delta = 0.07$
$v_s = 10V, v_o = 15V$	30%	2.7%
$v_s = 10V, v_o = 20V$	33%	7%
$v_s = 10V, v_o = 30V$	42%	11%
$v_s = 15V, v_o = 30V$	44%	12%
Tracking Error [V]:		
Steady-State Conditions	$\delta = 0.01$	$\delta = 0.07$
$v_s = 10V, v_o = 15V$	0.024	0.09
$v_s = 10V, v_o = 20V$	0.049	0.178
$v_s = 10V, v_o = 30V$	0.216	0.42
$v_s = 15V, v_o = 30V$	0.072	0.1
Output Voltage Ripple [Vpp]:		
Steady-State Conditions	$\delta = 0.01$	$\delta = 0.07$
$v_s = 10V, v_o = 15V$	0.095	0.36
$v_s = 10V, v_o = 20V$	0.163	0.54
$v_s = 10V, v_o = 30V$	0.43	0.62
$v_s = 15V, v_o = 30V$	0.236	0.377

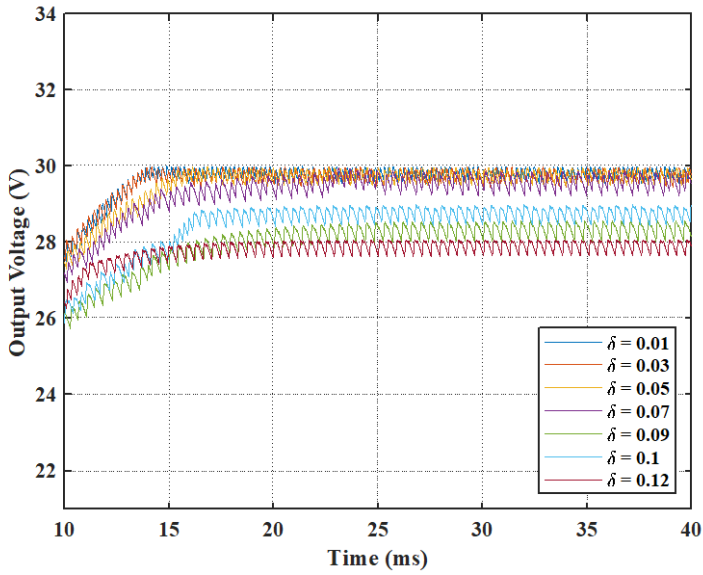


Figure 4.11: Start-up and steady-state operation ($v_s = 10V$ and $v_{o,ref} = 30V$)

evaluated when the output reference voltage was stepped up at $7.5ms$ from $15V$ to $30V$, where $v_s = 10V$. As can be seen from Figure 4.12, the converter achieves a regulated $30V$ output at approximately $19ms$ when $\delta = 0.01$ and at $23.5ms$ when $\delta = 0.07$. The event frequency increases as well as the inductor current during the step up in reference voltage. Once the converter reaches regulation, the inductor current is reduced. Results are summarized in Table 4.5.

Next, the output voltage reference is changed from $20V$ to $15V$ at $7.5ms$ for $\delta = 0.01$ and 0.07 with waveforms plotted in Figure 4.13. During the step down in reference voltage, switch S is OFF and the inductor current goes to zero allowing the capacitor to discharge into the load to reduce the output voltage. A subset of the results for different thresholds is summarized in Table 4.5.

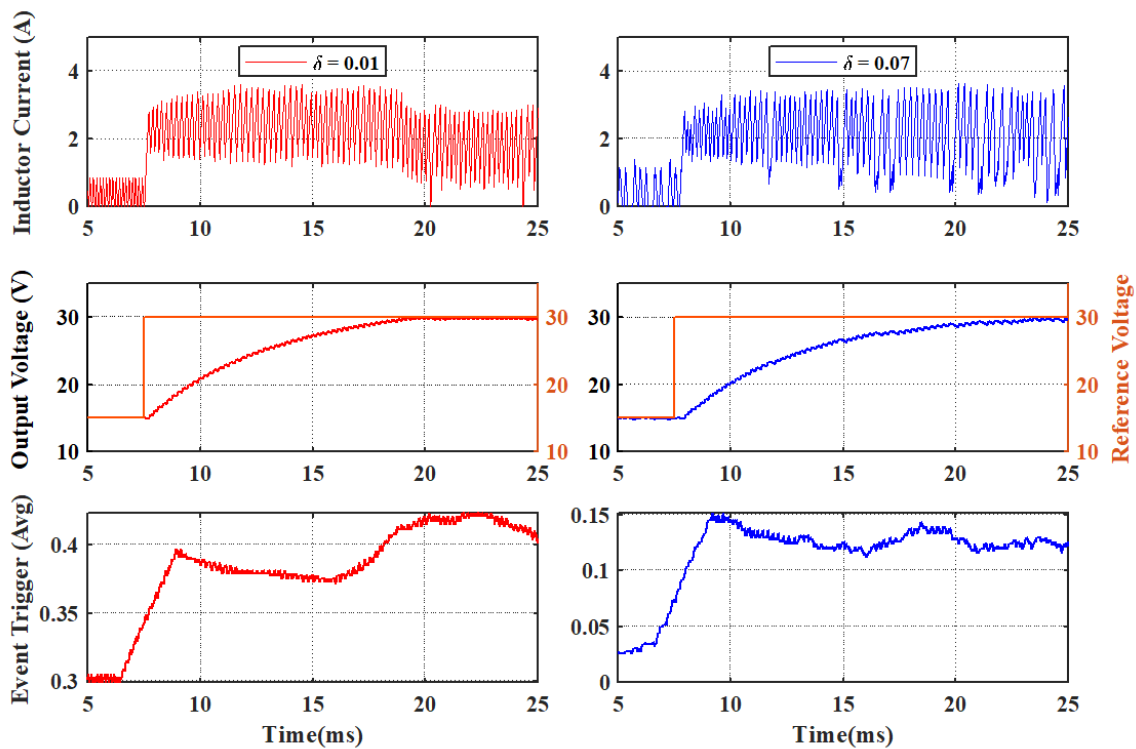


Figure 4.12: Reference voltage step-up from 15V to 30V (ET-MPC)

Table 4.5: Voltage Reference Converter Response for Different Event Thresholds

	$\delta = 0.01$	$\delta = 0.05$	$\delta = 0.07$
$v_{o,ref} = 15V \rightarrow 30V, v_s = 10V$			
Transient time [ms]	11.5	14	16
Event Frequency	42.5%	19.5%	15%
$v_{o,ref} = 20V \rightarrow 15V, v_s = 10V$			
Transient time [ms]	4.6	4.6	4.6
Event Frequency	28%	7.5%	2.5%

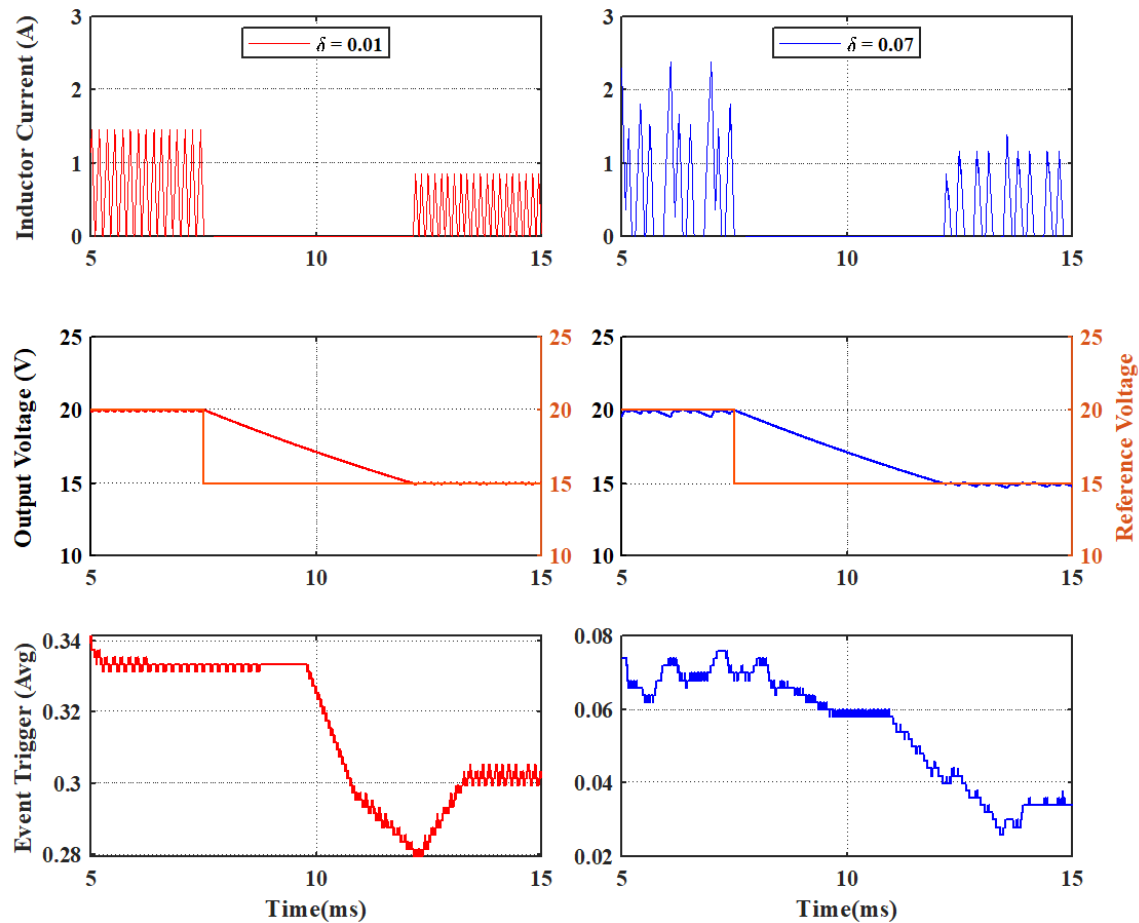


Figure 4.13: Reference voltage step-down from 20V to 15V (ET-MPC)

4.2.4 Event-Trigger Threshold Impact on Step Change in the Input Voltage

A step change in the input voltage from 10V to 15V at 20ms after steady state operation with $v_{o,ref}$ set to 30V was simulated. The line transient response of the converter for $\delta = 0.01$ and $\delta = 0.07$ are displayed in Figure 4.14. In both cases, event trigger frequency increases as the input voltage increases. The event frequency during the transient increases by 2% when $\delta = 0.01$, where as it only increases by 0.5% when $\delta = 0.07$. The output voltage remains almost undisturbed during the input transient as the response of the controller is almost immediate due to the feedforward effect of the input voltage to the controller.

4.2.5 Summary of results

This section explored the impact of the event-trigger threshold, δ , on the performance of ET-MPC for a DC-DC boost converter. The simulation results demonstrate the impact of the event-trigger threshold on the performance of the converter during different operating conditions. Generally, increasing the threshold trigger reduces the number of computations performed but increases the tracking error, voltage ripple, and inductor peak currents during steady state operation. A trade-off must be made between the number of computations and meeting specific performance targets.

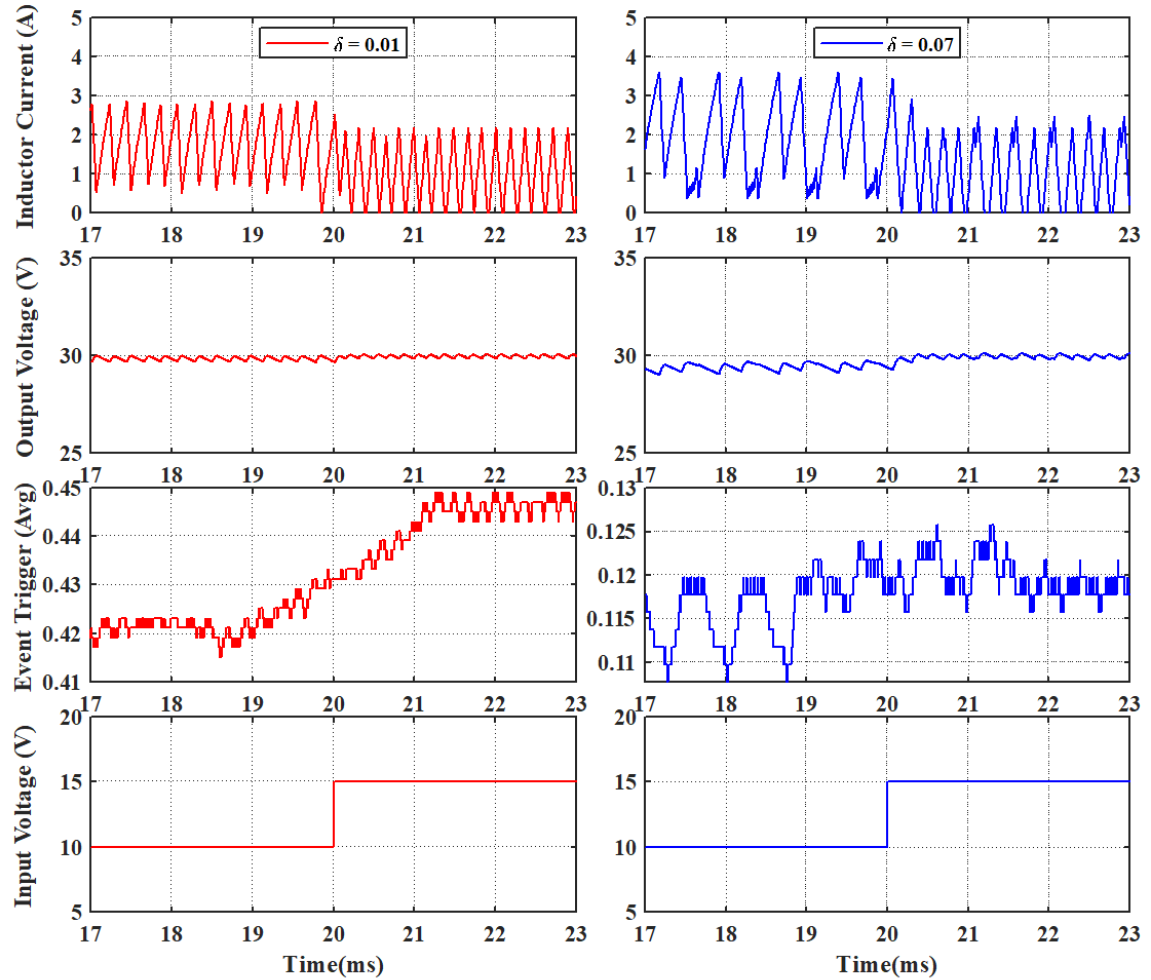


Figure 4.14: Input voltage step-up from 10V to 15V (ET-MPC)

CHAPTER FIVE

ET-MPC WITH KALMAN FILTER

5.1 Introduction and Key Concepts

MPC relies heavily on an accurate dynamic model to predict the optimal control action. Additionally, the optimal control action is determined by the initial state of the system which can be obtained by either a direct measurement or through the use of an observer for the states that cannot be directly measured. Direct measurements and observers can suffer from inaccuracies due to measurement errors, noise and tolerances on the components that are contained within the system model. This is why state estimation, which is the use of past data to determine the most likely value of the state at the current time, becomes a key component for MPC [8]. Figure 5.1 illustrates the concept of a state estimator to provide estimated states to mitigate inaccuracies.

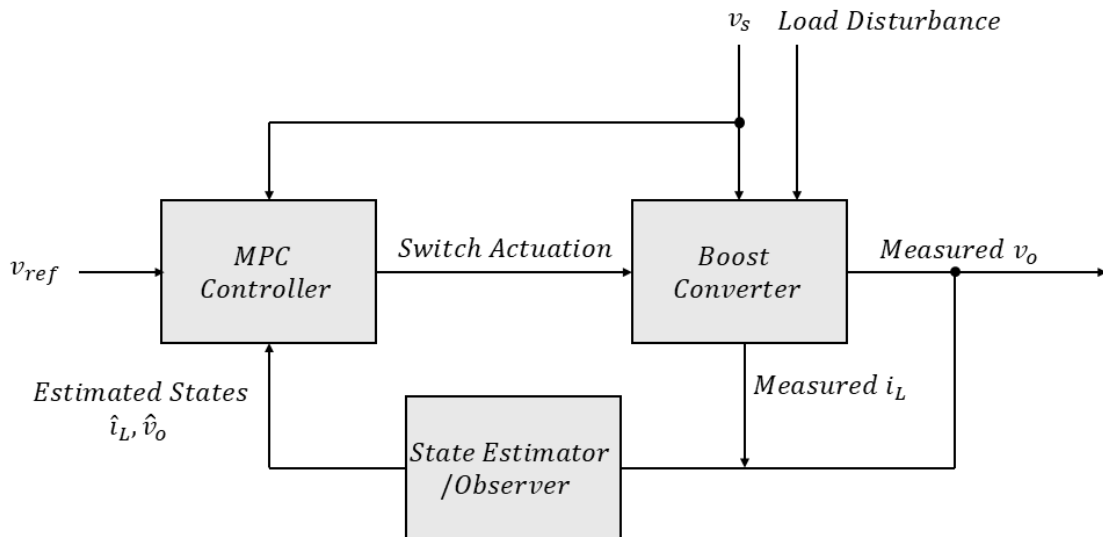


Figure 5.1: The use of a state estimator in MPC

Power converters will inevitably be exposed to disturbances or variations which will force the converter to deviate from nominal operating conditions. The control system needs to be designed so that the circuit could quickly adjust to these variations. One operating condition that has not been covered thus far is a load transient. During a load transient, the value of the resistor load changes while the nominal resistor value within the controller model, i.e., R , stays the same. Inaccuracies in the model introduced due to parameter tolerances will not allow the controller to regulate the voltage effectively. The regulation performance of the TT-MPC and ET-MPC boost converter during these conditions can be improved through the implementation of a Kalman Filter-based disturbance observer [110]. Including disturbance observers and state estimators into the MPC controller contribute to the overall robustness of the system [19, 111–114].

We will first start the chapter by reviewing key concepts related to disturbance observers and state estimation:

5.1.1 State Estimators, Observers and Filters

As discussed earlier, a state estimator estimates the state variables of a system. It does this through the examination of past data and uses current measurements along with the system model to determine the most likely value of the state at the current time. [8]

State Estimation is used to find an approximation of these variables when data may be incomplete, uncertain or unstable. A state estimator can be a filter or an observer. The term 'observer' generally refers to state estimation on a deterministic dynamical system, whereas, the term 'filter' is a mathematical tool which allows you to do state estimation on a stochastic system. Filters can also be thought of as an averaging tool for random measurements. A robust filter is one that uses a math model (e.g., a Kalman Filter).

State estimators can be divided into deterministic (e.g., Luenberger Observer) and Stochastic (e.g., Kalman Filter) state estimators. Nonlinear state estimators exist such as

Particle Filters, Extended Kalman Filters and Unscented Kalman Filters [115]. Moving Horizon Estimation is considered when using nonlinear models or considering constraints on the estimates [116]. Kalman Filters have been cited as being effective state estimators in cases of high model uncertainty and substantial noise [8, 117].

5.1.2 Observability and Disturbance Observers

Observability is the ability to observe system states without measuring the state directly. This is accomplished through an observer which uses the available measurements and a system model.

The role of a disturbance observer is to act as an inner-loop feedback controller which rejects external disturbances. Figure 5.2 shows the general concept of a disturbance observer which is to estimate the external disturbance and counteract it by subtracting from the model. Additionally, plant uncertainties can be lumped into the external disturbance as will be described below [118, 119]. The baseline controller is designed around the nominal system while the disturbance observer is designed so that the closed loop system recovers the nominal performance completely. The performance of the observer degrades gradually as the amount of disturbance and uncertainty increases [120].

5.2 Kalman Filter-based Disturbance Observer

A Kalman Filter is a state estimator for a system that has been perturbed by white noise. It uses measurements linearly related to the state but corrupted with white noise. It is especially useful to estimate a state when a direct measurement is not available, but can be inferred from indirect and noisy measurements. [121]. Kalman filtering uses the method of least squares which is the optimal estimate from noisy data [8].

For the purposes of our work, a Kalman Filter is an appropriate choice due to the use of a linearized model of the system. The Kalman filter is used to estimate the state and

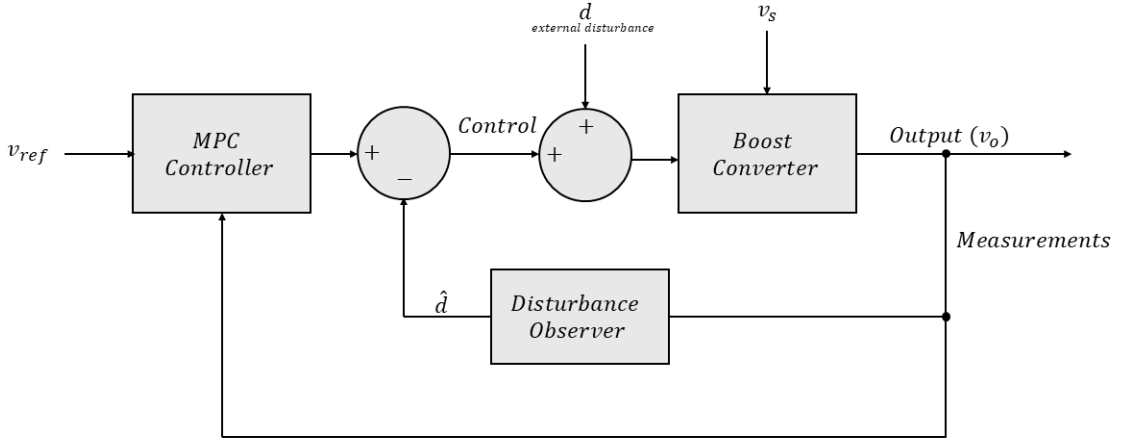


Figure 5.2: The use of a disturbance observer in MPC to eliminate the effect of disturbances

disturbances from the converter's inductor current and output voltage measurements. This is to enable tracking of the reference voltage despite the presence of model mismatch or unmeasured nonzero mean disturbances [19, 111–114].

We start with an assumption that our system and measurements contain disturbances. The system model becomes:

$$\mathbf{x}[k+1] = \mathbf{Ax}[k] + \mathbf{Bu} + w \quad (5.1a)$$

$$\mathbf{y}[k] = \mathbf{Cx}[k] + v \quad (5.1b)$$

where $\mathbf{x}[k]$ is the state variable, \mathbf{u} is the input, and \mathbf{y} is the output (or measurement). $\mathbf{x}[k+1]$ is the successor state. w represents disturbances in the model, and hence, the state, while v represents noise or inaccuracies in the measurement. w has a normal distribution with 0 mean and variance \mathbf{Q} , i.e., $w \sim N(0, \mathbf{Q})$. v also has a 0 mean and variance \mathbf{R} , i.e., $v \sim N(0, \mathbf{R})$. The larger the variance, the more uncertain we are about the parameter.

The Kalman algorithm starts with a prediction step, in which the predicted state and predicted error covariance are evaluated using the system model and previously computed state estimate and error covariance values. The second step is the estimation (or correction) step in which the Kalman gain and error covariances are computed. Additionally, the state estimate is computed using the measured value and Kalman gain. Kalman gains are updated as new measurements are obtained.

The Kalman filter is added to the MPC controller to address load variations and their effect on the model. During load transients, the value of R , in the model, changes. The disturbance estimator augments the math model of the boost converter with disturbances, i.e., we build a disturbance model. The disturbances introduced, i_e and v_e model the effect of the unmodelled load variations on the inductor current and output voltage respectively [59, 122]. The state variable is augmented with the disturbances as shown below in 5.2.

$$\mathbf{x}_{aug}[k] = \begin{bmatrix} i_L[k] & v_o[k] & i_e[k] & v_e[k] \end{bmatrix}^T \quad (5.2)$$

An augmented model of the system is generated in (5.3). The model is used in the prediction step of the Kalman Filter.

$$\mathbf{A}_{aug} = \begin{bmatrix} \mathbf{A}_m & \mathbf{0} \\ \mathbf{0} & \mathbf{I} \end{bmatrix} \quad (5.3a)$$

$$\mathbf{B}_{aug} = \begin{bmatrix} \mathbf{B}_m \\ \mathbf{0} \end{bmatrix} \quad (5.3b)$$

$$\mathbf{C}_{aug} = \begin{bmatrix} \mathbf{I} & \mathbf{I} \end{bmatrix} \quad (5.3c)$$

1. Predict state & Error Covariance before measurement:

$$\hat{\mathbf{x}}_{aug} = \mathbf{A}_{aug}\hat{\mathbf{x}}_{aug} + \mathbf{B}_{aug}v_s \quad (5.4)$$

$$\mathbf{P} = \mathbf{A}_{aug}\mathbf{P}\mathbf{A}_{aug}^{-1} + \mathbf{Q} \quad (5.5)$$

2. Calculate the Kalman gain:

$$K_m = \mathbf{P}\mathbf{C}_{aug}^{-1}/(\mathbf{C}_{aug}\mathbf{P}\mathbf{C}_{aug}^{-1} + \mathbf{R}) \quad (5.6)$$

3. Compute the estimate

Step a: Calculate the measurement residual

$$\mathbf{r}_{\text{residual}} = \begin{bmatrix} x(1) \\ x(2) \end{bmatrix} - \mathbf{C}_{aug}\hat{\mathbf{x}}_{aug} \quad (5.7)$$

Step b: Compute the estimate

$$\hat{\mathbf{x}}_{aug} = \hat{\mathbf{x}}_{aug} + K_m \mathbf{r}_{\text{residual}} \quad (5.8)$$

4. Update error covariance estimate based on measurement

$$\mathbf{P} = (\mathbf{I}(size(K_m, 1)) - K_m \mathbf{C}_{aug})\mathbf{P} \quad (5.9)$$

where m represents the different modes in (3.4) can be selected from any value $\{1, 2, 3, 4\}$ depending on the switch position and amplitude of inductor current. A_m , B_m and C represent the different state-space matrices of the original model in (3.4). P is the error covariance matrix; i.e. the variances of the estimation errors of the state vector. K_m are the Kalman gains for the different operating modes in Figure 3.6.

The covariance value, R , is adjusted so that the Kalman filter gives a lower weight to measurement errors by assigning a low value for R . This means that we have high confidence in our measurements and do not require compensation. However, a higher

weight is assigned to the disturbance states in Q in anticipation of process variability or model mismatches. The Kalman filter will estimate the disturbances i_e and v_e , where v_e will then be fed back to the MPC controller to compensate for the error by subtracting it from the reference. The updated reference becomes:

$$v'_{o,ref} = v_{o,ref} - v_e \quad (5.10)$$

5.3 Modified Objective Function

An additional improvement to our ET-MPC was introduced to penalize any control sequence that would allow the inductor current to deviate greatly from a reference inductor current that we define in (5.12b). The updated (OCP) is formulated as follows:

$$\min_{U_o} \sum_{\ell=k}^{k+N-1} (|v_{o,err}(\ell+1|k)| + \lambda_u |\Delta u(\ell|k)| + \lambda_{i_L} |i_{L,err}(\ell+1|k)|) \quad (5.11a)$$

$$\text{s.t. System dynamics (3.4)} \quad (5.11b)$$

where the absolute voltage error for the calculated output voltage is ($v_{o,err}(k) = v'_{ref} - v_o(k)$) and the difference in switch state is ($\Delta u(k) = u(k) - u(k-1)$). The weighting factor, λ_u , is applied to the difference between the two consecutive switching states to adjust the amount of switching. λ_{i_L} , is adjusted to control the influence of the inductor current error. The inductor current error is defined by: ($i_{L,err}(k) = i_{L,ref} - i_L(k)$), where, $i_{L,ref}$ in (5.12b) is derived through solving (5.12a):

$$v_s i_{L,ref} = R_L i_{L,ref}^2 + \frac{v'_{o,ref}^2}{R} \quad (5.12a)$$

$$i_{L,ref} = \frac{v_s}{2R_L} - \sqrt{\left(\frac{v_s}{2R_L}\right)^2 - \frac{v'_{o,ref}^2}{RR_L}} \quad (5.12b)$$

Equation (5.12a) represents the general power equation $P_{in} = P_{out}$, where the input power P_{in} , is equal to the inductor current $i_{L,ref}$ multiplied by the input voltage, v_s . As an

estimate, we equate P_{in} to the losses in the inductor series resistance, R_L , added to the power delivered to the load ($v_{o,ref}^2/R$). The updated algorithm is defined in (5.1).

The value of $i_{L,ref}$ in (5.12b) is dependent on the load impedance, R . During load transients, the value of R changes with time. One approach is to implement an adaptive Kalman filter to estimate this parameter in real-time similar to the method proposed in [123].

In order to compensate for load variations, the inductor current disturbance calculated by the Kalman filter is subtracted from the inductor current reference, so that the updated inductor current reference becomes $i'_{L,ref}$ in (5.13)

$$i'_{L,ref} = i_{L,ref} - i_e \quad (5.13)$$

5.4 Implementation and Simulation Results

The block diagram for the updated ET-MPC system with Kalman-Filter is shown in 5.3. Both output voltage and inductor current disturbances, v_e and i_e are introduced into the diagram to eliminate any disturbances caused by model mismatches.

The event-triggered Kalman-based MPC controller was implemented in MATLAB/SIMULINK. The parameters used in the simulation are listed in Table 5.1. The performance of the system is evaluated during start-up and step changes in the input voltage, reference voltage and load. TT-MPC is implemented using the same system, with the event-trigger threshold δ is set to 0.

By substituting the values in Table (5.1) in Eq. (3.14), we find that the minimum event frequency achievable is 1/12, or approximately 8.33%. The maximum computational savings per second can be found by substituting the parameters from Table (5.1) and the values found in Eq. (3.15)

Algorithm 5.1: Event-Triggered MPC Algorithm

```
procedure ETMPC( $u, U_{t1}, X_{t1}, t, i_L, v_o, v_s$ )
     $J^*(k) = \infty$ 
     $t \leftarrow t + T_s$ 
     $k \leftarrow$  select  $k$  from  $T$  using  $t$  see Table (3.1)
     $e \leftarrow$  compute (3.9)
    if  $e = 1$  then
         $t \leftarrow 0$ 
        for all  $U$  over  $N$  do
             $J = 0$ 
            for  $\ell = k$  to  $k + N - 1$  do
                 $x(\ell + 1) \leftarrow$  compute from (3.4), (5.2) and (5.3)
                 $J \leftarrow$  compute from (5.11)
            end
            if  $J < J^*(k)$  then
                 $J^*(k) = J, u = U(1)$ 
            end
        end
         $U_t \leftarrow U$ 
         $X_t \leftarrow x$ 
    end

    if  $e = 0$  then
         $u \leftarrow U_{t1}(k)$ 
         $U_t \leftarrow U_{t1}$ 
         $X_t \leftarrow X_{t1}$ 
    end
return  $u, t, U_t, X_t$ 
end procedure
```

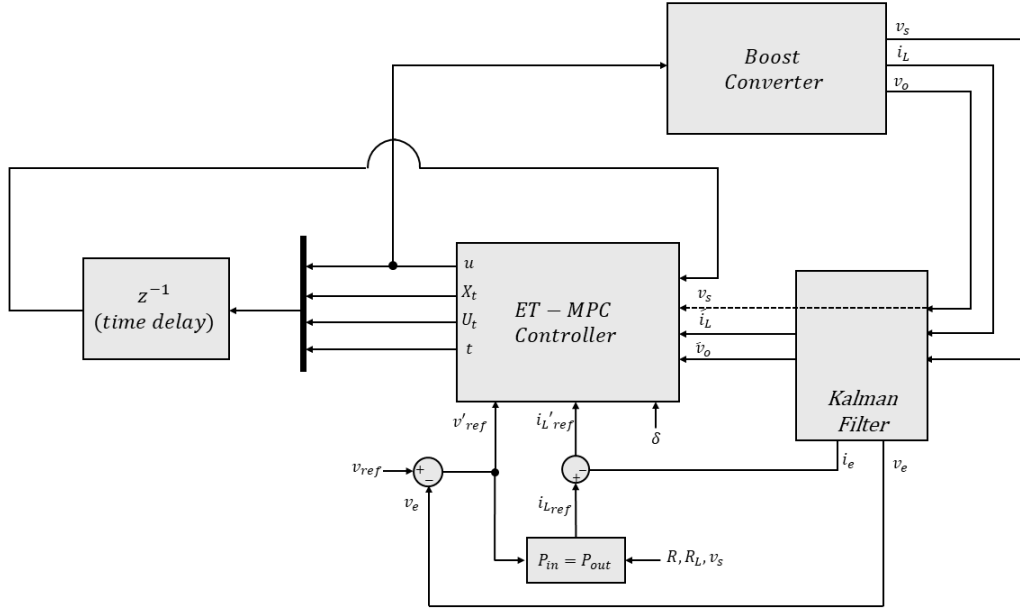


Figure 5.3: DC-DC boost converter with ET-MPC control and Kalman Filter-based DOB

5.4.1 Converter Startup

The startup time of the converter was evaluated at different input voltages and output voltage references for both the time-triggered and event-triggered controllers. The results are listed in Table 5.2. The startup time is comparable for both implementations with no overshoot observed. The simulated inductor current and output voltage waveforms for the test case $V_{in} = 10V, V_{out} = 15V$ are plotted in Figure 5.4 and Figure 5.5. The event-trigger threshold of the MPC controller was set to $\delta = 0.025$. The number of event triggers are averaged using a moving average window of 200 and plotted.

During startup, switch S remains in the open position allowing the output capacitor to charge and subsequently provide load current which causes an initial inrush of current. The current is only limited by the inductor resistance R_L . Limiting this inrush current in Boost converters cannot be done through the control of the switch, but can be achieved

through external means such as employing a pre-charge resistor. After the output capacitor voltage equals the input voltage (neglecting the diode voltage drop), the voltage across the inductor becomes zero. At that point, the inductor current begins to drop and the voltage across the inductor reverses ($v_L = L(di/dt)$) which allows the diode D to remain forward biased and the output voltage to rise above the input voltage. However, the output voltage cannot be maintained in this manner due to the load demand and will begin to slightly drop, at this point, the controller will begin to actuate the switch S , and the converter will boost the output voltage to the voltage setpoint ($v_{o,ref}$).

Note that during the converter's initial operation, the event frequency is at its highest value (50%) due to the difference between output voltage and reference voltage (Figure 5.5). Once the output voltage reaches the reference voltage in steady-state, the inductor current decreases. Once the converter reached DCM operation, the event frequency significantly decreased (15%). In [105], it was found that the start-up time was mostly independent on the selection of the event-trigger threshold δ value, but was dependent on operating conditions.

The plots in Figure 5.6 show the gate signals, counter and instances of event triggers during steady-state operation when $v_{in} = 10V$ and $v_{o,ref} = 15V$. Since k_{max} is set to 6, $T_s = 5\mu s$, $N_1 = 4$ and $n_s = 4$, the maximum counter value is calculated to be $60\mu s$ ($t_{max} = N_1 T_s + n_s(k_{max} - N_1)T_s$). In the actual implementation, we set the maximum counter value to $55\mu s$. The optimal switching sequences in the time duration $4ms$ and $5ms$ are listed in Table 5.3. Any switching values with an index above 6 are discarded in the control. If we analyze the behavior of the controller at time instance immediately before $4.3ms$. An event is triggered at that instant and the optimal switch sequence is found to be $U_t[k] = [0, 0, 0, 0, 0, 0]$. For the duration of $55\mu s$, the sequence $U_t[k]$ is reused to actuate the main switch before triggering the next event due to reaching the maximum limit set for the counter t . The next event is triggered at $4.39ms$ which still finds that the same optimal

Table 5.1: Simulation Parameters - Boost Converter with Kalman Filter

Converter and Controller Parameter	Value
Input Voltage (v_s)	15V
Output Voltage ($v_{o,ref}$)	30V
Inductor (L)	$450\mu H$
Inductor DC Resistance (R_L)	0.8Ω
Output Capacitance (C)	$220\mu F$
Load Resistance (R)	$73\Omega \rightarrow 42\Omega$
Sampling Period (T_s)	$5\mu s$
Prediction Horizon (N)	14
N_1	4
Move Blocking Coefficient (n_s)	4
Allowable Optimal Switching Elements (k_{max})	6
Switching - Weighting Factor (λ_u)	0.35
Inductor Current - Weighting Factor (λ_{iL})	0.1
Minimum event frequency (f_{min-ET})	8.33%

Table 5.2: Start-up Time Summary

Operating Conditions	TT-MPC	ET-MPC
$v_s = 10V, v_o = 15V$	1.4ms	1.4ms
$v_s = 10V, v_o = 20V$	3.5ms	3.25ms
$v_s = 10V, v_o = 25V$	7.3ms	7.5ms
$v_s = 10V, v_o = 30V$	14.5ms	14.5ms
$v_s = 15V, v_o = 20V$	1.5ms	1.5ms
$v_s = 15V, v_o = 25V$	2ms	2ms
$v_s = 15V, v_o = 30V$	3.75ms	3.75ms

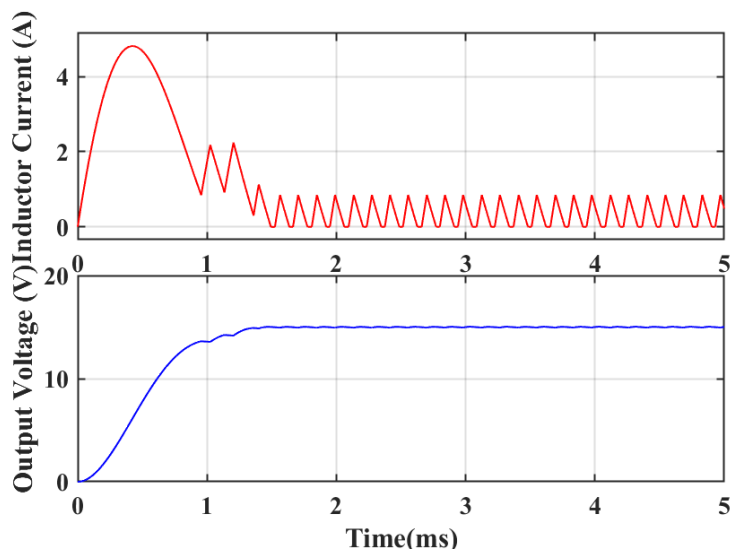


Figure 5.4: Start-up (TT-MPC)

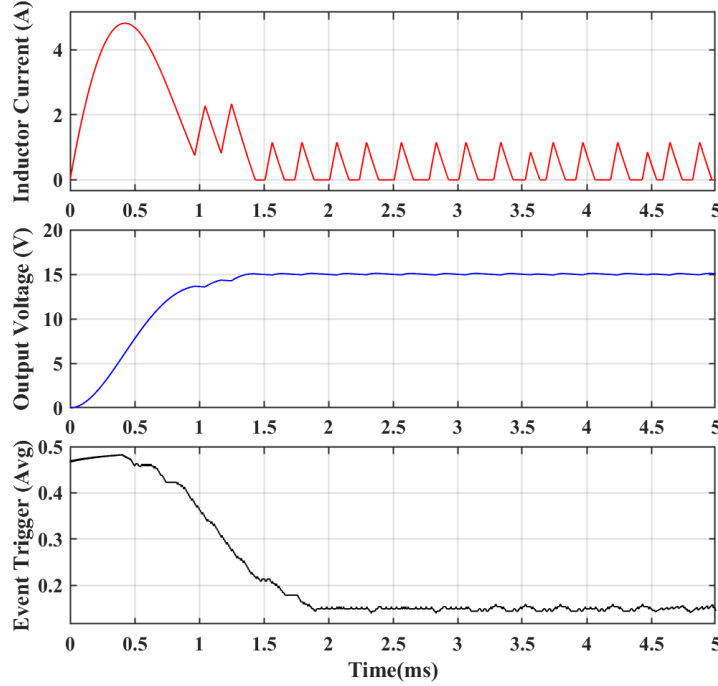


Figure 5.5: Start-up (ET-MPC)

switch state viable to maintain regulation, however, at $4.435ms$, the optimal switch sequence is updated to $U_t[k] = [1, 1, 1, 1, 1, 0]$.

5.4.2 Steady-state Operation

The performance evaluation of the ET-MPC boost converter in [104, 105] in addition to our findings here, show that increasing the trigger threshold δ significantly reduces the computational effort of the controller during steady-state operation but that the tracking error, calculated using (4.1), increased. Increasing δ also increased the output voltage ripple and peak inductor current, and in some cases, the converter was not able to reach regulation, thus, putting a limit to our threshold selection.

The converter and controller parameters in this work slightly differ from what was evaluated in the previous chapter, and the threshold value is selected differently to achieve

Table 5.3: Optimal Switching Sequences in time duration between $4ms$ and $5ms$ in Figure 5.6

Time Duration	$U_t[1]$	$U_t[2]$	$U_t[3]$	$U_t[4]$	$U_t[5]$	$U_t[6]$
$4ms \rightarrow 4.165ms$	0	0	0	0	0	0
$4.165ms \rightarrow 4.205ms$	0	1	1	1	1	0
$4.205ms \rightarrow 4.245ms$	1	1	1	1	0	0
$4.245ms \rightarrow 4.435ms$	0	0	0	0	0	0
$4.435ms \rightarrow 4.475ms$	1	1	1	1	1	0
$4.475ms \rightarrow 4.57ms$	0	0	0	0	0	0
$4.57ms \rightarrow 4.61ms$	0	1	1	1	1	0
$4.61ms \rightarrow 4.65ms$	1	1	1	1	0	0
$4.65ms \rightarrow 4.8ms$	0	0	0	0	0	0
$4.8ms \rightarrow 4.84ms$	0	1	1	1	1	0
$4.84ms \rightarrow 5ms$	0	0	0	0	0	0

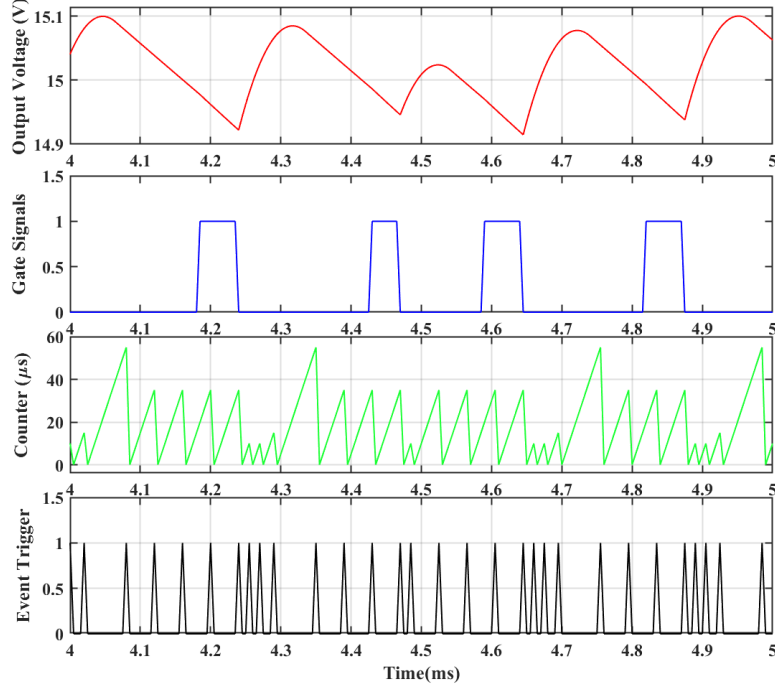


Figure 5.6: Steady-State (ET-MPC) $v_s = 10V$, $v_{o,ref} = 15V$

comparable results to a time-triggered controller. A comparison between TT-MPC and ET-MPC event frequency, tracking error and output ripple results are tabulated in Table 5.4.

As for our simulation results, the TT-MPC results are reported under $\delta = 0$. As the trigger threshold increases, the performance of the converter begins to degrade. Additionally, it was noted, that implementing an ET-MPC strategy results in reduced switching frequency from the TT-MPC formulation utilizing similar parameters. The switching frequency also reduces as the trigger-threshold is increased. Another observation is that the event frequency increases as the difference between the input and output voltage widens. A trade-off between the performance criteria and computational burden needs to be made when selecting the appropriate trigger-threshold [105].

Table 5.4: Event-trigger Impact on Steady-state Operation - Results Summary

Event Frequency:				
Steady-State Conditions	$\delta = 0.00$	$\delta = 0.01$	$\delta = 0.015$	$\delta = 0.025$
$v_s = 10V, v_o = 15V$	100%	24.6%	17.37%	15%
$v_s = 10V, v_o = 20V$	100%	34.7%	25.6%	17.3%
$v_s = 10V, v_o = 30V$	100%	37.5%	36%	28.5%
$v_s = 15V, v_o = 30V$	100%	34.4%	32.8%	23.8%

Tracking Error [V]:				
Steady-State Conditions	$\delta = 0.00$	$\delta = 0.01$	$\delta = 0.015$	$\delta = 0.025$
$v_s = 10V, v_o = 15V$	0.024	0.025	0.059	0.058
$v_s = 10V, v_o = 20V$	0.03	0.03	0.035	0.06
$v_s = 10V, v_o = 30V$	0.082	0.124	0.175	0.153
$v_s = 15V, v_o = 30V$	0.081	0.113	0.113	0.146

Output Ripple [Vp-p]:				
Steady-State Conditions	$\delta = 0.00$	$\delta = 0.01$	$\delta = 0.015$	$\delta = 0.025$
$v_s = 10V, v_o = 15V$	0.082	0.0945	0.1785	0.1854
$v_s = 10V, v_o = 20V$	0.097	0.11	0.177	0.219
$v_s = 10V, v_o = 30V$	0.134	0.24	0.273	0.31
$v_s = 15V, v_o = 30V$	0.085	0.24	0.24	0.12

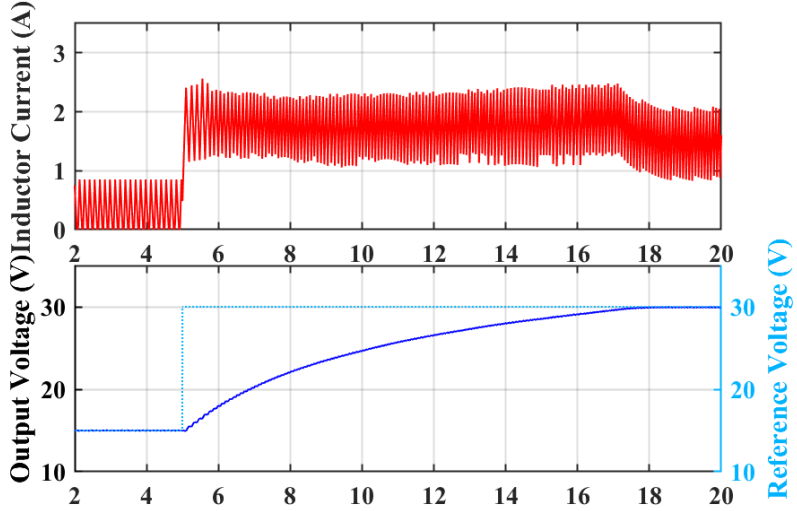


Figure 5.7: Reference voltage step-up from 15V to 30V (TT-MPC)

5.4.3 Step Changes in the Output Reference Voltage

Results were recorded while stepping up the output reference voltage from 15V to 30. The input voltage was set to 10V. The response time of the converter with different trigger thresholds was evaluated and recorded in Table 5.5. As observed from Figure 5.7 and Figure 5.8, the output achieves a regulated 30V within 13ms for both TT-MPC and ET-MPC. During the transition, the event frequency, switching frequency and inductor current increase. The inductor current rms increases due to increase in load demand. Once the converter reaches regulation, the inductor current and event frequency are reduced. The transient time is similar for both time-triggered and event-triggered, and as noted above, utilizing the ET-MPC controller results in a reduced switching frequency for similar operating conditions experience when using the TT-MPC controller.

Figure 5.9 and Figure 5.10 show simulation results when the voltage reference was stepped down from 25V to 15V. Switch S remains OFF as the inductor current reduces to zero allowing the capacitor to discharge into the load to reduce the output voltage. The

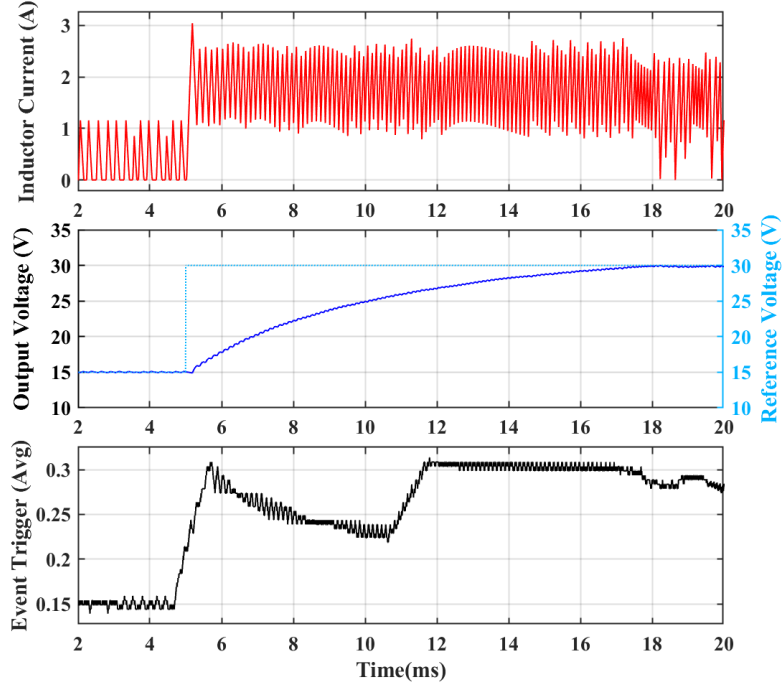


Figure 5.8: Reference voltage step-up from 15V to 30V (ET-MPC)

converter's regulation is almost equivalent for the two techniques, with the average number of computations significantly reduced with the latter method. The transient time was also similar for the two control techniques. The results for two different thresholds along with the TT-MPC implementation is summarized in Table 5.5.

One issue we had not accounted for originally in our work, prior to adding inductor current to the OCP (5.11), was inductor saturation. 5.11 shows the test result for when the reference voltage was stepped down from 20V to 15V at 10ms and $\delta = 0.005$. It was noted that without adding inductor information into the cost function, and in certain scenarios when the step down in reference voltage occurred as the inductor current was increasing (i.e. Switch S was *ON*), that the OCP would keep the switch *ON*, and only turn it to the *OFF* position to regulate the voltage. This is because the OCP found that to be

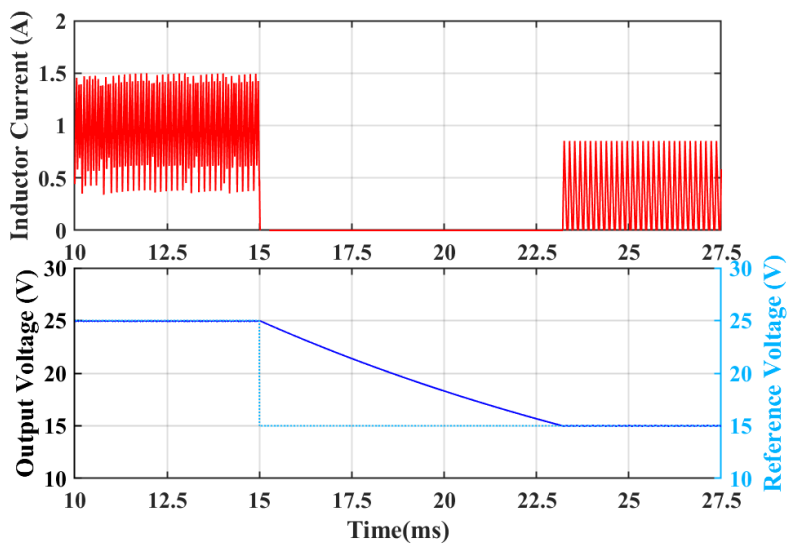


Figure 5.9: Reference voltage step-down from 25V to 15V (TT-MPC)

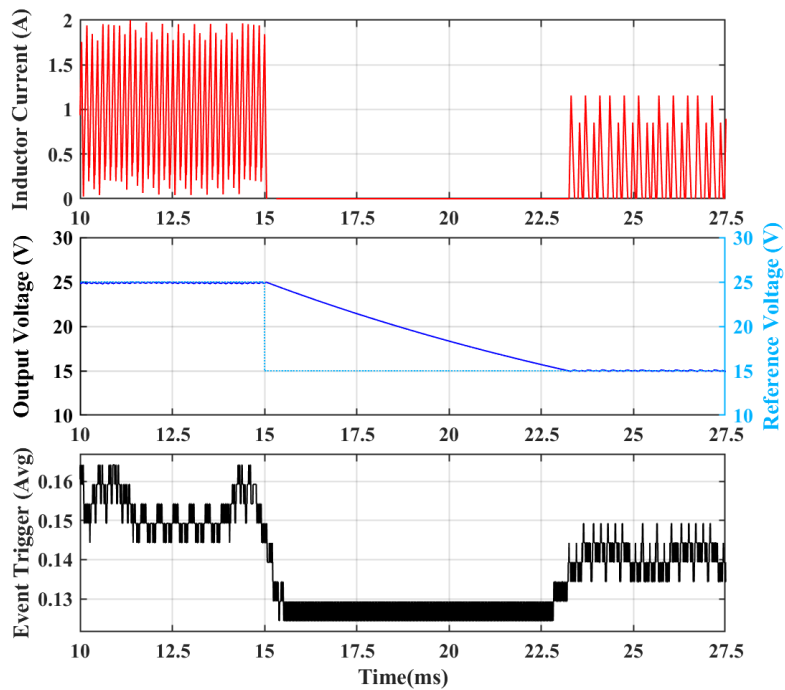


Figure 5.10: Reference voltage step-down from 25V to 15V (ET-MPC)

Table 5.5: Voltage Reference Converter Response for Different Event Thresholds

	$\delta = 0.00$	$\delta = 0.015$	$\delta = 0.025$
$v_{o,ref} = 15V \rightarrow 30V, v_s = 10V$			
Transient time [ms]	13ms	13ms	13ms
Event Frequency	100%	40%	30%
$v_{o,ref} = 25V \rightarrow 15V, v_s = 10V$			
Transient time [ms]	8ms	8ms	8ms
Event Frequency	100%	25%	13%

the optimal solution. One quick remedy for the issue is to shift the step-down in reference voltage so that it coincides with a decrease in inductor current (i.e. switch S is in the *OFF* position) as observed in Figure 5.12. While this fixes the issue, it is not a practical solution. Figure 5.13 shows the same operating conditions with the inductor current added to the cost function which solved the issue with inductor saturation.

5.4.4 Step Change in the Input Voltage

The ability of a converter to reject disturbances at the input source is a key requirement of any power converter controller. In Figure 5.14 and Figure 5.15, the input voltage is stepped up from 10V to 15V at 20ms after steady state operation with $v_{o,ref}$ set to 30V. The line transient response of the converter in both time-triggered and event-triggered formulations is similar showing that the converter is able to maintain the output voltage. The event frequency during the transient decreases by 6% as the difference between the input and output voltage decreases.

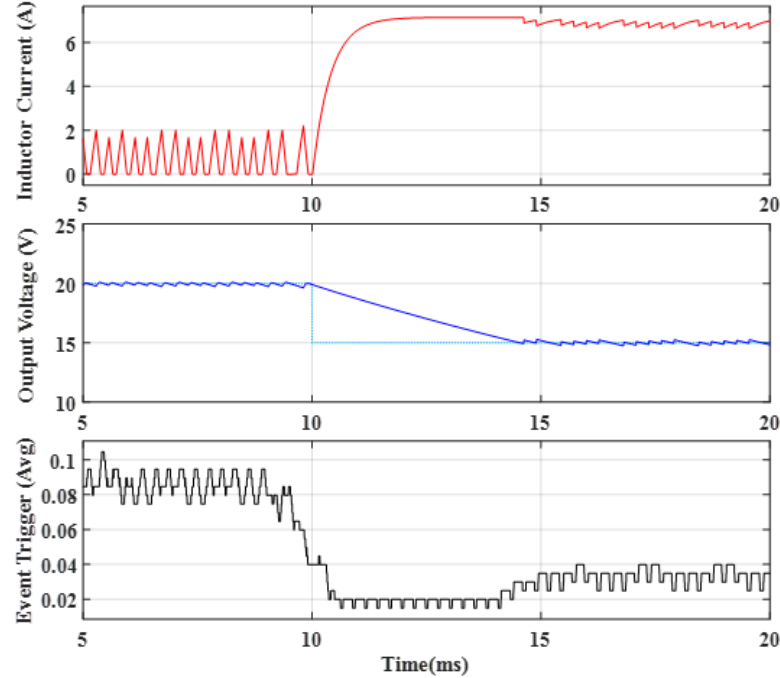


Figure 5.11: Inductor Saturation (No current information in OCP)

5.4.5 Response to Load Transients

The load resistance R is reduced from 73Ω to 42Ω to simulate an increase in load demand. The change in load resistance is not captured in the MPC controller which results in inaccuracies of the control. Without compensating for the change in load, the output voltage will begin to sag and the controller will not be able to regulate the converter to the reference voltage. The Kalman Filter is used to estimate the measured inductor current, output voltage and disturbance variables i_e and v_e . The estimated voltage error is then subtracted from the voltage reference to adjust for disturbances in the load. While the estimated inductor current error is subtracted from the inductor current reference.

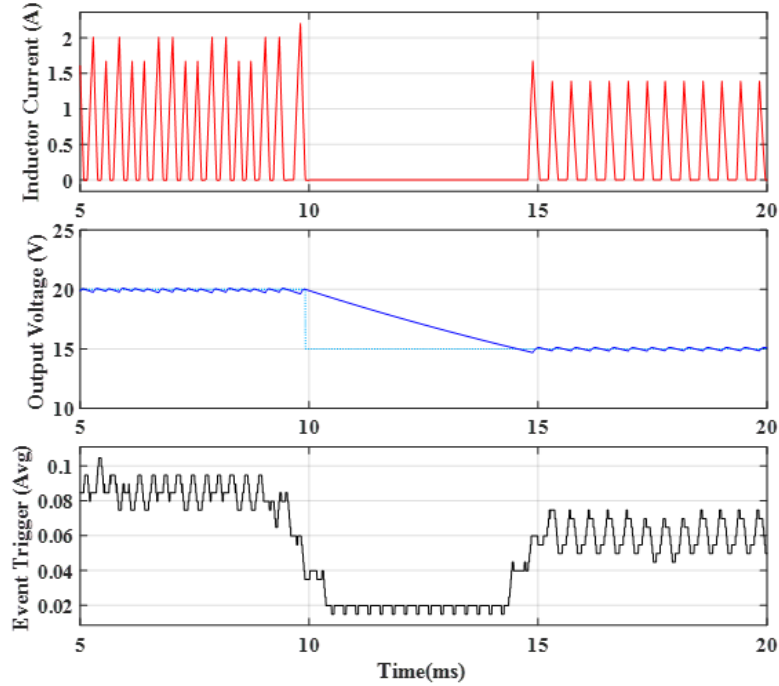


Figure 5.12: Inductor Saturation Addressed: Shifted Voltage Reference from 10ms to 9.92ms

The output reference voltage is set to 30V and input voltage set to 15V. The covariance matrices for process noise, Q , and measurement noise, R , are assigned the values in (5.14):

$$Q = \begin{bmatrix} 0.1 & 0 & 0 & 0 \\ 0 & 0.1 & 0 & 0 \\ 0 & 0 & 50 & 0 \\ 0 & 0 & 0 & 50 \end{bmatrix} R = \begin{bmatrix} 1 & 0 \\ 0 & 1 \end{bmatrix} \quad (5.14)$$

The time-triggered simulated waveform is shown in Figure 5.16. The undershoot measured 0.3V which is equivalent to 1% of the reference voltage. The settling time for the transient was 2ms and the converter was able to return to regulation.

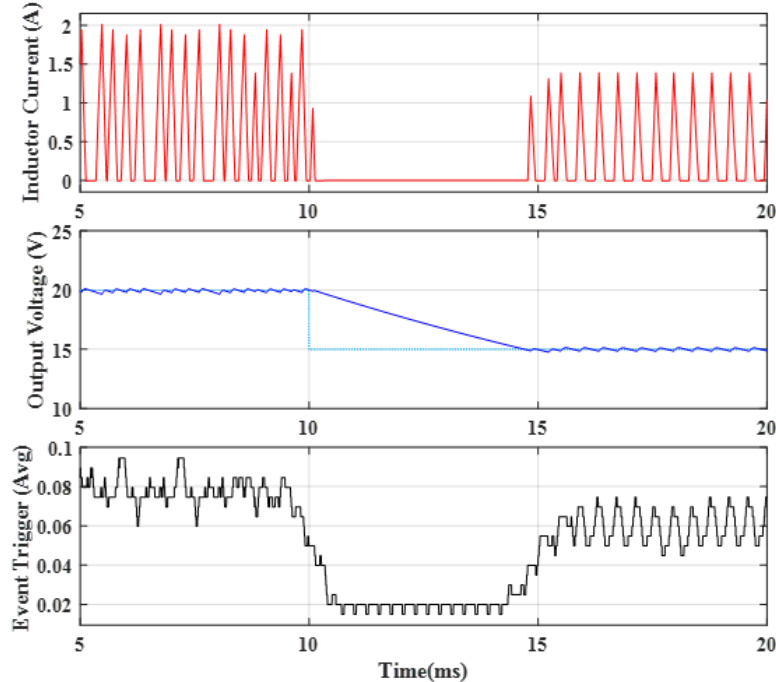


Figure 5.13: Inductor Saturation Addressed: Add Inductor Current to OCP

The output voltage when a load transient was applied to the converter using ET-MPC control with δ set to 0.01 is shown in Figure 5.17. The undershoot was 1%; similar with the TT-MPC result, but with a faster settling time 1.1ms. When the threshold was set to $\delta = 0.025$ the voltage was able to return to regulation within 1ms; the undershoot was also 1% (Figure 5.18). The aforementioned results are tabulated in Table 5.6. The results show that ET-MPC can reduce the overall computational burden of TT-MPC, but the trade-off is higher peak inductor current and output voltage ripple.

5.4.6 ET-MPC Impact on Efficiency

The efficiency of the converter is defined in (5.15)

$$\eta = \frac{P_{in} - P_{loss}}{P_{in}} \times 100\% \quad (5.15)$$

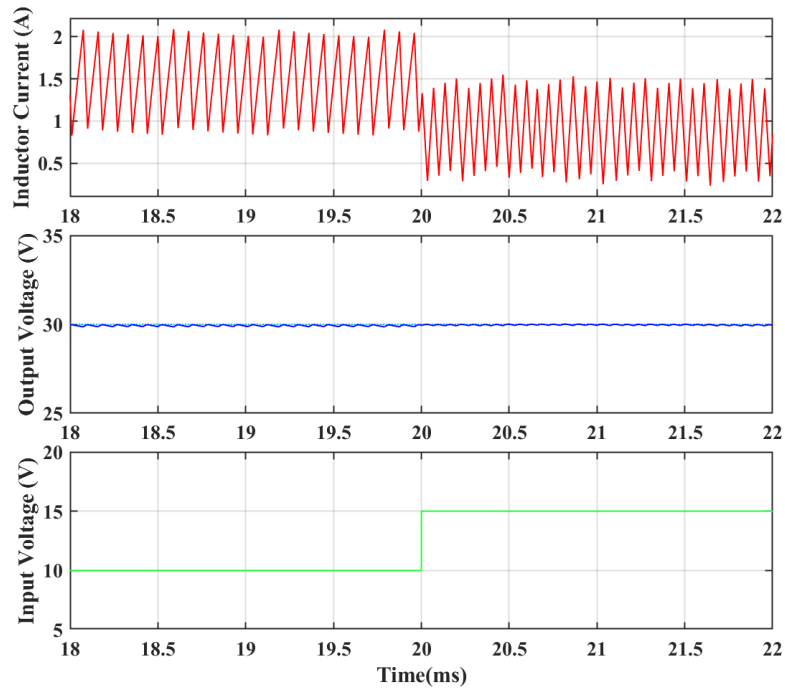


Figure 5.14: Input voltage step-up from 10V to 15V (TT-MPC)

Table 5.6: Load Transient Results

	$\delta = 0.00$	$\delta = 0.01$	$\delta = 0.025$
$R = 73\Omega \rightarrow 42\Omega$			
Undershoot (V)	$0.3V$	$0.3V$	$0.3V$
Undershoot (%)	1%	1%	1%
Settling time (ms)	$2ms$	$1.1ms$	$1ms$

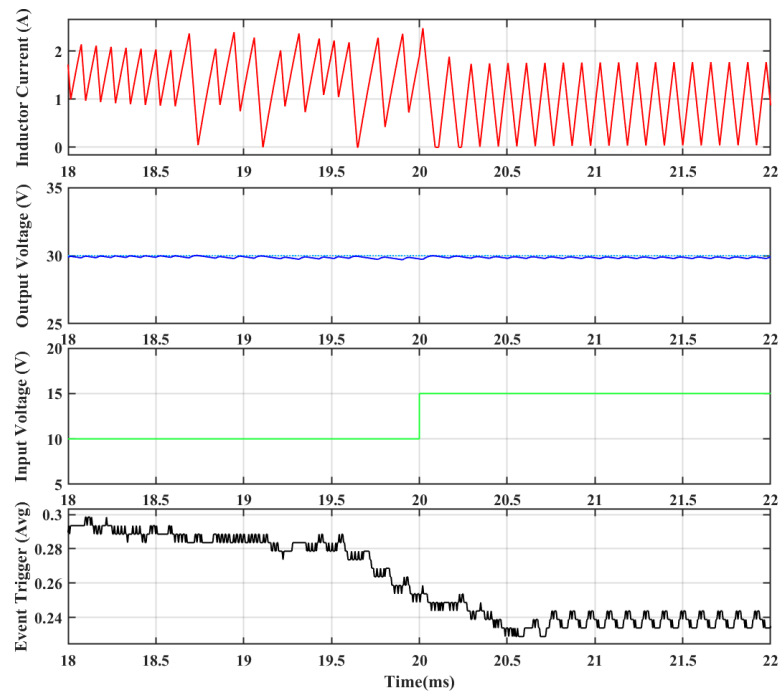


Figure 5.15: Input voltage step-up from 10V to 15V (ET-MCP)

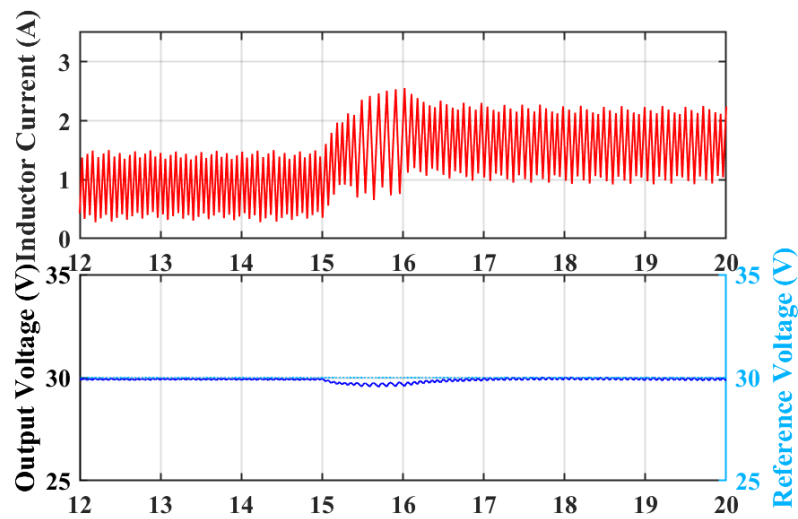


Figure 5.16: Load Transient for TT-MPC

Chapter 2 gave a brief introduction to the main components of converter power loss which can be divided into switching and conduction losses. In our example, the major power loss (P_{loss}) contributors in the boost converter are due to the non-idealistic characteristics of the power switch S , the inductor L and the diode D . Additional losses are due to magnetic core loss, capacitor $I_{rms}^2 ESR$ loss, and fixed power losses to power ancillary circuitry. These additional losses will be ignored in this evaluation. The total power loss can be approximated as shown in (5.16):

$$P_{loss} = P_{Switch} + P_{Diode} + P_{L,inductor} \quad (5.16)$$

To evaluate the impact of ET-MPC to the baseline TT-MPC, the following assumptions are made:

- The boost converter is operating at light load in which switching losses are dominant at 30% of the total loss. Switching losses are directly proportional to the switching frequency.
- While the on-resistance of the MOSFET, $R_{ds,on}$, was not included in our analysis, a general assumption is made in which conductive losses in switch S are approximately 20% of the total loss. Conductive losses in the switch increase quadratically as the rms current increases; i.e., $I^2 R$ losses.
- Inductor losses are estimated to be 30% of the total loss. Similar to the switch, these losses increase quadratically as the inductor rms current increases.
- Diode conductive losses are estimated to be 20% of the total loss and are directly proportional to the increase of diode current ($P_{diode} = I_D V_D$).

With these assumptions, a general evaluation of the impact of ET-MPC to the efficiency of the converter can be conducted. Table 5.7 compares the rms currents in the

inductor, switch and diode to the baseline TT-MPC converter when the load is set to 42Ω ($v_s = 15V, v_{o,ref} = 30V$). The factors are then used to calculate the impact of ET-MPC to power loss.

Table 5.7: ET-MPC Impact to Efficiency

	$\delta = 0.00$	$\delta = 0.01$	$\delta = 0.025$
Inductor current (rms)	I_L	$1.02 \times I_L$	$1.01 \times I_L$
Diode current (rms)	I_D	$1.025 \times I_D$	$1.07 \times I_D$
Switch current (rms)	I_S	$1.01 \times I_S$	$1.09 \times I_S$
Switching frequency (kHz)	f_{sw}	$0.73 \times f_{sw}$	$0.61 \times f_{sw}$
P_{loss}	P_{loss}	$0.93 \times P_{loss}$	$0.87 \times P_{loss}$

It was found that the power loss is reduced when ET-MPC is implemented on the TT-MPC boost converter. This is mainly due to the switching loss being the major contributor to power loss at light loads. ET-MPC reduces the switching frequency by a factor of approximately 0.73 when $\delta = 0.01$ which leads to the reduction in switching losses. An increase in the trigger threshold δ also reduces the switching losses and hence, further reduction in power losses can be achieved. These assumptions and findings can be verified through hardware implementation.

5.5 Remarks

In this chapter, several improvements were introduced to enhance the performance of the event-trigger MPC scheme for the boost converter. The first was the introduction of

a Kalman Filter-based disturbance observer which enabled the controller to provide offset-free tracking of the reference voltage. This was done through augmenting the system model by introducing disturbances [112]. There are several parameters that impact the performance of our boost converter ET-MPC controller. The influence of the trigger threshold, δ , was briefly evaluated in this work while its selection criteria and performance impact was extensively explored in [105]. Generally, increasing the trigger threshold reduces the computational burden, but increases tracking error, output ripple and peak inductor current. Additional parameters include the switching weighting factor λ_u which penalizes switching and can be used to control the switching frequency. The inductor current weighting factor λ_{i_L} , penalizes the error between the inductor reference and measured inductor current. Increasing this value increases the tightness of current control and prevents inductor saturation but excessively increasing this value can cause the controller to lose voltage regulation. Another factor is k_{max} , which is the maximum allowable number of elements that can be used in the switching sequence. Reducing this number improves the performance of the control but increases the computational burden as more events are triggered.

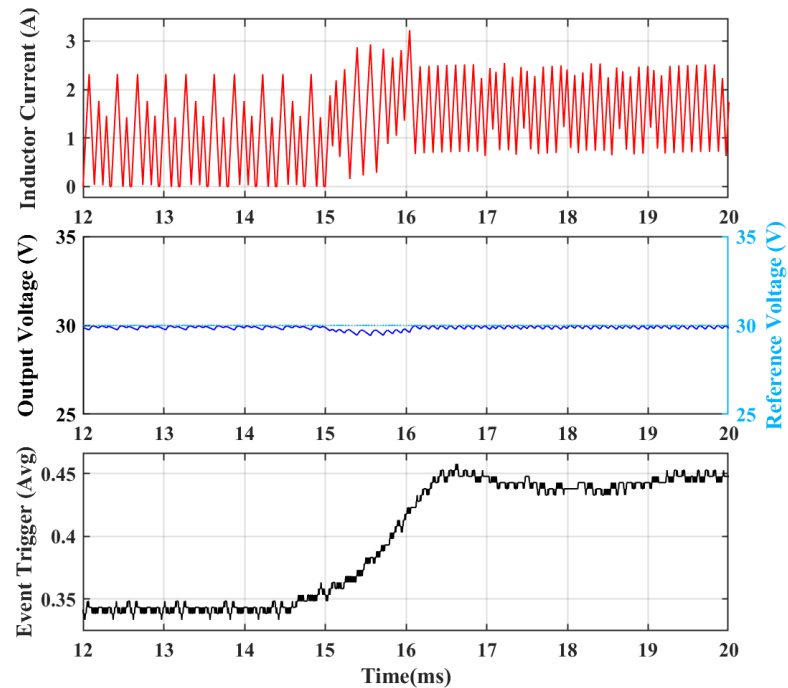


Figure 5.17: Load Transient for ET-MPC, $\delta = 0.01$

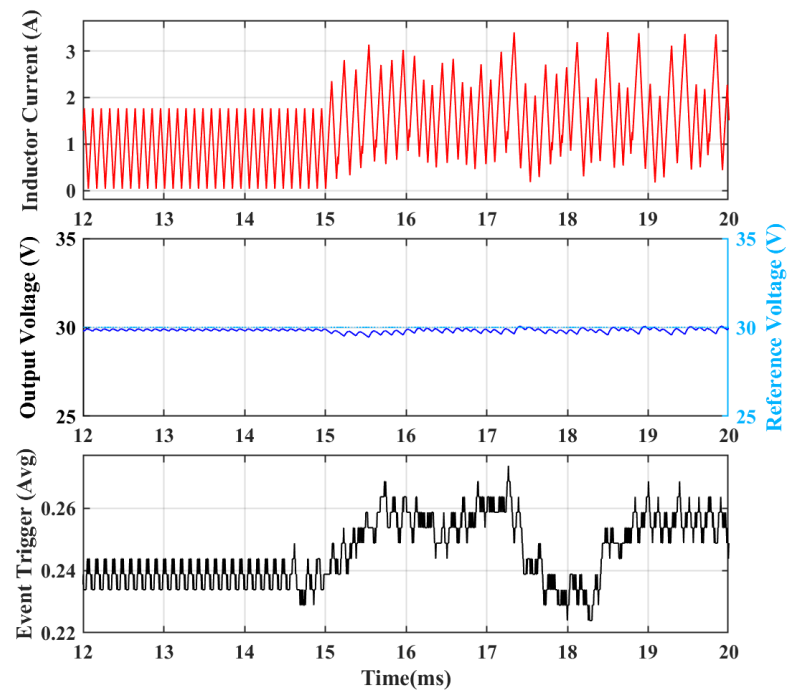


Figure 5.18: Load Transient for ET-MPC, $\delta = 0.025$

CHAPTER SIX

ET-MPC FOR BUCK CONVERTER

6.1 Buck Converter

A buck converter is a step-down converter that provides an output voltage that is less than its input voltage. Buck converters are prevalent in power conversion applications since power is transmitted more efficiently at higher voltages while loads typically require lower voltages for operation either for safety or other reasons. Buck converters can be found in many applications such as battery chargers, computers and audio amplifiers. Isolated buck-derived converters, such as full-bridge isolated converters, which are found on hybrid and electric vehicles, can convert power from the 400V battery to charge the 12V battery and provide power to the 12V bus.

The topology of a dc-dc buck converter is shown in Figure 6.1. Unlike the boost converter, the inductor current flows continuously to the output and so the output capacitor does less work in supporting the output and sees less AC currents [46].

Similar to our previous work on the boost converter, we will develop the main components of the time-triggered enumerated-based MPC controller for the buck converter and then implement a similar event-triggered MPC controller.

6.2 Discrete Mathematical Model

6.2.1 Continuous-time Model

Three different operating modes can be defined for the buck converter 6.1 depending on the position of switch S and the inductor current during a single time step, T_S . The first mode is when the switch is *ON* and inductor current is positive and increasing. In this mode, the diode is *OFF*. The second mode is when the switch is *OFF*. In this case, the inductor will induce a voltage that will force the current to continue

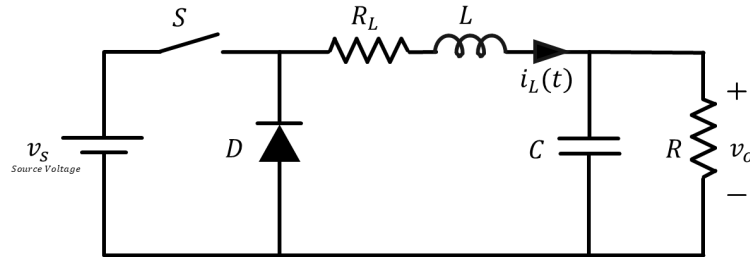


Figure 6.1: Buck converter circuit diagram

flowing in the same direction through the diode to the load. The third mode is when the switch is *OFF* and the inductor current reaches zero, in this case, the diode is also *OFF*. This corresponds to Discontinuous Conduction Mode (DCM).

The next step is to develop state-space equations for each mode using the state variable defined in 3.1, where i_L is the inductor current and v_o is the output voltage (capacitor voltage).

The state-space equations for each mode are defined in 6.1.

Mode 1 is realized when Switch S is *ON*, i_L is positive and increasing, and diode D is not conducting. This mode is represented with (6.1a) state equation:

$$\dot{x}(t) = \begin{bmatrix} -\frac{R_L}{L} & -\frac{1}{L} \\ \frac{1}{C} & -\frac{1}{RC} \end{bmatrix} x(t) + \begin{bmatrix} -\frac{1}{L} \\ 0 \end{bmatrix} v_s(t) \quad (6.1a)$$

Mode 2 is realized when Switch S is *OFF*, i_L is positive and decreasing, and diode D is conducting. This mode is represented with (6.1b):

$$\dot{x}(t) = \begin{bmatrix} -\frac{R_L}{L} & -\frac{1}{L} \\ \frac{1}{C} & -\frac{1}{RC} \end{bmatrix} x(t) + \begin{bmatrix} 0 \\ 0 \end{bmatrix} v_s(t) \quad (6.1b)$$

Mode 3 is realized when Switch S is *OFF*, i_L is 0, and diode D is not conducting. This mode is represented with (6.1c):

$$\dot{x}(t) = \begin{bmatrix} 0 & 0 \\ 0 & -\frac{1}{RC} \end{bmatrix} x(t) + \begin{bmatrix} 0 \\ 0 \end{bmatrix} v_s(t) \quad (6.1c)$$

6.2.2 Discrete-time Model

The forward Euler approximation (3.3) is then used to derive a discrete-time model from the continuous-time model in (6.1) where the time increment is defined by T_s .

Where $f(x[k])$ is substituted with the equations in 6.1 for each mode. The discrete-time model shares the same three modes as the continuous-time model, and a fourth mode (Mode 3) is added to represent the moment the inductor current decreases from a positive value and reaches 0. This instant is defined as τ_1 . Hence, the converter operates in four different modes, depending on the shape of the inductor current and switch position:

1. Mode 1 represents the converter when switch S is ON and the inductor current is increasing.
2. Mode 2 is when switch S is OFF and the inductor current is decreasing and is positive.

3. Mode 3 is the average of Modes 2 and 4 and includes the moment the inductor current decreases from a positive value to 0, which is defined as τ_1 .

4. Mode 4 is when both switch S and diode D are OFF and the inductor current is 0.

The discrete-time state space matrices for all four modes are included below (6.2).

Mode 1 (6.2a):

$$x[k+1] = \begin{bmatrix} 1 - \frac{R_L T_s}{L} & -\frac{T_s}{L} \\ \frac{T_s}{C} & 1 - \frac{T_s}{RC} \end{bmatrix} x[k] + \begin{bmatrix} -\frac{T_s}{L} \\ 0 \end{bmatrix} v_s[k] \quad (6.2a)$$

Mode 2 (6.2b):

$$x[k+1] = \begin{bmatrix} 1 - \frac{R_L T_s}{L} & -\frac{T_s}{L} \\ \frac{T_s}{C} & 1 - \frac{T_s}{RC} \end{bmatrix} x[k] + \begin{bmatrix} 0 \\ 0 \end{bmatrix} v_s[k] \quad (6.2b)$$

Mode 3 (6.2c):

$$x[k+1] = \begin{bmatrix} 1 - \frac{R_L \tau_1}{L} & -\frac{\tau_1}{L} \\ \frac{\tau_1}{C} & 1 - \frac{T_s}{RC} \end{bmatrix} x[k] + \begin{bmatrix} 0 \\ 0 \end{bmatrix} v_s[k] \quad (6.2c)$$

Mode 4 (6.2d):

$$x[k+1] = \begin{bmatrix} 1 & 0 \\ 0 & 1 - \frac{T_s}{RC} \end{bmatrix} x[k] + \begin{bmatrix} 0 \\ 0 \end{bmatrix} v_s[k] \quad (6.2d)$$

Output:

$$y[k] = \begin{bmatrix} 0 & 1 \end{bmatrix} x[k] \quad (6.2e)$$

6.3 Implementation and Simulation Results

The block diagram for the buck ET-MPC system with Kalman-Filter is shown in 6.2. One modification was made with regards to the estimation of the inductor current as the inductor is connected directly to the output capacitor, C and load resistor R . As an estimate, the inductor current can be made equal to the load current:

$$i_{L,ref} = \frac{v_{o,ref}}{R} \quad (6.3)$$

TT-MPC is implemented using the same system, with the event-trigger threshold δ is set to 0.

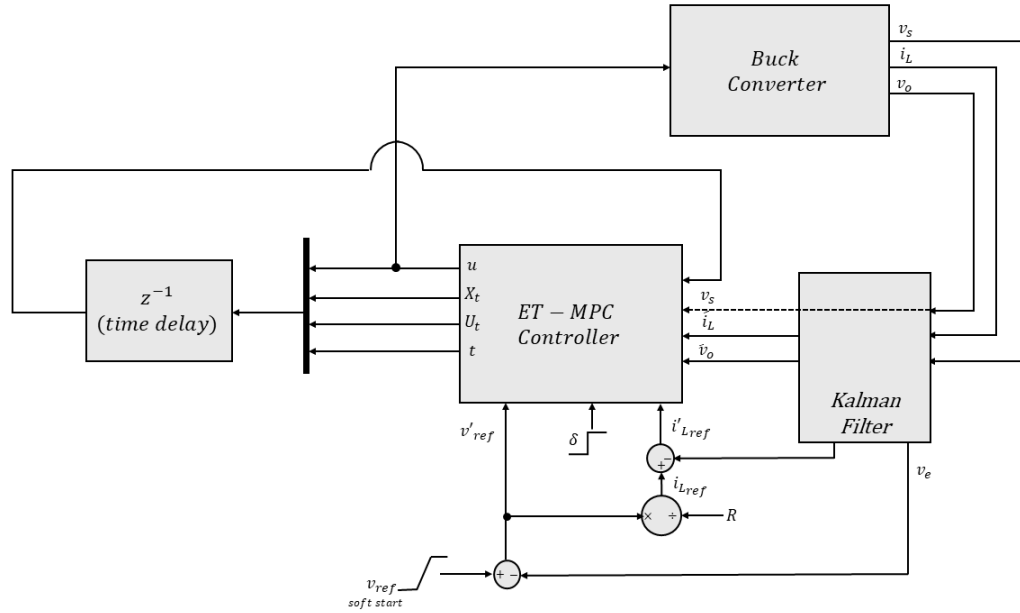


Figure 6.2: Buck Converter ET-MPC Implementation Block Diagram

Table 6.1: Simulation Parameters - Buck Converter with Kalman Filter

Converter and Controller Parameter	Value
Input Voltage (v_s)	16V
Output Voltage ($v_{o,ref}$)	5V
Inductor (L)	$100\mu H$
Inductor DC Resistance (R_L)	0.3Ω
Output Capacitance (C)	$220\mu F$
Load Resistance (R)	$36\Omega \rightarrow 18\Omega$
Sampling Period (T_s)	$2.5\mu s$
Prediction Horizon (N)	8
N_1	4
Move Blocking Coefficient (n_s)	4
Allowable Optimal Switching Elements (k_{max})	7
Switching - Weighting Factor (λ_u)	0.05
Inductor Current - Weighting Factor (λ_{iL})	0.05
Minimum event frequency (f_{min-ET})	6.25%

The event-triggered Kalman-based MPC controller was implemented in MATLAB/SIMULINK. The parameters used in the simulation are listed in Table 6.1. A smaller prediction horizon, N is selected, as the buck converter does not experience non-minimum phase behavior as in the case of a boost converter. The performance of the system is evaluated during start-up and step changes in the input voltage, reference voltage and load.

6.3.1 Buck Converter Startup

The time-triggered and event-triggered MPC with Kalman Filter formulations were implemented on the buck converter. During ET-MPC operation, it was found during startup that an event would not trigger, i.e., e remained 0, since the difference between the output voltage measured and optimal project state variable ($X_{t1}[2, k]$) was less than the event-trigger threshold δ . The output in this condition remained at 0V, or in other words, the converter did not start up. To remedy this, the event-trigger threshold, δ , was applied with a delay time $0.5ms$ in order for the converter to trigger and start up.

During start-up, the reference voltage was applied at $0.1ms$. This delay was applied in order to observe the startup sequence with more clarity. The observations from both TT-MPC and ET-MPC controllers show that the buck converter experienced an overshoot at the output before returning to regulation at $3ms$ during startup. This is due to switch S going to the *ON* state for a duration long enough to allow an inrush of current into the output capacitor and raises the voltage to $v_{o,ref} = 5V$. The switch then turned *OFF*. During this scenario, the inductor current finds an alternate path through the diode, D by forward biasing the diode and allowing the current to continue to flow to the output which in this case, causes the capacitor to charge up to a higher voltage; approximately $7V$. For the remainder of the duration in which the switch, S is *OFF* the output capacitor voltage falls as it discharges through the load resistor R to $5V$. When this happens, the controller begins to actuate the switch, and normal conversion takes place for which the buck converter is able to reach regulation.

In order to avoid an overshoot scenario, a Soft-Start (SS) scheme is applied to the converter to ramp the reference voltage up. The operation of the TT-MPC and ET-MPC without and with soft-start are shown in Figure 6.3 and Figure 6.4, respectively. Table 6.2 summarizes important attributes to during startup for both TT-MPC and ET-MPC. Both

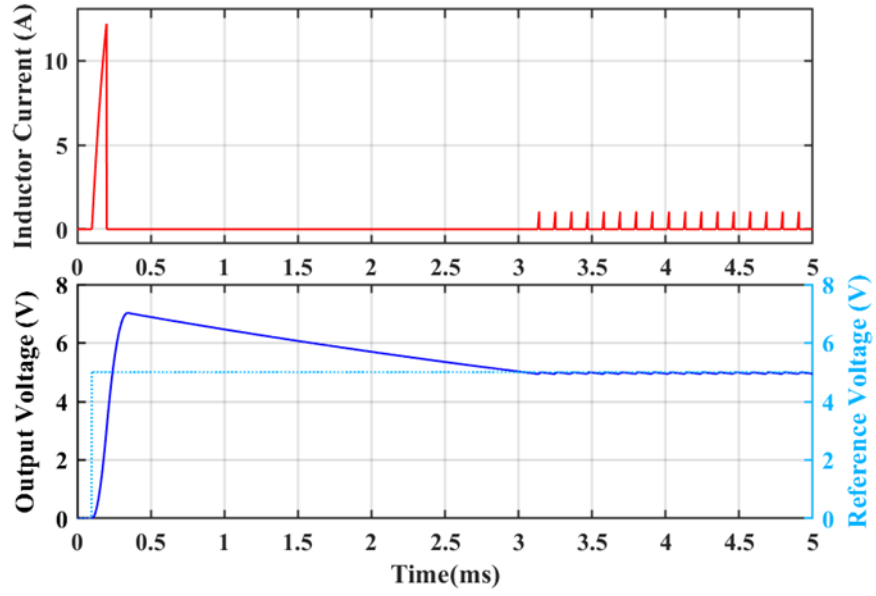
Table 6.2: Start-up Attributes Summary-Buck Converter

	TT-MPC		ET-MPC	
Operating Conditions	no SS	with SS	no SS	with SS
Overshoot (%)	40%	0%	40%	0%
Peak Inductor current (A)	12.2A	1.8A	12.2A	3A

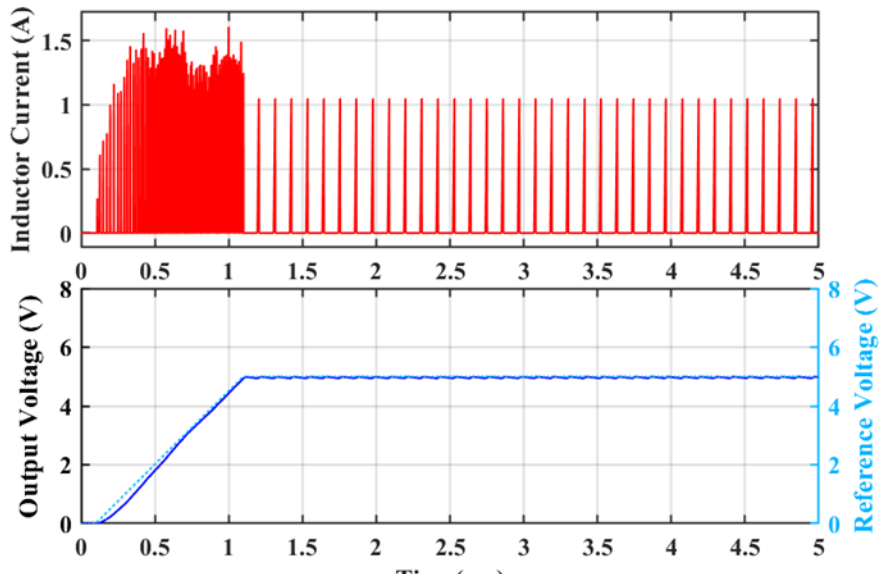
formulations exhibited similar overshoot and start-up times. However, the key difference between the methods is the peak inductor current which is different as a result of the switching frequency. Since ET-MPC results in a lower switching frequency 55kHz when compared to TT-MPC 125kHz , the inductor peak current is higher during start-up for ET-MPC. An additional observation is the reduction in computational burden achieved by utilizing the event-trigger formulation, in which the OCP is only triggered only approximately 10% of the time once the converter reaches steady-state.

6.3.2 Steady-state Operation

The buck converter was evaluated for different steady-state conditions and trigger thresholds which are listed in Table (6.3). The table includes the event frequency, tracking error and output ripple. Similar to the boost converter results, increasing the trigger threshold δ significantly reduces the computational effort of the controller during steady-state operation but tracking error, calculated using (4.1), increased. Additionally, increasing δ also increased the output voltage ripple, peak inductor current and reduced the switching frequency. The number of events increased as the difference between the input and output voltage increases.



(a) without soft-start (SS)



(b) with soft-start (SS)

Figure 6.3: Buck Converter Start-up without (a) and with Soft-Start (b) (TT-MPC)

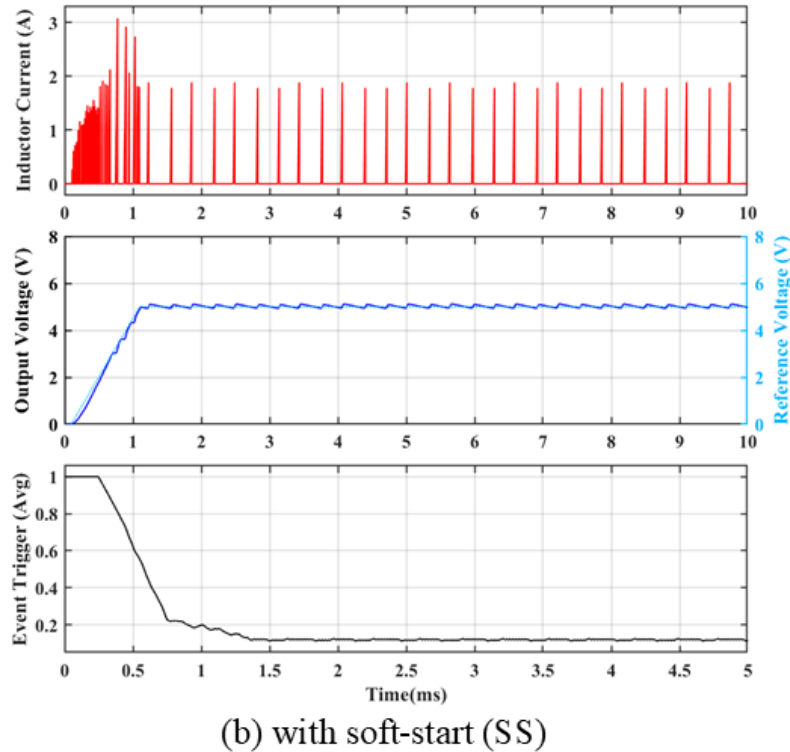
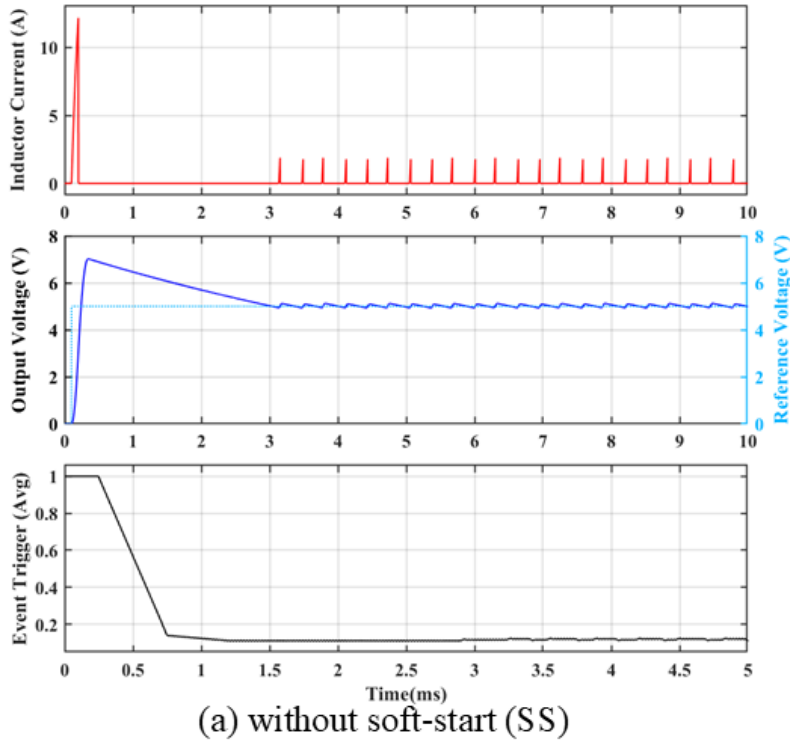


Figure 6.4: Buck Converter Start-up without and with Soft-Start (ET-MPC - $\delta = 0.025$)

When events are not triggered, we are able to skip the optimization problem after an event is triggered for up to 16 time steps

$(N_1 = 4, k_{max} = 7, n_s = 4 \rightarrow (4 + ((7 - 4) \times 4)) = 16)$ if an event is not triggered. The minimum event frequency possible for the buck converter is found to be 6.25% using (3.14). The minimum event average frequency was found to be 6.65% when the input voltage was 12V and output voltage reference was 3.3V. The computational savings in this scenario are realized by reducing the number of times the OCP is triggered by 93%.

6.3.3 Step Changes in the Output Reference Voltage

Figure 6.5 shows the results for a step-up in reference voltage from 3.3V to 5V. The reference voltage was applied with a slew rate approximately equal to $4V/msec$. In both formulations, the inductor current and switching frequency increase during the transition.

Next, the output voltage reference is stepped-down from 5V to 3.3V at $10ms$. The response of the converter using both TT-MPC and ET-MPC methods are illustrated in Figure 6.6. Both control methods allow the converter to reach regulation within $3ms$ with the latter achieving similar performance with significantly reduced calculations. On average, the OCP is only triggered 9% of the time duration when compared to TT-MPC. A similar operation occurs during the step down in reference voltage as the boost converter, in which the inductor current goes to zero allowing the capacitor to discharge into the load to reduce the output voltage to the new reference voltage.

6.3.4 Step Change in the Input Voltage (Line Transient)

Results for both TT-MPC and ET-MPC for a line transient case are shown in Figure 6.7. The input voltage is stepped down from 16V to 12V at $10ms$ after steady state operation with $v_{o,ref}$ set to 5V. The line transient response of the converter in both

Table 6.3: Event-trigger Impact on Steady-state Operation - Results Summary

Event Frequency:				
Steady-State Conditions	$\delta = 0.00$	$\delta = 0.015$	$\delta = 0.025$	$\delta = 0.035$
$v_s = 12V, v_o = 3.3V$	100%	10.93%	7.95%	6.65%
$v_s = 12V, v_o = 5V$	100%	18.2%	11.33%	7.48%
$v_s = 16V, v_o = 3.3V$	100%	12.34%	8.16%	6.84%
$v_s = 16V, v_o = 5V$	100%	19.80%	11.98%	9.13%

Tracking Error [V]:				
Steady-State Conditions	$\delta = 0.00$	$\delta = 0.015$	$\delta = 0.025$	$\delta = 0.035$
$v_s = 12V, v_o = 3.3V$	0.034V	0.033V	0.047V	0.064V
$v_s = 12V, v_o = 5V$	0.066V	0.053V	0.051V	0.053V
$v_s = 16V, v_o = 3.3V$	0.033V	0.029V	0.052V	0.053V
$v_s = 16V, v_o = 5V$	0.035V	0.039V	0.059V	0.050

Output Ripple [Vp-p]:				
Steady-State Conditions	$\delta = 0.00$	$\delta = 0.015$	$\delta = 0.025$	$\delta = 0.035$
$v_s = 12V, v_o = 3.3V$	0.048	0.116	0.161	0.219
$v_s = 12V, v_o = 5V$	0.086	0.135	0.171	0.210
$v_s = 16V, v_o = 3.3V$	0.060	0.101	0.163	0.163
$v_s = 16V, v_o = 5V$	0.055	0.128	0.193	0.165

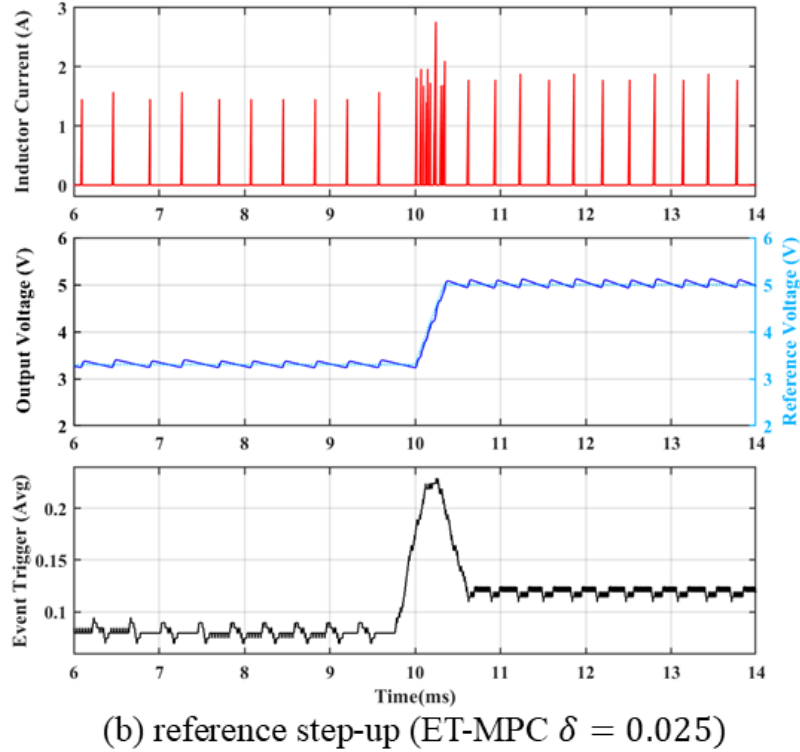
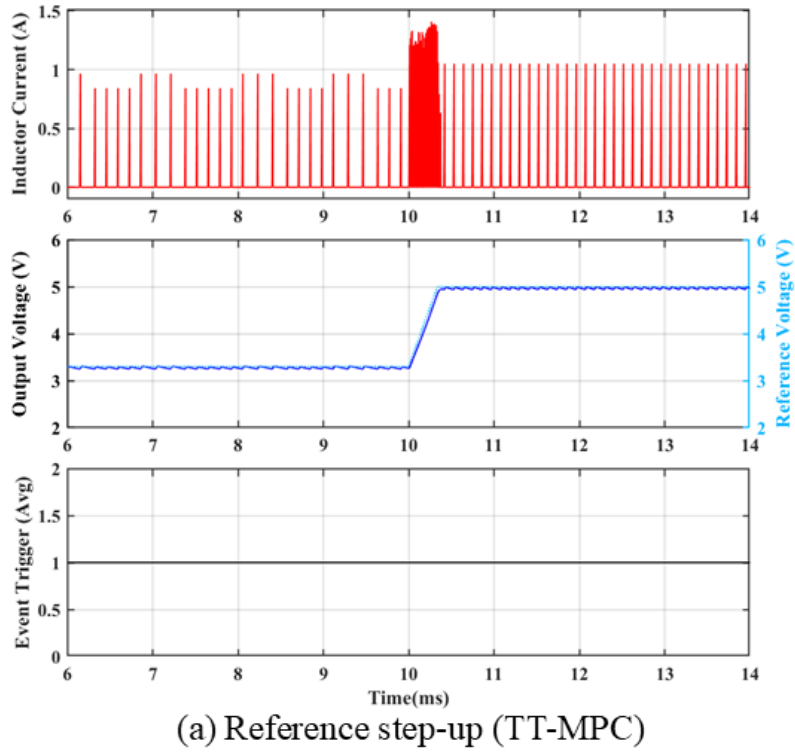
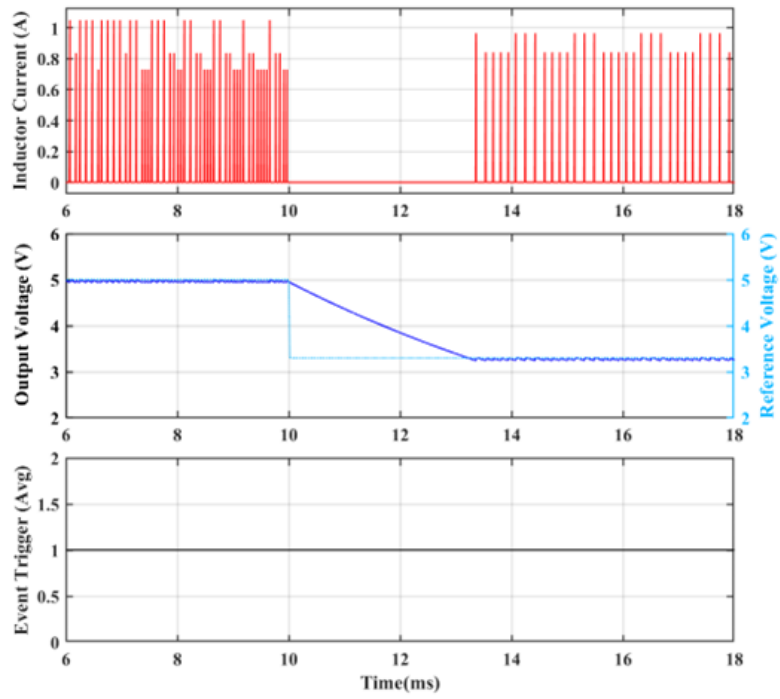
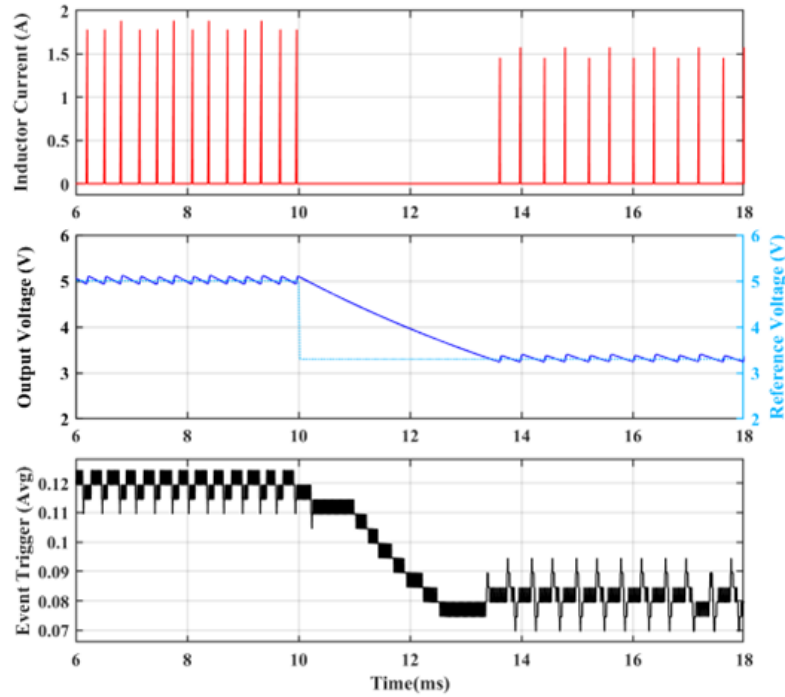


Figure 6.5: Reference voltage step-up from 3.3V to 5V (TT-MPC and ET-MPC)



(a) Reference step-down (TT-MPC)



(b) reference step-down (ET-MPC $\delta = 0.025$)

Figure 6.6: Reference voltage step-down from 5V to 3.3V (TT-MPC and ET-MPC)

Table 6.4: Voltage Reference Converter Response for Different Event Thresholds

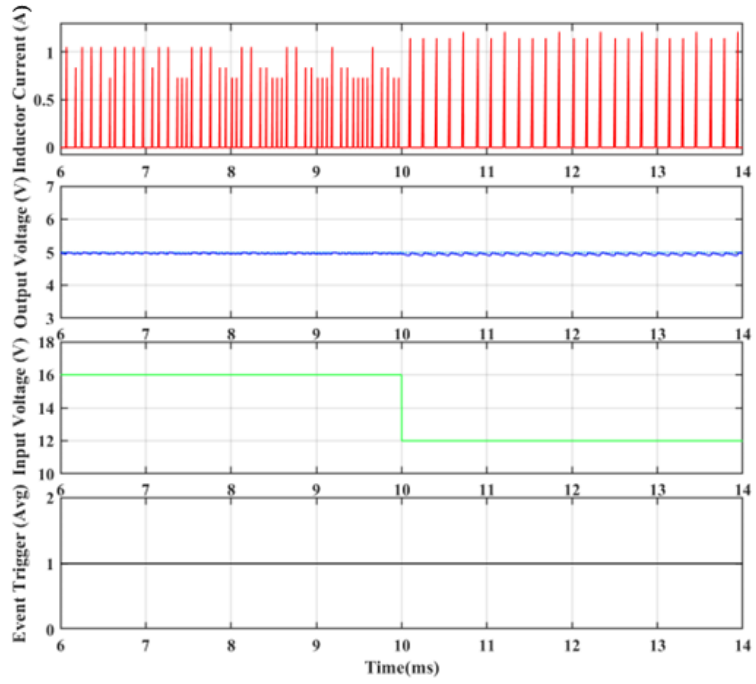
	$\delta = 0.00$	$\delta = 0.025$
$v_{o,ref} = 3.3V \rightarrow 5V, v_s = 16V$		
Transient time [ms]	0.5ms	0.5ms
Event Frequency	100%	23.5%
$v_{o,ref} = 5V \rightarrow 3.3V, v_s = 16V$		
Transient time [ms]	3.5ms	3.5ms
Event Frequency	100%	9%

time-triggered and event-triggered formulations is similar showing that the converter is able to maintain the output voltage within regulation. The event frequency during the transient decreases is maintained at approximately 12%. An additional note can be made about the TT-MPC controller, where it experiences lower frequency as the input voltage decreases.

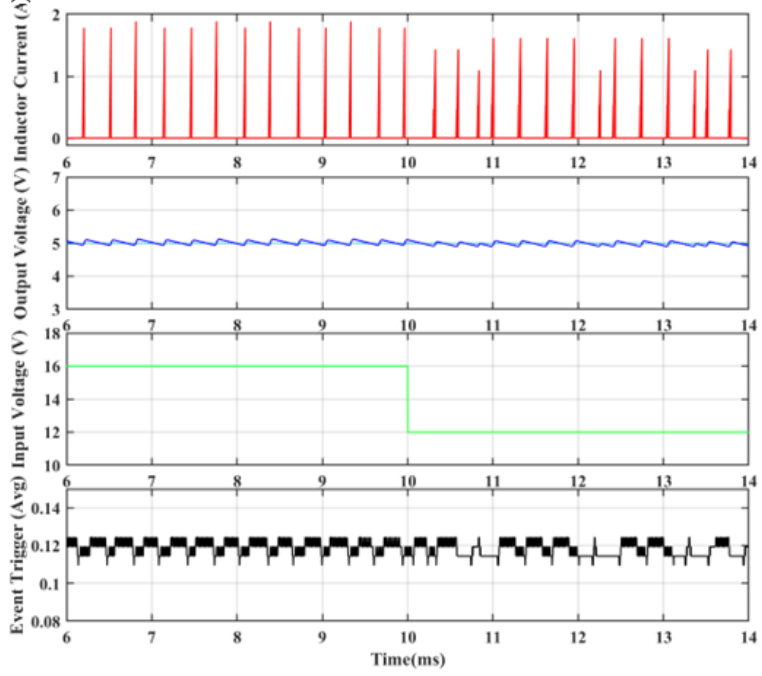
6.3.5 Response to Load Transients

The load resistance R is reduced from 36Ω to 18Ω to simulate an increase in load demand. The Kalman Filter is used to estimate the measured inductor current, output voltage and disturbance variables i_e and v_e which are fed back to the controller to adjust the inductor current and output voltage references and compensate for the load disturbance.

The output reference voltage is set to $5V$ and input voltage set to $16V$. The covariance matrices for process noise, Q , and measurement noise, R , are assigned the values in (6.4). The results comparing the TT-MPC and ET-MPC controllers are reported



(a) Input voltage step-down (TT-MPC)



(b) Input voltage step-down (ET-MPC $\delta = 0.025$)

Figure 6.7: Input voltage step-down from 12V to 16V (TT-MPC and ET-MPC ($\delta = 0.025$))

in Figure 6.8. Both controllers were able to regulate the output voltage with no undershoot.

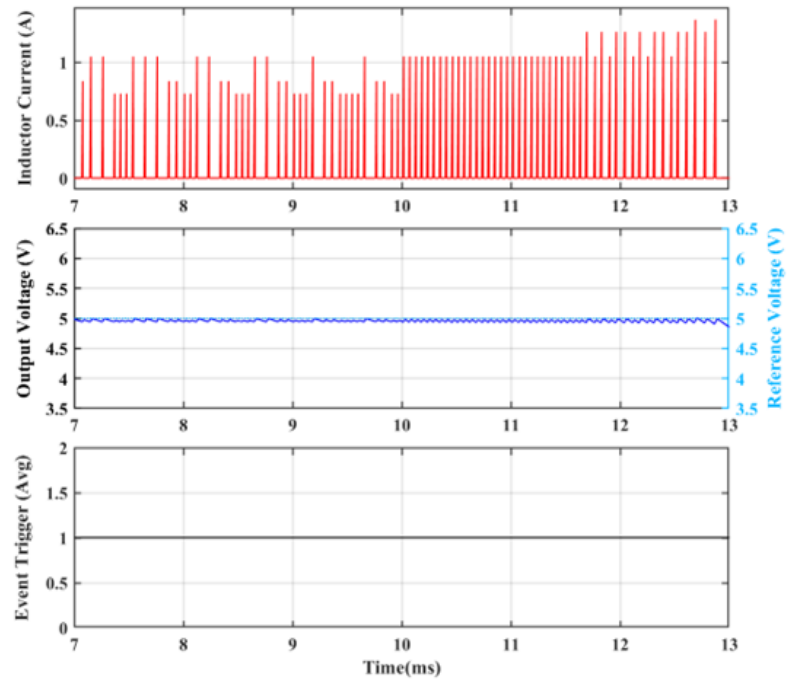
The ET-MPC controller was also evaluated for different event-trigger thresholds. The waveforms in Figure 6.9 display a general trend in which increasing the event-trigger threshold generally reduces the event frequency and switching frequency of the converter while increasing the peak inductor currents and output voltage ripple. However, the transient response throughout all plots show favorable operation in which the converter is able to maintain regulation with the increase in load current.

$$Q = \begin{bmatrix} 0.1 & 0 & 0 & 0 \\ 0 & 0.1 & 0 & 0 \\ 0 & 0 & 50 & 0 \\ 0 & 0 & 0 & 50 \end{bmatrix} R = \begin{bmatrix} 1 & 0 \\ 0 & 1 \end{bmatrix} \quad (6.4)$$

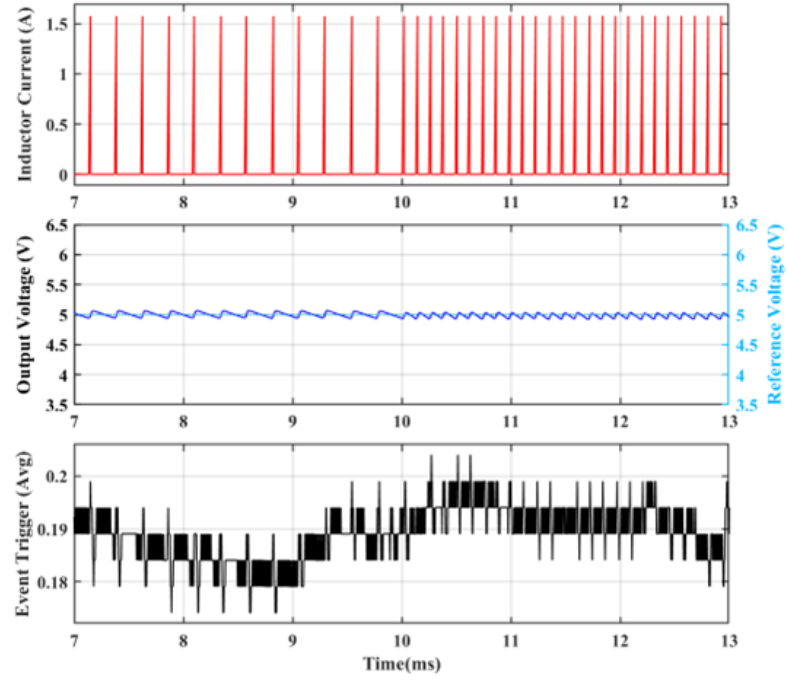
6.4 Remarks

The results reported for the buck converter show that ET-MPC is a promising control method to reduce the computational burden of an enumeration-based TT-MPC. During specific operating conditions the computational burden was reduced by almost 94%. The controller also performed very well against load transients showing no undershoot at the load transition.

A future evaluation would include a trade-off study which would examine the impact of reducing the prediction horizon even further while achieving performance requirements. Additional studies would include tuning the weighting factors and event-trigger threshold to maintain a constant switching frequency throughout steady-state operation and during transients.



(a) Load transient ($36\Omega \rightarrow 18\Omega$ (TT-MPC))



(b) Load transient ($36\Omega \rightarrow 18\Omega$ (ET-MPC $\delta = 0.015$))

Figure 6.8: Load Transient for TT-MPC and ET-MPC ($\delta = 0.15$) - Buck Converter

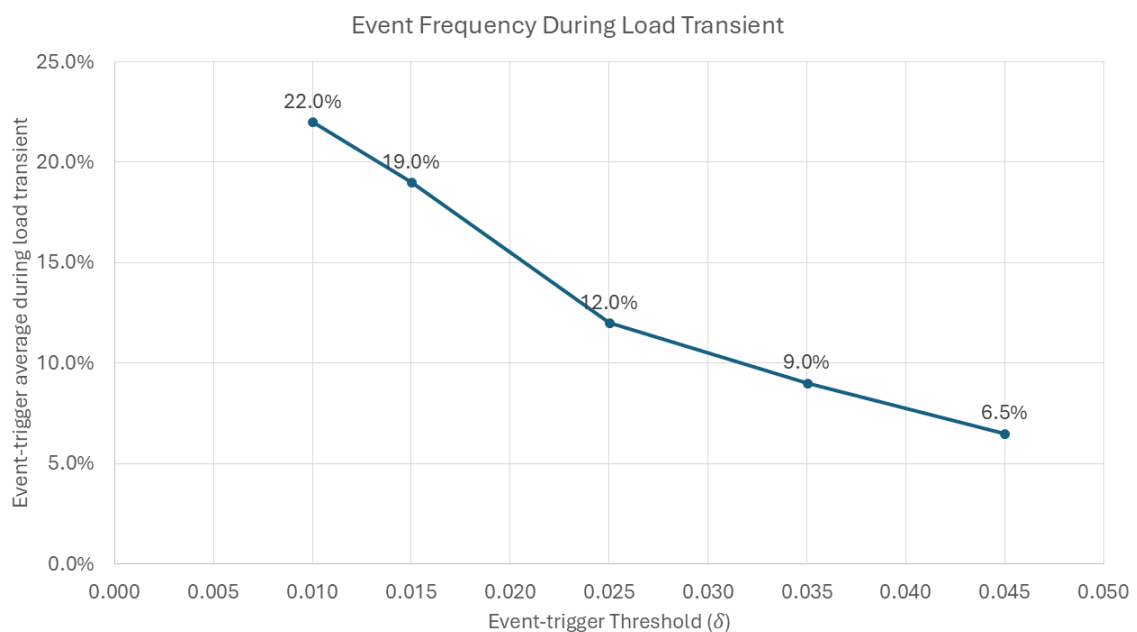


Figure 6.9: Average event frequency during load transient - ($\delta = 0.01$, $\delta = 0.015$, $\delta = 0.035$, $\delta = 0.045$)

CHAPTER SEVEN

CONCLUSION AND FUTURE WORK

7.1 Remarks

This work introduces an effective method to reduce the computational burden associated with a finite control set enumeration-based model predictive control used for the direct control of DC-DC converters. The strategy has been implemented on both boost and buck converters. Simulation results demonstrate that the performance of the proposed event-triggered MPC is comparable with the conventional time-triggered MPC while achieving reduction in the computational burden of the controller. While there is a reduction in the computational burden, the selected microcontroller and resource utilization remains unchanged. In other words, ET-MPC does not reduce system resource allocation.

There are several parameters that impact the performance of the ET-MPC controller. The influence of the trigger threshold, δ , including its selection criteria and performance impact was explored. Generally, increasing the trigger threshold reduces the computational burden, but increases tracking error, output ripple and peak inductor current. Additional parameters include the switching weighting factor λ_u which penalizes switching and can be used to control the switching frequency. The inductor current weighting factor λ_{iL} penalizes the error between the inductor reference and measured inductor current. Increasing this value increases the tightness of current control and prevents inductor saturation but excessively increasing this value can cause the controller to lose voltage regulation. Another factor is k_{max} , which is the maximum allowable number of elements that can be used in the switching sequence. Reducing this number

improves the performance of the control but increases the computational burden as more events are triggered. The effect of changing these values was evaluated in this work.

7.2 Future Work

Ideas for future work as it relates to event-trigger control for power converters include:

1. Implementation of the proposed control algorithms in hardware to verify the stability of real-time implementation .
2. Explore applicability of this method to different DC-DC, AC-DC, AC-AC, DC-AC topologies.
3. Explore applicability of this method to different MPC control strategies including but not limited to direct MPC with hysteresis bounds, direct MPC with implicit PWM modulator and Indirect MPC.
4. Setting trigger threshold criteria to encompass deviation of inductor current from reference value.
5. Conduct a stability analysis of the proposed method.

Additional ideas as they relate to optimization and the field of power converter control include the use of math models and Kalman Filters in power converter diagnostics and prognostics.

APPENDIX A
NOTATION

A.1 Mathematical Notation

.	general placeholder for any variable
\in	is an element of
\forall	for all
$=$	equal
\neq	not equal
\geq	greater than or equal
\leq	less than or equal
\preceq	element-wise inequality
\mapsto	maps to
s.t.	subject to
	such that
$ \cdot $	absolute value
$\ x\ _p$	ℓ_p -norm, $\ x\ _p = (x_1 ^p + x_2 ^p + \dots + x_n ^p)^{1/p}, (p \geq 1)$
\max	maximum
\min	minimum
\mathbb{N}	integers
\mathbb{N}^+	positive integers
$N(m, P)$	normal distribution (mean m , covariance P), $x \sim N(m, P)$
\mathbb{R}	real numbers
\mathbb{R}^n	real valued n -vectors
$\mathbb{R}^{m \times n}$	real valued $m \times n$ -matrices
\mathbf{S}_+^n	set of symmetric positive semi-definite matrices

A.2 Symbols

a	scalar
a	vector
A, B, C	system matrices, discrete time, $x[k + 1] = Ax[k] + Bu[k], y = Cx[k]$
\mathbf{A}^T	matrix transpose
\mathbf{A}^{-1}	inverse of a square matrix
I	identity matrix
$\mathcal{O}(\cdot)$	used to indicate an upper bound on time taken by an algorithm and its behavior as the input increases
u	switch state (manipulated variable)
u	input vector in Chapter 5
\mathbf{U}_o	optimal switching sequence — TT-MPC (Chapter 3)
\mathbf{U}_t	optimal switching sequence — ET-MPC
\mathbf{U}_{t1}	optimal switching sequence after single time delay
v	output disturbance (measurement error)
w	disturbance to the state evolution (process error)
x	state vector
$\dot{\mathbf{x}}(t)$	derivative of the state vector with respect to time
$\mathbf{x}[k]$	evolution of state vector in discrete-time domain
$\hat{\mathbf{x}}$	state estimate
\mathbf{x}_e	disturbance state
\mathbf{x}^*	optimal solution (Chapter 1)
\mathbf{x}^T	row vector
\mathbf{X}_t	optimal state trajectory
\mathbf{X}_{t1}	optimal state trajectory after single time delay
0	zero matrix

A.3 Acronyms

AC	Alternating Current
CCM	Continuous Conduction Mode
CRM	Critical Conduction Mode
DC	Direct Current
DCM	Discontinuous Conduction Mode
DOB	Disturbance Observer
DP	Dynamic Programming
ET-MPC	Event-Triggered Model Predictive Control
FCS	Finite Control Set
LQR	Linear Quadratic Regulator
LQG	Linear Quadratic Gaussian
MPC	Model Predictive Control
LP	Linear Programming
LTI	Linear Time-Invariant
MILP	Mixed Integer Linear Programming
MIMO	Multiple-Input Multiple-Output
MIQP	Mixed Integer Quadratic Programming
MPC	Model Predictive Control
OCP	Optimal Control Problem
OPS	Operations per Second
PI	Proportional Integral
PID	Proportional Integral Derivative
PWM	Pulse Width Modulation
RL	Reinforced Learning
RMS	Root Mean Square (rms)
TT-MPC	Time-Triggered Model Predictive Control

REFERENCES

- [1] John G Kassakian, David J Perreault, George C Verghese, and Martin F Schlecht. *Principles of power electronics*. Cambridge University Press, 2023.
- [2] Robert W Erickson and Dragan Maksimovic. *Fundamentals of power electronics*. Springer Science & Business Media, 2007.
- [3] Jose Rodriguez and Patricio Cortes. *Predictive control of power converters and electrical drives*. John Wiley & Sons, 2012.
- [4] Minghao Han, Han He, Xingtao Wang, Zheng Dong, and Zhenbin Zhang. Current-sensorless model predictive control of dual active bridge converters with kalman filter. In *2021 IEEE International Conference on Predictive Control of Electrical Drives and Power Electronics (PRECEDE)*, pages 663–667, 2021.
- [5] Erliza Serri and Abu Zaharin Ahmad. Comparative study of short prediction mpc-kf with pi controller for dc-dc buck converter. In *2016 IEEE International Conference on Automatic Control and Intelligent Systems (I2CACIS)*, pages 219–224, 2016.
- [6] Mostafa Ahmed, Mohamed Abdelrahem, Ralph Kennel, and Christoph M. Hackl. A robust maximum power point tracking based model predictive control and extended kalman filter for pv systems. In *2020 International Symposium on Power Electronics, Electrical Drives, Automation and Motion (SPEEDAM)*, pages 514–519, 2020.
- [7] Mostafa Ahmed, Mohamed Abdelrahem, Ralph Kennel, and Christoph M. Hackl. Maximum power point tracking based model predictive control and extended kalman filter using single voltage sensor for pv systems. In *2020 IEEE 29th International Symposium on Industrial Electronics (ISIE)*, pages 1039–1044, 2020.
- [8] James Blake Rawlings, David Q Mayne, Moritz Diehl, et al. *Model predictive control: theory, computation, and design*, volume 2. Nob Hill Publishing Madison, WI, 2017.
- [9] Petros Karamanakos, Eyke Liegmann, Tobias Geyer, and Ralph Kennel. Model predictive control of power electronic systems: Methods, results, and challenges. *IEEE Open Journal of Industry Applications*, 1:95–114, 2020.
- [10] Naoto Umeno and Hidenori Maruta. Stabilization improvement of mpc based dc-dc converter with load estimation. In *2020 9th International Conference on Renewable Energy Research and Application (ICRERA)*, pages 295–300. IEEE, 2020.
- [11] Jun Chen, Zhaojian Li, and Xiang Yin. Optimization of energy storage size and operation for renewable-ev hybrid energy systems. In *2021 IEEE Green Technologies Conference*, Denver, CO, April 7–9, 2021.

- [12] Jun Chen, Aman Behal, and Chong Li. Active cell balancing by model predictive control for real time range extension. In *2021 IEEE Conference on Decision and Control*, Austin, TX, USA, December 13–15, 2021.
- [13] Jun Chen, Man Liang, and Xu Ma. Probabilistic analysis of electric vehicle energy consumption using MPC speed control and nonlinear battery model. In *2021 IEEE Green Technologies Conference*, Denver, CO, April 7–9, 2021.
- [14] Yan Liang, Zehua Liang, Dongdong Zhao, Yigeng Huangfu, Liang Guo, and Ben Zhao. Model predictive control of interleaved dc-dc boost converter with current compensation. In *2019 IEEE International Conference on Industrial Technology (ICIT)*, pages 1701–1706, 2019.
- [15] Yanhui Xie, Reza Ghaemi, Jing Sun, and James S Freudenberg. Implicit model predictive control of a full bridge dc–dc converter. *IEEE Transactions on Power Electronics*, 24(12):2704–2713, 2009.
- [16] Petros Karamanakos and Tobias Geyer. Guidelines for the design of finite control set model predictive controllers. *IEEE Transactions on Power Electronics*, 35(7):7434–7450, 2019.
- [17] David J Perreault and George C Verghese. Time-varying effects and averaging issues in models for current-mode control. *IEEE Transactions on Power Electronics*, 12(3):453–461, 1997.
- [18] Michal Kvasnica. Implicit vs explicit mpc — similarities, differences, and a path towards a unified method. In *2016 European Control Conference (ECC)*, pages 603–603, 2016.
- [19] Andrea Giovanni Beccuti, Sébastien Mariethoz, Sébastien Cliquennois, Shu Wang, and Manfred Morari. Explicit model predictive control of dc–dc switched-mode power supplies with extended kalman filtering. *IEEE Transactions on Industrial Electronics*, 56(6):1864–1874, 2009.
- [20] Mizanur Rahman, Subroto K. Sarkar, Sajal K. Das, and Yuan Miao. A comparative study of lqr, lqg, and integral lqg controller for frequency control of interconnected smart grid. In *2017 3rd International Conference on Electrical Information and Communication Technology (EICT)*, pages 1–6, 2017.
- [21] Faryad Darabi Sahneh, Guoqiang Hu, and Lihua Xie. Extremum seeking control for systems with time-varying extremum. In *Proceedings of the 31st Chinese Control Conference*, pages 225–231, 2012.
- [22] Mingduo Lin, Bo Zhao, Derong Liu, Xi Liu, and Fangchao Luo. Generalized policy iteration-based reinforcement learning algorithm for optimal control of

- unknown discrete-time systems. In *2021 33rd Chinese Control and Decision Conference (CCDC)*, pages 3650–3655, 2021.
- [23] Nafees Ahamad, Gagan Singh, Shahala Khan, and Afzal Sikander. Design and performance analysis of optimal reduced order h-infinity controller: L1 norm based genetic algorithm technique. In *2017 International Conference on Power and Embedded Drive Control (ICPEDC)*, pages 8–13, 2017.
 - [24] Stephen P Boyd and Lieven Vandenberghe. *Convex optimization*. Cambridge university press, 2004.
 - [25] Alberto Bemporad, Francesco Borrelli, and Manfred Morari. Robust model predictive control: Piecewise linear explicit solution. In *2001 European Control Conference (ECC)*, pages 939–944. IEEE, 2001.
 - [26] Michael R Garey and David S Johnson. *Computers and intractability*, volume 174. freeman San Francisco, 1979.
 - [27] Erwin Kreyszig. *Advanced Engineering Mathematics 9th Edition with Wiley Plus Set*, volume 334. John Wiley & Sons US, 2007.
 - [28] Christodoulos A Floudas. *Nonlinear and mixed-integer optimization: fundamentals and applications*. Oxford University Press, 1995.
 - [29] M. M. Guignard and K. Spielberg. Mixed-integer algorithms for the (0,1) knapsack problem. *IBM Journal of Research and Development*, 16(4):424–430, 1972.
 - [30] Joseph Vithayathil. Power electronics: principles and applications. (*No Title*), 1995.
 - [31] Irving M Gottlieb. Power supplies, switching regulators, inverters, and converters. (*No Title*), 1994.
 - [32] Petros P Karamanakos. *Model predictive control strategies for power electronics converters and ac drives*. PhD thesis, National Technical University of Athens, 2013.
 - [33] Ned Mohan, Tore M Undeland, and William P Robbins. *Power electronics: converters, applications, and design*. John wiley & sons, 2003.
 - [34] S Joe Qin and Thomas A Badgwell. A survey of industrial model predictive control technology. *Control engineering practice*, 11(7):733–764, 2003.
 - [35] Z. Ding and B.W. Hogg. Multivariable self-tuning control of a boiler-turbine system. In *1991 International Conference on Advances in Power System Control, Operation and Management, APSCOM-91.*, pages 498–502 vol.2, 1991.

- [36] Qinghua He, S.J. Qin, and A.J. Toprac. Computationally efficient modeling of wafer temperatures in a low-pressure chemical vapor deposition furnace. *IEEE Transactions on Semiconductor Manufacturing*, 16(2):342–350, 2003.
- [37] Michael G Forbes, Rohit S Patwardhan, Hamza Hamadah, and R Bhushan Gopaluni. Model predictive control in industry: Challenges and opportunities. *IFAC-PapersOnLine*, 48(8):531–538, 2015.
- [38] Jun Chen and Zonggen Yi. Comparison of event-triggered model predictive control for autonomous vehicle path tracking. In *IEEE Conf. Control Technology and Applications*, San Diego, CA, Aug. 8–11, 2021.
- [39] Jun Chen, Xiangyu Meng, and Zhaojian Li. Reinforcement learning-based event-triggered model predictive control for autonomous vehicle path following. In *American Control Conference*, Atlanta, GA, June 8–10, 2022.
- [40] A. Bonfiglio, A. Oliveri, R. Procopio, F. Delfino, G.B. Denegrí, M. Invernizzi, and M. Storace. Improving power grids transient stability via model predictive control. In *2014 Power Systems Computation Conference*, pages 1–7, 2014.
- [41] Ján Drgoňa. *Model Predictive Control with Applications in Building Thermal Comfort Control*. PhD thesis, Slovak University of Technology in Bratislava Bratislava, Slovakia, 2017.
- [42] Hongliang Zhou, Levent Güvenç, and Zhiyuan Liu. Design and evaluation of path following controller based on mpc for autonomous vehicle. In *2017 36th Chinese Control Conference (CCC)*, pages 9934–9939, 2017.
- [43] Jiawei Tian. Vehicle adaptive cruise control based on model predictive algorithm. In *2024 International Conference on Intelligent Robotics and Automatic Control (IRAC)*, pages 467–470, 2024.
- [44] Patricio Cortes, Samir Kouro, Bruno La Rocca, Rene Vargas, Jose Rodriguez, Jose I. Leon, Sergio Vazquez, and Leopoldo G. Franquelo. Guidelines for weighting factors design in model predictive control of power converters and drives. In *2009 IEEE International Conference on Industrial Technology*, pages 1–7, 2009.
- [45] Sergio Vazquez, Jose I. Leon, Leopoldo G. Franquelo, Jose Rodriguez, Hector A. Young, Abraham Marquez, and Pericle Zanchetta. Model predictive control: A review of its applications in power electronics. *IEEE Industrial Electronics Magazine*, 8(1):16–31, 2014.
- [46] Robert A Mammano. *Fundamentals of power supply design: technology from Unitrode/Texas Instruments Power Supply Design Seminars*. Texas Instruments Incorporated, 2017.

- [47] Kefan Yu, Fang Zhuo, Feng Wang, Xinyu Jiang, and Yating Gou. Mpc-based startup current shaping strategy with state-space model of dab in dc distribution system. *IEEE Journal of Emerging and Selected Topics in Power Electronics*, 10(4):4073–4089, 2022.
- [48] Liwei Zhou and Matthias Preindl. Variable-switching constant-sampling frequency critical soft switching mpc for dc/dc converters. *IEEE Transactions on Energy Conversion*, 36(2):1548–1561, 2021.
- [49] Jaroslaw Luszcz. Modeling of common mode currents induced by motor cable in converter fed ac motor drives. In *2011 IEEE International Symposium on Electromagnetic Compatibility*, pages 459–464, 2011.
- [50] Muslem Uddin, Galina Mirzaeva, Graham Goodwin, and Pericle Zanchetta. Computationally efficient model predictive control for ac-dc-ac converter with common mode voltage elimination. In *2018 IEEE Energy Conversion Congress and Exposition (ECCE)*, pages 6418–6423, 2018.
- [51] Arthur G. Bartsch, Christian J. Meirinho, Yales R. de Novaes, Mariana S. M. Cavalca, and José de Oliveira. Analysis of predictive control for boost converter in power factor correction application. In *2016 12th IEEE International Conference on Industry Applications (INDUSCON)*, pages 1–8, 2016.
- [52] Md Juel Rana, M. Shaiful Alam, A. Hussein, and M. A. Abido. Transient performance improvement of active front end rectifier using finite set model predictive control. In *2018 IEEE 19th Workshop on Control and Modeling for Power Electronics (COMPEL)*, pages 1–6, 2018.
- [53] Clayton R Paul, Robert C Scully, and Mark A Steffka. *Introduction to electromagnetic compatibility*. John Wiley & Sons, 2022.
- [54] Cristian Castillo, Cristian García, Daniel Sanchez, Baldomero Araya, Chenwei Ma, S. Alireza Davari, Bo Long, and Jose Rodriguez. Fcs-mpc with computational efficiency and dv/dt mitigation in multilevel converters. In *2024 IEEE Energy Conversion Congress and Exposition (ECCE)*, pages 3386–3392, 2024.
- [55] Samir Kouro, Patricio Cortés, René Vargas, Ulrich Ammann, and José Rodríguez. Model predictive control—a simple and powerful method to control power converters. *IEEE Transactions on Industrial Electronics*, 56(6):1826–1838, 2008.
- [56] Felipe A Villarroel, José R Espinoza, Marcelo A Pérez, Roberto O Ramírez, Carlos R Baier, Daniel Sbárbaro, José J Silva, and Mauricio A Reyes. Stable shortest horizon fcs-mpc output voltage control in non-minimum phase boost-type converters based on input-state linearization. *IEEE Transactions on Energy Conversion*, 36(2):1378–1391, 2021.

- [57] N. Snehal, W. Pooja, and K. Sonam. Model predictive control for dc-dc buck converter using enumeration. In *2020 52nd North American Power Symposium (NAPS)*, pages 1–6, 2021.
- [58] Shudan Jin, Shengrong Zhuo, and Yigeng Huangfu. Offset-free model predictive control of interleaved boost converter based on extended state observer. In *2022 4th International Conference on Smart Power & Internet Energy Systems (SPIES)*, pages 268–273, 2022.
- [59] Tobias Geyer, Georgios Papafotiou, Roberto Frasca, and Manfred Morari. Constrained optimal control of the step-down dc-dc converter. *IEEE transactions on power electronics*, 23(5):2454–2464, 2008.
- [60] Yan Liang, Zehua Liang, Dongdong Zhao, Yigeng Huangfu, and Liang Guo. Model predictive control for interleaved dc-dc boost converter based on kalman compensation. In *2018 IEEE International Power Electronics and Application Conference and Exposition (PEAC)*, pages 1–5, 2018.
- [61] James Scoltock, Tobias Geyer, and Udaya Madawala. Model predictive direct power control for a grid-connected converter with an lcl-filter. In *2013 IEEE International Conference on Industrial Technology (ICIT)*, pages 588–593, 2013.
- [62] Muhammad Saleh Murtaza Gardezi and Ammar Hasan. Machine learning based adaptive prediction horizon in finite control set model predictive control. *IEEE Access*, 6:32392–32400, 2018.
- [63] Wenyuan Ding, Faramarz Faraji, Vijesh Jayan, Wang Zuo, Amer MYM Ghias, and Honnyong Cha. Finite control set model predictive control for five-level modified active nested neutral point clamped converter. In *2022 IEEE Energy Conversion Congress and Exposition (ECCE)*, pages 1–5. IEEE, 2022.
- [64] Salvatore R Di Salvo, Riccardo Leuzzi, Giulia Tresca, Norma Anglani, and Pericle Zanchetta. Self-tuning finite-state model predictive control with grid impedance estimation in a grid-tied inverter. In *2022 IEEE Energy Conversion Congress and Exposition (ECCE)*, pages 1–7. IEEE, 2022.
- [65] Liang Chen, Yunyang Xu, and Nian Heng. Improved finite set model predictive current control of grid side converter in weak grid using kalman filter. In *2019 IEEE PES Asia-Pacific Power and Energy Engineering Conference (APPEEC)*, pages 1–5, 2019.
- [66] Tobias Geyer, Georgios Papafotiou, and Manfred Morari. Hybrid model predictive control of the step-down dc-dc converter. *IEEE Transactions on Control Systems Technology*, 16(6):1112–1124, 2008.

- [67] Xiaofeng Dong and Hui Li. Model predictive control for a pll-less sic grid-tied inverter with zero-voltage-ride-through capability. In *2022 IEEE Energy Conversion Congress and Exposition (ECCE)*, pages 1–7. IEEE, 2022.
- [68] Yufan Li, Yichao Sun, Carlos Teixeira, Liye Wu, Brendan Peter McGrath, and Donald Grahame Holmes. Model predictive control of a modular multilevel dc transformer under quasi-square modulation. In *2022 IEEE Energy Conversion Congress and Exposition (ECCE)*, pages 1–8. IEEE, 2022.
- [69] Zehua Liang, Dongdong Zhao, Rui Ma, Haiyan Li, and Yigeng Huangfu. Continuous model predictive control of current-fed half-bridge isolated dc/dc converter. In *2020 IEEE Industry Applications Society Annual Meeting*, pages 1–7. IEEE, 2020.
- [70] Thomas Effenberger, Hannes Börngen, Eyke Liegmann, Michael Hoerner, Petros Karamanakos, and Ralph Kennel. Modeling of an interleaved dc-dc boost converter for a direct model predictive control strategy. In *2022 24th European Conference on Power Electronics and Applications (EPE'22 ECCE Europe)*, pages 1–11. IEEE, 2022.
- [71] Paul Gistain Ipoum-Ngome, Daniel Legrand Mon-Nzongo, Rodolfo CC Flesch, Joseph Song-Manguelle, Mengqi Wang, and Tao Jin. Model predictive current control based on a generalised adjacent voltage vectors approach for multilevel inverters. *IET Power Electronics*, 12(13):3590–3599, 2019.
- [72] Petros Karamanakos, Tobias Geyer, Nikolaos Oikonomou, Frederick D Kieferndorf, and Stefanos Manias. Direct model predictive control: A review of strategies that achieve long prediction intervals for power electronics. *IEEE Industrial Electronics Magazine*, 8(1):32–43, 2014.
- [73] Ajay Shetgaonkar, Aleksandra Lekić, José Luis Rueda Torres, and Peter Palensky. Microsecond enhanced indirect model predictive control for dynamic power management in mmc units. *Energies*, 14(11):3318, 2021.
- [74] Mohamed E Albira and Mohamed A Zohdy. Adaptive model predictive control for dc-dc power converters with parameters’ uncertainties. *IEEE Access*, 9:135121–135131, 2021.
- [75] Noda Yuya and Hidenori Maruta. A study on model based control of dc-dc converter with simple enumeration and pruning restriction computation. In *IECON 2019-45th Annual Conference of the IEEE Industrial Electronics Society*, volume 1, pages 1567–1572. IEEE, 2019.
- [76] Benfei Wang, Venkata Ravi Kishore Kanamarlapudi, Liang Xian, Xiaoyang Peng, Kuan Tak Tan, and Ping Lam So. Model predictive voltage control for

- single-inductor multiple-output dc–dc converter with reduced cross regulation. *IEEE transactions on industrial electronics*, 63(7):4187–4197, 2016.
- [77] Koya Taguchi and Hidenori Maruta. A study on effect of dynamic quantized resolution on mpc based dc-dc converter with combinatorial optimization. In *2020 9th International Conference on Renewable Energy Research and Application (ICRERA)*, pages 289–294. IEEE, 2020.
 - [78] N Snehal, W Pooja, and K Sonam. Model predictive control for dc-dc buck converter using enumeration. In *2020 52nd North American power symposium (NAPS)*, pages 1–6. IEEE, 2021.
 - [79] Qianling Chen, Benfei Wang, Weiwen Peng, and Jose Rodriguez. Cost function decoupling of fs-mpc for power converter using event-triggered mechanism. In *2021 IEEE International Conference on Predictive Control of Electrical Drives and Power Electronics (PRECEDE)*, pages 104–108. IEEE, 2021.
 - [80] Xing Liu, Lin Qiu, Wenjie Wu, Jien Ma, Youtong Fang, Zhouhua Peng, Dan Wang, and Jose Rodríguez. Event-triggered eso-based robust mpc for power converters. *IEEE Transactions on Industrial Electronics*, 70(2):2144–2152, 2022.
 - [81] Shudan Jin, Shengrong Zhuo, and Yigeng Huangfu. Offset-free model predictive control of interleaved boost converter based on extended state observer. In *2022 4th International conference on smart power & internet energy systems (SPIES)*, pages 268–273. IEEE, 2022.
 - [82] Liang Chen, Yunyang Xu, and Nian Heng. Improved finite set model predictive current control of grid side converter in weak grid using kalman filter. In *2019 IEEE PES asia-pacific power and energy engineering conference (APPEEC)*, pages 1–5. IEEE, 2019.
 - [83] Yan Liang, Zehua Liang, Dongdong Zhao, Yigeng Huangfu, and Liang Guo. Model predictive control for interleaved dc-dc boost converter based on kalman compensation. In *2018 IEEE international power electronics and application conference and exposition (PEAC)*, pages 1–5. IEEE, 2018.
 - [84] Xinwei Wei, Hongliang Wang, Kangliang Wang, Kui Li, Minying Li, and An Luo. Robust two-layer model predictive control for full-bridge npc inverter-based class-d voltage mode amplifier. *Electronics*, 8(11), 2019.
 - [85] Malek Ghanes, Mohamed Trabelsi, Haitham Abu-Rub, and Lazhar Ben-Brahim. Robust adaptive observer-based model predictive control for multilevel flying capacitors inverter. *IEEE Transactions on Industrial Electronics*, 63(12):7876–7886, 2016.

- [86] Dae-Keun Choi and Kyo-Beum Lee. Dynamic performance improvement of ac/dc converter using model predictive direct power control with finite control set. *IEEE Transactions on Industrial Electronics*, 62(2):757–767, 2015.
- [87] Sangshin Kwak and Sung-ki Mun. Model predictive control methods to reduce common-mode voltage for three-phase voltage source inverters. *IEEE Transactions on Power Electronics*, 30(9):5019–5035, 2015.
- [88] Guoqing Gao, Wanjun Lei, Yao Cui, Kai Li, Xiufang Hu, Jinghui Xu, and Gaotai Lv. Model predictive control of dual active bridge converter based on the lookup table method. In *2019 IEEE 10th International Symposium on Power Electronics for Distributed Generation Systems (PEDG)*, pages 183–186, 2019.
- [89] Jianfeng Liu, Qing Yan, Zhiwu Huang, and Cheng Luo. Model predictive control of dc/dc converter for ultracapacitors energy storage union based on t-s model. In *2014 IEEE Energy Conversion Congress and Exposition (ECCE)*, pages 2316–2321, 2014.
- [90] Xiangdong Sun, Yonghang Zhou, Guitao Chen, and Biying Ren. Model predictive control of a phase-shifted full-bridge dc-dc converter. In *2020 IEEE 9th International Power Electronics and Motion Control Conference (IPEMC2020-ECCE Asia)*, pages 2710–2714, 2020.
- [91] Junaid Saeed, Liuping Wang, and Nuwantha Fernando. Model predictive control of phase shift full-bridge dc–dc converter using laguerre functions. *IEEE Transactions on Control Systems Technology*, 30(2):819–826, 2022.
- [92] Ronaq Nazir, Tabish Nazir Mir, Abdul Hamid Bhat, and Naira Jeelani. Finite control set model predictive current control of non-isolated ac-ac converters. In *2022 Second International Conference on Power, Control and Computing Technologies (ICPC2T)*, pages 1–6, 2022.
- [93] Males Tomlinson, Toit Mouton, Ralph Kennel, and Peter Stolze. Model predictive control of an ac-to-ac converter with input and output lc filter. In *2011 6th IEEE Conference on Industrial Electronics and Applications*, pages 1233–1238, 2011.
- [94] Patricio Cortes, Gabriel Ortiz, Juan I. Yuz, JosÉ Rodriguez, Sergio Vazquez, and Leopoldo G. Franquelo. Model predictive control of an inverter with output lc filter for ups applications. *IEEE Transactions on Industrial Electronics*, 56(6):1875–1883, 2009.
- [95] Patricio CortÉs, JosÉ RodrÍguez, Patrycjusz Antoniewicz, and Marian Kazmierkowski. Direct power control of an afe using predictive control. *IEEE Transactions on Power Electronics*, 23(5):2516–2523, 2008.

- [96] Eduardo I. Silva, Brendan P. McGrath, Daniel E. Quevedo, and Graham C. Goodwin. Predictive control of a flying capacitor converter. In *2007 American Control Conference*, pages 3763–3768, 2007.
- [97] Florian David Brunner, W. P. M. H. Heemels, and Frank Allgöwer. Robust event-triggered mpc with guaranteed asymptotic bound and average sampling rate. *IEEE Transactions on Automatic Control*, 62(11):5694–5709, 2017.
- [98] Alina Eqtami, Dimos V. Dimarogonas, and Kostas J. Kyriakopoulos. Novel event-triggered strategies for model predictive controllers. In *2011 50th IEEE Conference on Decision and Control and European Control Conference*, pages 3392–3397, 2011.
- [99] Li Deng, Zhan Shu, and Tongwen Chen. Event-triggered robust model predictive control with stochastic event verification. *Automatica*, 146:110638, 2022.
- [100] Alina Eqtami, Dimos V Dimarogonas, and Kostas J Kyriakopoulos. Novel event-triggered strategies for model predictive controllers. In *2011 50th IEEE Conference on Decision and Control and European Control Conference*, pages 3392–3397, Orlando, FL, December 12-15, 2011.
- [101] Jaehyun Yoo and Karl H Johansson. Event-triggered model predictive control with a statistical learning. *IEEE Transactions on Systems, Man, and Cybernetics: Systems*, 51(4):2571–2581, 2021.
- [102] Huiping Li and Yang Shi. Event-triggered robust model predictive control of continuous-time nonlinear systems. *Automatica*, 50(5):1507–1513, 2014.
- [103] Kazumune Hashimoto, Shuichi Adachi, and Dimos V Dimarogonas. Self-triggered model predictive control for nonlinear input-affine dynamical systems via adaptive control samples selection. *IEEE Transactions on Automatic Control*, 62(1):177–189, 2016.
- [104] Ranya Badawi and Jun Chen. Enhancing enumeration-based model predictive control for dc-dc boost converter with event-triggered control. In *European Control Conference*, London, UK, July 12–15, 2022.
- [105] Ranya Badawi and Jun Chen. Performance evaluation of event-triggered model predictive control for boost converter. In *2022 IEEE Vehicle Power and Propulsion Conference (VPPC)*, pages 1–6, 2022.
- [106] Benfei Wang, Jingjing Huang, Changyun Wen, Jose Rodriguez, Cristian Garcia, Hoay Beng Gooi, and Zheng Zeng. Event-triggered model predictive control for power converters. *IEEE Transactions on Industrial Electronics*, 68(1):715–720, 2020.

- [107] Nupur Rathore and Deepak Fulwani. Event triggered control scheme for power converters. In *IECON 2016-42nd Annual Conference of the IEEE Industrial Electronics Society*, pages 1342–1347. IEEE, 2016.
- [108] Chenxuan Liang, Zheng Dong, Qiaoge Zhang, Tongli Cao, Xianjin Gao, Ning Wang, and Zhenbin Zhang. Event-triggered mpc for current-source-mode single-inductor multiple-port dc-dc converter. In *2023 IEEE 14th International Symposium on Power Electronics for Distributed Generation Systems (PEDG)*, pages 932–937. IEEE, 2023.
- [109] Hao Lin, Jianxing Liu, Xiaoning Shen, Yunfei Yin, Jose I Leon, Leopoldo G Franquelo, and Ligang Wu. Event-triggered continuous control set-model predictive control for three-phase power converters. In *IECON 2021–47th Annual Conference of the IEEE Industrial Electronics Society*, pages 1–6. IEEE, 2021.
- [110] Ranya Badawi and Jun Chen. Event-triggered boost converter model predictive control with kalman filter. *Systems Science & Control Engineering*, 12(1):2438866, 2024.
- [111] Gabriele Pannocchia and Alberto Bemporad. Combined design of disturbance model and observer for offset-free model predictive control. *IEEE Transactions on Automatic Control*, 52(6):1048–1053, 2007.
- [112] Gabriele Pannocchia. Offset-free tracking mpc: A tutorial review and comparison of different formulations. In *2015 European control conference (ECC)*, pages 527–532. IEEE, 2015.
- [113] Gerasimos Rigatos, Krishna Busawon, Pierluigi Siano, and Masoud Abbaszadeh. A kalman filter-based disturbance observer for state-of-charge estimation in ev batteries. In *2018 AEIT International Annual Conference*, pages 1–6. IEEE, 2018.
- [114] PJ Hargrave. A tutorial introduction to kalman filtering. In *IEE colloquium on Kalman filters: introduction, applications and future developments*, pages 1–1. IET, 1989.
- [115] Marion McAfee, Mandana Kariminejad, Albert Weinert, Saif Huq, Johannes D. Stigter, and David Tormey. State estimators in soft sensing and sensor fusion for sustainable manufacturing. *Sustainability*, 14(6), 2022.
- [116] Devyani Varshney, Sachin C. Patwardhan, Mani Bhushan, and Lorenz T. Biegler. Moving horizon estimator for nonlinear and non-gaussian stochastic disturbances. *Journal of Process Control*, 116:234–254, 2022.
- [117] Kumar E Vinodh, Jerome Jovitha, and S Ayyappan. Comparison of four state observer design algorithms for mimo system. *Archives of Control Sciences*, 23(2), 2013.

- [118] Wen-Hua Chen, Jun Yang, Lei Guo, and Shihua Li. Disturbance-observer-based control and related methods—an overview. *IEEE Transactions on Industrial Electronics*, 63(2):1083–1095, 2016.
- [119] Juhoon Back and Hyungbo Shim. An inner-loop controller guaranteeing robust transient performance for uncertain mimo nonlinear systems. *IEEE Transactions on Automatic Control*, 54(7):1601–1607, 2009.
- [120] Hyungbo Shim. Disturbance observers. In *Encyclopedia of Systems and Control*, pages 622–629. Springer, 2021.
- [121] Mohinder S Grewal and Angus P Andrews. *Kalman filtering: Theory and Practice with MATLAB*. John Wiley & Sons, 2014.
- [122] J.B. Rawlings, E.S. Meadows, and K.R. Muske. Nonlinear model predictive control: A tutorial and survey. *IFAC Proceedings Volumes*, 27(2):185–197, 1994. IFAC Symposium on Advanced Control of Chemical Processes, Kyoto, Japan, 25-27 May 1994.
- [123] Mohamed Ahmeid, Matthew Armstrong, Shady Gadoue, Maher Al-Greer, and Petros Missailidis. Real-time parameter estimation of dc–dc converters using a self-tuned kalman filter. *IEEE Transactions on Power Electronics*, 32(7):5666–5674, 2017.